Catarina Gato Cardadeiro

Bachelor of Science

Model-based comparative biomechanics and muscle function analysis of simulated crouch gait by healthy children and crouch gait in CP children

Dissertation submitted in partial fulfilment of the requirements for the degree of

Master of Science in
Biomedical Engineering

Adviser: Prof. Doutor António Prieto Veloso, Full Professor, Faculty of Human Kinetics

Co-adviser: Prof.ª Doutora Cláudia Quaresma, Assistant Professor, NOVA University of Lisbon

November 2021

FACULDADE DE CIÊNCIAS E TECNOLOGIA
UNIVERSIDADE NOVA DE LISBOA

Model-based comparative biomechanics and muscle function analysis of simulated crouch gait by healthy children and crouch gait in CP children

Agradecimentos

Agradecimentos

Os contributos para esta dissertação foram muito diversificados, quer pela forma como se manifestaram, quer pela intensidade e frequência com que ocorreram. Este percurso foi marcado por uma situação conturbada relativa à pandemia que levou a muitos condicionalismos e que, naturalmente, dificultaram o desenvolvimento desta tese.

Neste contexto, os meus primeiros agradecimentos vão para o Professor Doutor António Veloso, pelo seu valioso contributo durante todo este processo. Agradeço pela sua orientação científica que me proporcionou novos conhecimentos, e pelo apoio ao trabalho desenvolvido. Um especial obrigado ao Mestre Rodrigo Mateus, pela sua completa disponibilidade durante todo este percurso, tendo sido uma ajuda preciosa nos momentos mais complicados. Agradeço pela sua dedicação e capacidade de me motivar, e por todos os momentos de reflexão que muito me ensinaram. Estou ainda grata à Professora Doutora Filipa João que me ajudou na resolução de diversos problemas ao longo da tese. À Professora Doutora Filomena Carnide, agradeço a disponibilidade e colaboração na resolução dos problemas de estatística que fui encontrando.

Esta dissertação não marca só o final de um estudo de investigação, mas o final de um percurso de 5 anos de grande aprendizagem e diversas vivências na Faculdade de Ciências e Tecnologia. Um último agradecimento a todos os professores que ao longo destes anos me marcaram e ajudaram a definir o meu percurso profissional.

Quero agradecer a todos os meus amigos pela constante presença na minha vida e pelo precioso valor da vossa amizade. Um especial obrigado à Mónica Cepeda, Madalena Gomes, Madalena Marques, Joana Santos, Madalena Maia, Tiago Amaral, Beatriz Barrocas, Nuno Infante, Catarina Pires e Teresa Chambel, pelo constante incentivo e momentos de partilha durante este longo processo.

Por fim, o meu maior agradecimento vai para a minha família pelo apoio incondicional e por serem os meus grandes pilares. Aos meus pais por tudo o que sempre me proporcionaram, e pelo amor e apoio que nunca me faltou. Aos meus irmãos Diogo e Francisco pela cumplicidade e constante partilha nas várias áreas da minha vida.

Gostaria de dedicar esta tese ao meu avô paterno por tudo o que sempre me ensinou, e por ter sido a minha grande inspiração na escolha desta área de engenharia. Obrigada por ter sempre acreditado em mim.

Trabalho integrado no projeto

Referência do Projeto: PTDC/EMD-EMD/5804/2020
Título: Desenvolvimento de uma plataforma de simulação biomecânica baseada em modelos músculo-esqueléticos preditivos do efeito de intervenção ortopédica na melhoria da marcha em crianças com paralisia cerebral

Resumo

Patologias neurológicas como a paralisia cerebral levam a perturbações severas do movimento, sendo a capacidade de andar significativamente afetada. A marcha em agachamento (*crouch gait*) é o padrão de marcha mais comum adotado por crianças com paralisia cerebral. Atualmente, as causas associadas a esta marcha patológica não são facilmente identificadas, pelo que a decisão clínica relativa ao tratamento adequado para cada caso baseia-se num diagnóstico pouco preciso. Os principais objetivos desta dissertação são investigar a biomecânica da marcha, as forças musculares, e as contribuições musculares individuais para a aceleração do centro de massa em crianças com paralisia cerebral e que apresentem *crouch gait*, e crianças saudáveis a simular este padrão de marcha. Foram considerados três grupos de estudo, incluindo o grupo de controlo: três crianças com paralisia cerebral com *crouch gait* considerado severo, seis crianças saudáveis a simular esta padrão de marcha patológica, e as mesmas crianças consideradas saudáveis a andar em marcha normal (grupo de controlo). Todos os parâmetros foram estimados através de simulações músculo-esqueléticas realizadas no software OpenSim. Por sua vez, o processamento de dados e a análise cinemática inversa foram realizados no Visual3D. Foi possível concluir que os sujeitos saudáveis mostraram capacidade de simular a marcha em agachamento. Os resultados indicam que o *crouch gait* simulado e o real apresentam um comportamento muscular semelhante durante toda a fase da marcha, solicitando essencialmente os mesmos grupos musculares. Isto indicia que as diferenças mais significativas entre o *crouch gait* e a marcha normal estão mais provavelmente relacionadas com a postura de agachamento adotada do que propriamente disfunções musculares. As contribuições musculares individuais para a aceleração do centro de massa mostraram que os principais responsáveis pelo suporte durante a marcha são os mesmos em todos os grupos de estudo, sendo os vastos, o solear e os gastrocnémios muito importantes para sustentar a postura de agachamento.
Palavras-chave: Marcha em agachamento, Paralisia cerebral, Marcha simulada, Modelação Musculoesquelética, Otimização dinâmica, Análise de acelerações induzidas

Abstract

Neurologic dysfunctions like cerebral palsy lead to serious disorders of movement, being walking really affected. Crouch gait is the most common abnormal gait pattern adopted by children with cerebral palsy. Nowadays, the causes associated with this pathological gait cannot be clearly identified, therefore the clinical decision on the appropriate treatment is dependent on an inaccurate diagnosis. The goal of this dissertation is to investigate gait biomechanics, the muscle forces, and individual muscle contributions to vertical and fore-aft acceleration of the mass centre during stance of CP children with crouch gait and healthy children simulating this abnormal gait pattern. There were considered three study groups, one of which was the control group: three children with cerebral palsy walking in severe crouch gait, six typically developing children simulating crouch gait, and the same typically developing children performing unimpaired gait (control group). The parameters were estimated through musculoskeletal simulations performed in OpenSim. Data processing and inverse kinematics analysis were performed in Visual3D. The healthy subjects showed ability to simulate crouch gait in a reproducible manner. The results indicate that simulated and real crouch gait present a similar muscle behaviour throughout the stance phase, relying mostly on the same muscle groups. This suggests that the most significant differences between this pathological gait and normal walking are more likely to be related to the crouch posture adopted than muscular dysfunctions. The individual muscle contributions to vertical and fore-aft acceleration of the mass centre showed that the major contributors to vertical acceleration are the same in all of the research groups, being the vasti, soleus and gastrocnemius very important in supporting the crouch posture.

Keywords: Crouch gait, Cerebral palsy, Simulated crouch gait, OpenSim, Musculoskeletal modelling, Computed Muscle Control, Induced Acceleration Analysis

Contents

List of Figures

List of Tables

List of Acronyms

AFOs	Ankle-foot orthoses
CG	Crouch gait
CMC	Computed Muscle Control
CP	Cerebral palsy
EMG	Electromyography
IAA	Induced Accelerations Analysis
ID	Inverse Dynamics
MIMF	Maximum isometric muscle forces
NICE	National Institute for Health and Care Excellence
PCSA	Muscle's physiological cross-sectional area
RMS	Root mean square
RRA	Residual Reduction Algorithm
TD	Typically developing
TDC	Typically developing children simulating crouch gait
TDN	Typically developing children performing normal walking

1. Introduction

1.1 Problem Definition

The ability to walk can significantly contribute to the physical health and overall well-being of someone, independent of the age group. However, in children it can have a greater impact because they are much more active than adults. Moving disabilities are major constraints in the learning process of a child and in his ability to socialize. According to the National Institute for Health and Care Excellence (NICE), cerebral palsy (CP) is the most common cause of physical disability in children and young people in the developed world (NICE, 2020). Overall, the CP rate is between 2 and 3 per 1000 live-births. This rate increases to 40-100 per 1000 live births among babies born very early or with very low birthweight (Krägeloh-Mann & Cans, 2009). As it is not associated with a high mortality rate in the developed countries, there are as many adults with CP as children (Gage et al., 2009).

Cerebral palsy is a permanent neurologic dysfunction caused by serious cerebral damages of the fetal or neonatal brain (before its development is complete), primarily leading to disorders of movement and posture. It can also cause mental dysfunctions or disturbances in gait, cognition, growth, and sensation. Although the brain damages are not progressive, their expression can change over time. This disorder largely affects the motor control of gait. Consequently, it is considered to be a key aspect when it comes to the diagnosis.

The diversity of gait deviations observed in children with cerebral palsy has led to a lot of research in gait classification systems to assist in the diagnostic process and clinical decision making. Crouch gait (CG) is one of the identified gait patterns related to this disease, characterized by excessive knee flexion, increased hip flexion and increased ankle dorsiflexion, leading to bone deformities and joint pain (van Gelder et al., 2017). There are several factors that can contribute to this pattern like muscle contractures, weakness, or foot deformities.

Gait analysis has been performed in the clinical setting to assist surgical planning in children with cerebral palsy and other neurologic disorders, for the last decades (Khouri and Desailly, 2017). In its simplest form, motion capture systems are used to track the movements of the lower limbs. It enables us to obtain joint kinematics and other direct measurements, but it does not provide musculoskeletal information that can be really helpful for an accurate diagnosis. The acquisition of ground reaction forces made it possible to also calculate the kinetics of the joints, which helps in interpreting the gait data. Thus, it was needed to obtain data from inside the body, such as muscle

forces and joint contact forces, to complement what was already being done with motion capture. Unfortunately, direct methods for measuring this type of force are extremely invasive and non-viable, which led us to consider musculoskeletal modelling and simulation to do so.

Classically, data gathered from gait analysis is compared to a healthy population with normal gait to determine gait deviations of CP patients. Most of these dysfunctions reflect the impact of the pathological posture adopted by the CP patient, which are normally addressed as primary deviations caused by the characteristic neurological disorders in these children. However, some of the gait deviations identified are direct consequences of secondary deviations due to postural or muscle compensations, and bone deformities caused by muscle force unbalance on the bones during growth (Gage & Novacheck, 2001).

Knowing the primary causes of the gait abnormalities is very important for clinicians to choose the appropriate corrective treatment and, especially, to define which surgical intervention should be applied. One of the approaches that has been studied, to better understand these different causes, is comparing the gait results from analysing patients with cerebral palsy performing their abnormal gait relatively to those of healthy subjects imitating characteristic CP patterns. There are only a few studies that investigate the possibility to use this approach, and they are mainly focused on analysing the differences in gait kinematics and kinetics. So, using this comparison to better understand the muscle forces and behaviour in this type of gait abnormalities may be helpful in clinical decision-making.

1.2 Objectives and Contributions

The main purpose of this dissertation was to compare gait biomechanics and muscle function of CP children with crouch gait and healthy children simulating this abnormal gait pattern, using musculoskeletal modelling. Therefore, several goals were set: (1) to estimate and compare muscle forces during stance in simulated and real crouch; (2) to investigate the individual muscle contributions to vertical and fore-aft acceleration of the mass centre in both simulated and real crouch gait and compare it, not only between them but also with unimpaired gait; (3) to evaluate the capacity of neurologically intact children to imitate crouch gait.

It was expected that this study could contribute to a better distinction between primary gait deviations, related with the neurological disorder, and secondary deviations, due to compensatory body mechanisms. Other studies had already examined and compared the kinematics between induced crouch gait and real crouch, but the muscle contributions have not been investigated for simulated crouch. Additionally, this research could also provide some inside on the efficiency of the gait pattern performed by CP children, by comparing them with healthy children simulating that same gait posture.

The use of musculoskeletal models to have a more precise diagnosis about pathological gait disfunctions is not being used yet in clinical practice, although it has been shown to have promising results. This work might constitute an additional contribution for its validation to that purpose. In conclusion, this dissertation aimed to contribute to improve the diagnosis of crouch gait in children with cerebral palsy and so helping with treatment planning.

1.3 Thesis Organization

This dissertation is divided into seven main chapter, which are described below:

Chapter 1: comprises a brief description of what motivated this dissertation, the objectives defined for this work and its contributions to this scientific area.

Chapter 2: overview of the most pertinent and relevant existing research related to this work.

Chapter 3: description of the relevant theory and the analytical concept.

Chapter 4: introduces the workflow for this dissertation. In this chapter, the subjects and all the details on how data acquisition was performed are described. Both Visual3D and OpenSim implementations are detailed in this chapter.

Chapter 5: this chapter comprises a detailed description of the results obtained.

Chapter 6: presents the discussion on the findings from the previous chapter. This discussion also relates the results obtained with existing research.

Chapter 7: summarizes the main conclusions of this dissertation, identifies the limitations of this dissertation, and describes future developments that could be included on further studies.

2. Literature Review

The study of the motion of the body has gained increasing importance over the years in clinical diagnosis, especially in understanding movement dysfunctions caused by neurological disorders. Among these, those which lead to gait abnormalities are pretty common and debilitating for the patients. It is known that specific features of gait might develop earlier than other signs and symptoms and can offer important clues leading to the diagnosis of the underlying disorder (Nonnekes et al., 2018).

Gait analysis is a very broad term to describe different ways to explain the motion of the body during gait. It can mean many different methods, from a brief observation performed by professionals to sophisticated computerized measurements. Considering the existing technology, this analysis uses physical measurements and models, including the movement of the person's centre of mass, joint kinematics, ground-reaction forces, the resultant loads, body segment energy variation, and muscular work (Surer and Kose, 2011).

Research on gait analysis has been conducted since the late 19th century, and its widespread application in biomedical engineering began with the availability of video camera systems (Tao et al., 2012). Around that time, Eadweard Muybridge developed the first technique to capture images sequences to analyse equine gait (Baker, 2007). The standard gait analysis method is now based on high-speed multi-camera motion capture, that tracks the changing positions and orientations of the body segments, and the acquisition of ground-reaction forces using a force platform. This process can require expensive equipment and other space limitations, so the use of wearable sensors to acquire inertial measurements has been presented as an alternative.

The main goal of gait analysis is the acquisition of quantitative information about the mechanics of the musculoskeletal system while executing a motor task (Surer and Kose, 2011). In order to obtain the values needed, motion capture and inertial measurements are performed. Motion capture is the process of digitally record the movement of a person. The data is acquired through external sensors and it is processed using mathematical models. On the other hand, inertial measurements are taken by using accelerometers, gyroscopes and magnetometers attached to the person to measure acceleration, angular velocity, and magnetic field, respectively. Through gait analysis, each gait phase can be identified, the kinematic and kinetic parameters of human gait can be determined, and musculoskeletal functions can be quantitatively evaluated. In traditional marker-based approaches, body models are used to estimate the kinematics of the task that is being

performed. In these models, a skeleton is defined as a set of joints and the bones between these joints. It is parameterized on the lengths of the bones and the rotation of each joint, with pose being described by the joint angles (Chimera et al., 2017).

Recent interest in using modelling and simulation to study movement is driven by the belief that this approach can provide insight into how the nervous system and muscles interact to produce coordinated motion of the body parts. The data we get from the motion capture provides a quantitative description of the kinematics and dynamics of body-segmental movement, but they do not explain how muscles work together to produce a coordinated gait pattern (Pandy, 2001). Computer modelling and simulation softwares have been created to fill in this gap in the gait analysis.

Computational musculoskeletal modelling provides the tools needed to understand the force profiles of individual muscles in performing a certain task. With this analysis, it is possible to identify neuro-musculoskeletal impairments and to know how these are affecting walking, and other important tasks of our daily routine. Although the potential of these technologies has been highlighted in the last ten years, it is still not being used in routine clinical gait analysis. There are already available a variety of computational techniques to estimate motion muscle forces and so, these modelling approaches have already been applied in many research studies related to sport performance and clinical interventions. The musculoskeletal models available nowadays incorporate different methods and optimization techniques, among them, to calculate and estimate the same gait motion parameters, and they also sometimes use different experimental inputs. These variations in model assumptions may result in different force estimations, which makes it difficult to select the most adequate approach for clinical use.

The potential feasibility and utility of muscle force modelling in clinical movement analysis has not been thoroughly studied and defined. Thereupon, Ursula Trinler aimed to study the applicability of current muscle force estimation approaches to clinical practice in her systematic review (Trinler et al., 2018). This paper showed a broad agreement, between the models analysed, in predicting when specific muscles were active during the unimpaired gait cycle. On the other hand, it found significant differences when estimating the peak muscle forces, and the reasons for this are not yet clear. Albeit, it couldn't identify a model preferable to others, so more research is needed to differentiate each technique and its potential.

Even though these models are not being used in clinical practice, there is research being done on analysing abnormal gait related to neurologic pathologies, as cerebral palsy. The most common gait pattern associated with this disease in children is crouch gait, so it is important to study and

understand the motions generated by muscle forces in order to determine the cause and appropriate treatment.

In 2008, Jennifer Hicks and colleagues aimed to determine how crouched postures affect the capacity of muscles to extend the hip and the knee joint during the single-limb stance gait phase (Hicks et al., 2008). They grouped the subjects into three different groups according to the severity of the crouch gait, and so they could relate the capacity of the extension to each representative crouched posture. In this analysis, they defined the muscle's extension capacity based only on the orientation and inertial properties of the body segments, not considering either the muscle's activation level or force-generating capacity. As it was expected, the reduced capacity to extend these joints was identified for all crouch severity levels. Compared to normal gait, these groups showed major reductions in the joints' accelerations generated for important stance-phase muscles and increases in the joints' accelerations induced by gravity. So, they concluded that an individual in crouch gait must generate more energy to maintain that posture, as was reported in previous experimental studies (Rose et al., 1990; Hsu et al., 1993; Waters and Mulroy, 1999). Furthermore, they demonstrated that the negative impacts of this abnormal gait pattern increase with worsening crouch severity, which indicates that crouch gait is not sustainable. By using a previously developed technique to simulate torsional bone deformities, they created a musculoskeletal model that accounts for various tibial torsion angles and they found that the increase in the angle of deformity implied a reduction in the hip and knee extension accelerations. These findings indicate that small interventions as correcting a patient's tibial alignment may lead to a significant improvement in the patient's gait efficiency. However, the problem in determining the adequate clinical approach for each individual patient remains.

Joint pain is one of the most debilitating consequences of walking in crouch gait. Cartilage and bone growth and regeneration depend on the loads applied, so abnormal loads can cause joint pain, bone deformities and cartilage deterioration. Understanding how joint loads change during gait may help in developing successful treatment strategies. Steele et al. aimed to study the relation between muscle forces and compressive tibiofemoral force change with the increasing knee flexion, associated with crouch gait (Steele, DeMers, et al., 2012). A previous research examined knee forces in a static crouched posture, which reported increasing compressive tibiofemoral force with increasing knee flexion (Perry et al., 1975). Thus, much higher forces are expected during dynamic activities like walking, due to the need to support the body weight and propel the body forward. Steele et al. compared muscle forces and compressive loads on the tibia in typically developing (TD) children with unimpaired gait and children with cerebral palsy who walked in different levels of crouch severity. They concluded that children with moderate and severe crouch experience

substantially greater compressive tibiofemoral forces that individuals with unimpaired gait, which is due to an increase in quadriceps force required to support the body. Therefore, surgeries that result in a more upright posture may help in reducing the excessive joint loading and prevent joint paint and cartilage regeneration.

In a more recent study, Steele et al. (Steele, van der Krogt, et al., 2012) examined how much muscle strength could be weakened before crouch gait becomes impossible. Muscle weakness is one of the most common suggested causes of crouch gait in children with cerebral palsy, and so understanding how this muscle disability can contribute to crouch posture can assist in defining the most adequate clinical approach. The effect of strength training in CP children is not yet completely clear but knowing in which muscle groups weakness contributes the most to the individual's abnormal gait may be important to define better the targets for strength training programs. They used musculoskeletal modelling to simulate weakness by reducing the force-generating capacity of particular muscle groups. This study suggested that crouch gait requires greater quadriceps strength than unimpaired gait and it worsens with crouch severity, which had already been reported in previous studies (Perry et al., 1975; Hsu et al., 1993) . In addition to this, Steele's results also indicate that crouch gait requires less hip abductor and ankle plantar flexor strength than normal gait.

Other than study which muscle groups are more responsible for crouch posture in children with cerebral palsy, knowing the role of each individual muscle during the gait cycle can be very useful in planning surgical interventions to improve gait dynamics. Several studies have analysed how muscles accelerate the joints and mass centre in unimpaired gait (Anderson and Pandy, 2003; Neptune et al., 2004; Arnold et al., 2005; Kimmel and Schwartz, 2006; Liu et al., 2006). They report that during early stance the vasti and gluteus maximus are responsible for the body support and slow forward progression, while gastrocnemius and soleus are mostly active during late stance, supporting the body weight and propelling the body forward. In 2010, Katherine Steele and colleagues (Steele et al., 2010) examined the muscles contribution to mass centre accelerations and joint angular accelerations during single-limb gait, in CP children diagnosed with crouch gait. This work was the first to use muscle-driven simulations to analyse these muscle contributions in subjects with crouch. These simulations indicate that crouch gait requires larger muscle forces than normal gait to support the body and propel the body forward. The muscle groups required for body support are the same in both gaits, but different muscles are used to propel the mass centre forward. During crouch gait, support muscles are active throughout single limb stance, while in unimpaired gait the same muscles follow a precise activation sequence. These different strategies to support and progression during single limb stance suggest that some children with cerebral palsy

may adopt crouch gait as a feasible gait pattern given their neurological limitations (Steele et al., 2010).

In a more recent study, the same research group aimed to examine if muscle contributions to vertical and fore-aft accelerations differ between crouch gait and unimpaired gait, and also understand how it changes with crouch severity (Steele et al., 2013). Previous studies have reported that, during unimpaired gait, the vasti and gluteus maximus accelerate the mass centre upward and backward in early stance, the gluteus medius accelerates the body upward in mid stance, and the ankle plantarflexors are the major responsible for the mass centre upward and forward accelerations in late stance (Neptune et al., 2001; Anderson & Pandy, 2003; Liu et al., 2008). Similar results were found in Steele's research regarding the quadriceps and ankle plantarflexors role during single limb stance in crouch gait. Even so, at the same time, these muscles also produce large opposing fore-aft accelerations throughout the gait cycle, which do not happen in unimpaired gait and turns out to be quite inefficient for the gait dynamics.

Normally to analyse kinematics and muscle contributions of crouch gait, researches compare it with known values for unimpaired gait, which truly helps in understanding this pathological gait. However, the comparison with healthy subjects walking in a crouched posture can also contribute to a better understanding of the biomechanics of the pathological gait. It is expected that this can help to better distinguish between primary deviations directly induced by neurological troubles and secondary compensatory deviations related to the gait performed.

Matjačić and Olenšek sought to characterize biomechanically three different crouch walking patterns, artificially induced in neurologically intact subjects, to compare them with cases of real crouch walking (Matjačić & Olenšek, 2007). They used a method to artificially emulate muscle contracture of the hamstrings and iliopsoas muscles so that they could make conclusions about changes in the kinematic and kinetic gait patterns. The results of this study showed that hamstring contraction can work to extend the hip and flex the knee, while the ankle joint needs to shift to a more dorsiflexion than normal as a compensatory effect during stance. Additionally, it was verified that contracture of iliopsoas directly forces the hip into flexion and can act to accelerate knee flexion, which increases the knee moment during terminal stance. These findings can help relating the gait features to the muscles which tightness causes the particular abnormal walking.

Although the analysis of simulated pathological gait by healthy subjects may be relevant to determine the most adequate clinical approach for each particular case, it is important to study the ability of the neurologically intact subjects to imitate the abnormal gait patterns. Therefore, Rezgui et al. (Rezgui et al., 2013) aimed to investigate that ability to simulate two typical CP gaits, jump gait

and crouch gait, and its relevance to clinical diagnosis. It has been demonstrated that healthy subjects are able to simulate these gait patterns in a reproducible manner. An obvious limitation of this study is that all gait imitations were performed by adults, being children the usual target patient population.

Another work concerning the analysis of artificially induce kinematic constraints was done by Balzer et al. (Balzer et al., 2013) and they wanted to explore if an artificially induced bilateral knee flexion contracture could cause compensatory mechanisms in the foot motion during gait in healthy children. In this case, they used children to simulate crouch gait, which is an added value compared with the study mentioned above. On average, their data showed that participants compensated for the induced knee flexion with dorsiflexion, eversion, and external rotation of the hindfoot, which is often seen in pathological crouch gait. This may indicate that any therapeutic treatment aiming to improve knee extension in CP children can also reduce the risk of possible compensation mechanisms around the foot.

Inducing physical constraints in healthy subjects, in order to simulate abnormal walking patterns commonly seen in children with neurological disorders as cerebral palsy, has been proven to be useful for a better understanding of the causes behind the pathological gait. This is especially important for progressive gait deviations like crouch gait. However, little research has been done on this approach.

3. Theoretical Concepts

3.1 Cerebral Palsy

Cerebral palsy is a permanent neurologic dysfunction caused by serious cerebral damages or malformations of the fetal or infant brain. As this occurs when the brain is still in development, the damages can happen before or during birth, and even in the first years of the child's life. The motor area of the cerebral cortex is the most affected, which is a region of the brain located in the frontal lobe and it is responsible for the planning, control, and execution of voluntary movements. So, CP patients present mostly movement disorders and difficulty in maintaining posture and balance. However, it can also cause disturbances of sensation, perception, cognition, communication, and behaviour, by epilepsy or secondary musculoskeletal problems (Gage et al., 2009).

There are several possible causes for this disease, which depend on the time at which the brain is affected. The majority of the children have congenital cerebral palsy, which means that they are already born with this disease. Acquired cerebral palsy is related to the development of this disorder after birth, that may be caused by brain infections (such as bacterial meningitis or viral encephalitis), problems with blood flow to the brain, or head injury from an accident. During the gestation period, the brain of the unborn child is still developing, so it is subject to having its white matter damaged, it can suffer abnormal developments or bleeding episodes, and it may have a lack of oxygen support. All of these situations can cause cerebral palsy to the child (CDC, 2019).

The most relevant risk factors for this condition are low birthweight, premature birth, multiple gestation, intrauterine viral infections, and maternal thyroid abnormalities (Jacobsson & Hagberg, 2004). It is known that premature birth, especially before 28 weeks of gestation, is the leading risk factor for the development of this dysfunction. Among neonates who were born prior to 28 weeks, the prevalence of cerebral palsy is 8,2%, and it decreases to 0,14% at 36 weeks of gestation (Stavsky et al., 2017). A recent study has suggested that postterm pregnancy at 42 weeks or later can also increase the risk of this condition (Moster et al., 2010).

3.1.1 Clinical classification

Cerebral palsy mostly affects the motor area of the cerebral cortex, which is the part of the brain that controls all body movements and maintain posture and balance. Although the brain damages are not progressive, their expression can change over time (Stavsky et al., 2017). There are a lot of classification systems proposed for cerebral palsy, and the first most comprehensive system to classify this disease was provided by Minear in 1956 (Gage et al., 2009). Nowadays, the most used are based on the nature of the motor disorders and on the functional motor abilities. Considering first the nature of the motor disorders, cerebral palsy can be categorized as:

1) Spastic cerebral palsy – it is the most common form of CP and it has to do with the stiffness of the muscles, which means that the muscle has an increased muscle tone. This can affect the arm, hand, and leg of only one side of the body (spastic hemiplegia), mostly the legs instead of the arms (spastic diplegia), or the muscles of the four limbs in the same way (spastic quadriplegia), which is the most severe.

2) Dyskinetic cerebral palsy – it is characterized by abnormal patterns of posture and/or movement also accompanied by involuntary, uncontrolled, recurring, and occasionally stereotyped movements (Himmelmann et al., 2009). Although it is not the most prevalent form of CP, it is one of the most disabling forms. Some patients have difficulty in doing basic activity as breathing and speaking.

3) Ataxic cerebral palsy – this mainly affects balance and depth perception. Children with ataxic CP often have poor coordination and walk unsteadily with a wide-based gait.

This classification system was described in the Reference and Training Manual of Surveillance of Cerebral Palsy in Europe (Rosenbaum et al., 2007). Children can also have symptoms that don't correspond to any single type of cerebral palsy but are a mix of types. Sometimes, there are patients who have some muscles that are too tight and others that are too relaxed, which does not fit in any of the types above.

The classification based on functional motor abilities is internationally used among health professionals. The Gross Motor Function Classification System (Palisano et al., 1997) is the most used in clinical terms to group patients with CP into one of five levels based on functional mobility or activity limitation. This system is explained in table 1.

Table 1. Gross Motor Function Classification System.

Gross Motor Function Classification System					
Levels	1	2	3	4	5
Description	Independent ambulators. Children are able to perform gross motor skills such as running and jumping, but speed, balance and coordination are limited. 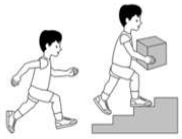	Independent ambulators. Children walk in most settings and climb stairs holding onto a railing. They may experience difficulty walking long distances. 	Non-independent ambulators. Children need assistive devices for walking, have to be supervised to climb stairs and use wheeled mobility when traveling long distances. 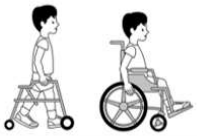	Non-independent ambulators. Children are mostly wheelchair-bound but are able to stand for short periods with assistance and resist gravity. 	Non-independent ambulators. Children are totally dependent, have limited ability to maintain antigravity head and trunk postures, and to control leg and arm movements. 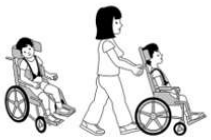

3.1.2 Gait patterns in cerebral palsy

As it was mentioned before, cerebral palsy is related to neuromuscular deficits which result in gait abnormalities, commonly seen in children with spastic CP. Clinical gait analysis aims to determine what is causing the abnormal gait of a patient, by collecting and analysing data. A gait cycle starts at the instant where one foot touches the floor and stops as the same foot comes into contact for the next step. It can be divided into different phases: the stance phase, the first 60% of the cycle, followed by the swing phase, the rest 40% of the cycle. In turn, the stance is characterized by the double support periods, which take place in the first (early stance), and last (pre-swing) 10% of this phase, and the single support period, which corresponds to the remaining 40% of the stance and it is divided into mid-stance and terminal stance (Neptune et al., 2001).

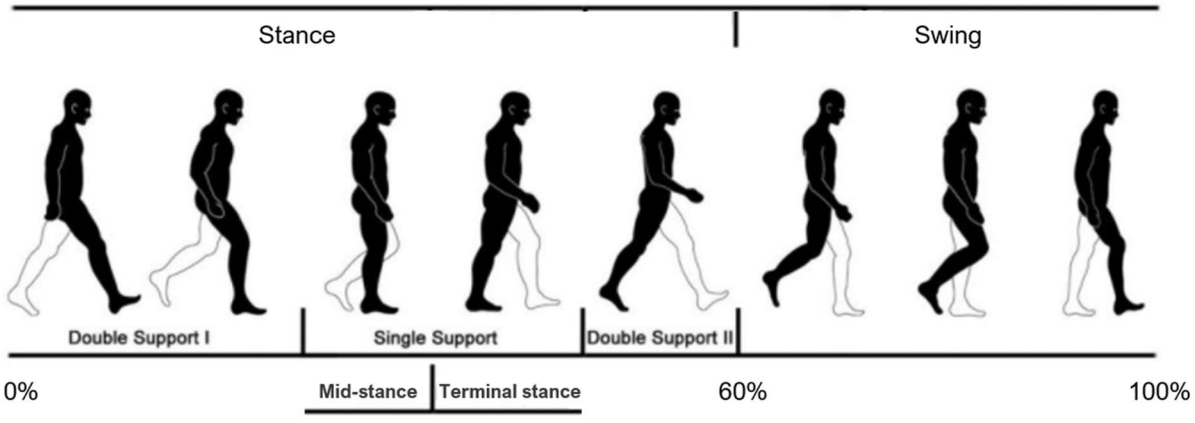

Figure 1. Some phases of the gait cycle.

There is a wide variety of gait deviations that can be observed in CP patients and they are mostly related to spastic cerebral palsy. Some gait patterns do not fit in only one classification type, because they result from a combination of deviations, so these are not described in the groups below. The classification system mostly used for CP gait patterns differs unilateral from bilateral

spastic cerebral palsy (Armand et al., 2016). Normally, the classification is based on the observation of the kinematics in the sagittal plane. Therefore, the two groups in which it is divided are:

1) Unilateral spastic CP – the first approach to classify this category was proposed by Winters et al (Winters et al., 1987). The impairments are grouped into four types in view of the severity and localization of the dysfunction.

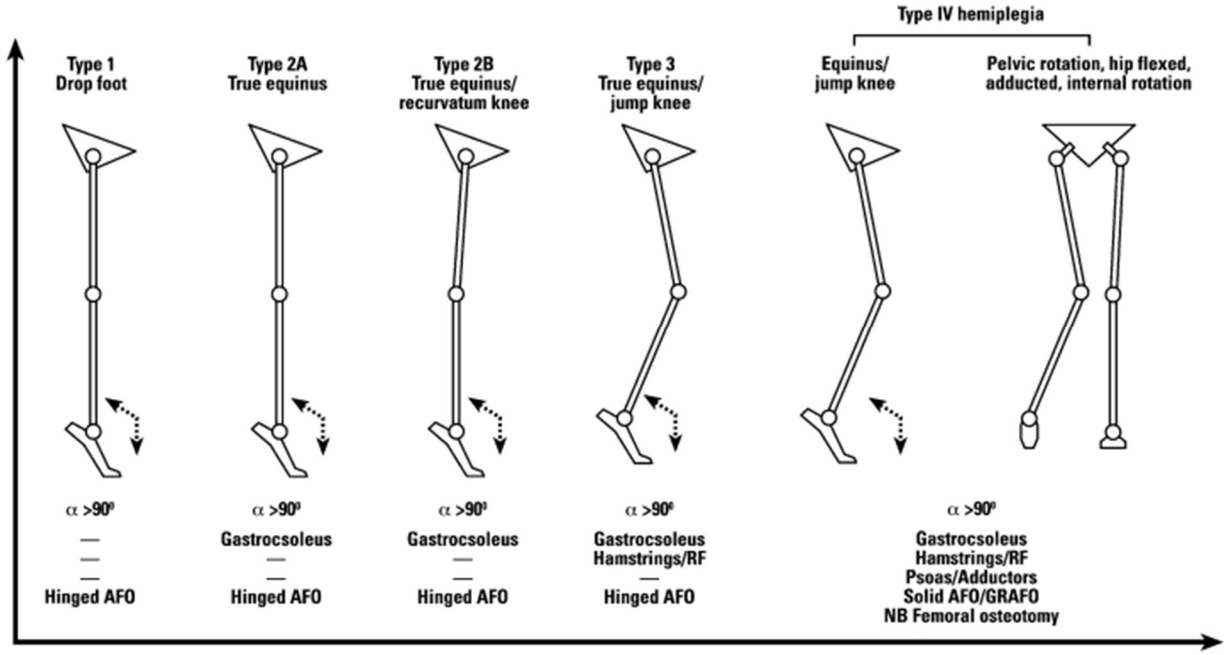

Figure 2. Gait patterns for unilateral spastic cerebral palsy. Adapted from (Rodda and Graham, 2001).

2) Bilateral spastic CP – in this classification proposed by Rodda and Graham (Rodda and Graham, 2001), they consider the kinematics of the ankle, knee, hip, and pelvis as a whole, and subdivide it also into four types.

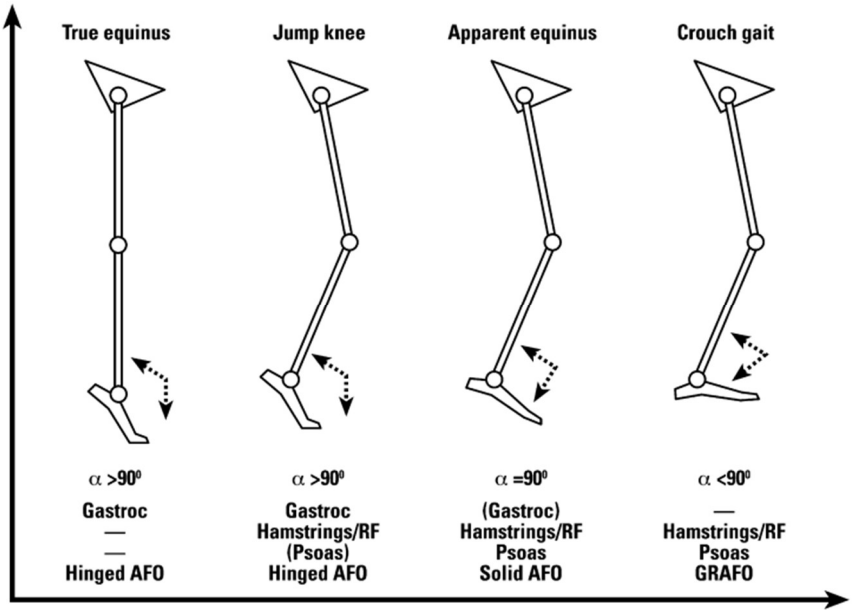

Figure 3. Gait patterns for bilateral spastic cerebral palsy. Adapted from (Rodda and Graham, 2001).

3.1.3 Crouch gait

3.1.3.1 Description

Crouch gait is a pattern commonly observed in children with bilateral spastic cerebral palsy and it is defined as excessive ankle dorsiflexion with increased knee and hip flexion during the stance phase. This is a pattern characteristic of children with severe diplegia or quadriplegia, because of substantial weakness, decreased selective motor control, and increased spasticity of lower limb muscles. This type of gait overloads the joints and it requires a much higher energy cost compared to unimpaired gait, so it is extremely inefficient and unsustainable in the long run (Kedem and Scher, 2016). Furthermore, crouch gait refers to progressive gait deviations that include primary musculoskeletal abnormalities, related directly to neurological disorders, but also secondary deviations that are induced by compensatory effects of the abnormal gait performed.

3.1.3.2 Treatment Approaches

The main goal of the clinical approaches used nowadays is to control and improve the gait efficiency, in order to delay the progression of the abnormal walking pattern. A crouched posture reduces the capacity of muscles to extend the knee and hip, and so it requires a lot more energy than normal gait. Higher muscle forces lead to higher joint reaction forces, which may contribute over time to higher rates of joint pain and degenerative arthritis (Galey et al., 2017). Because of its progressive nature, it should not be left untreated.

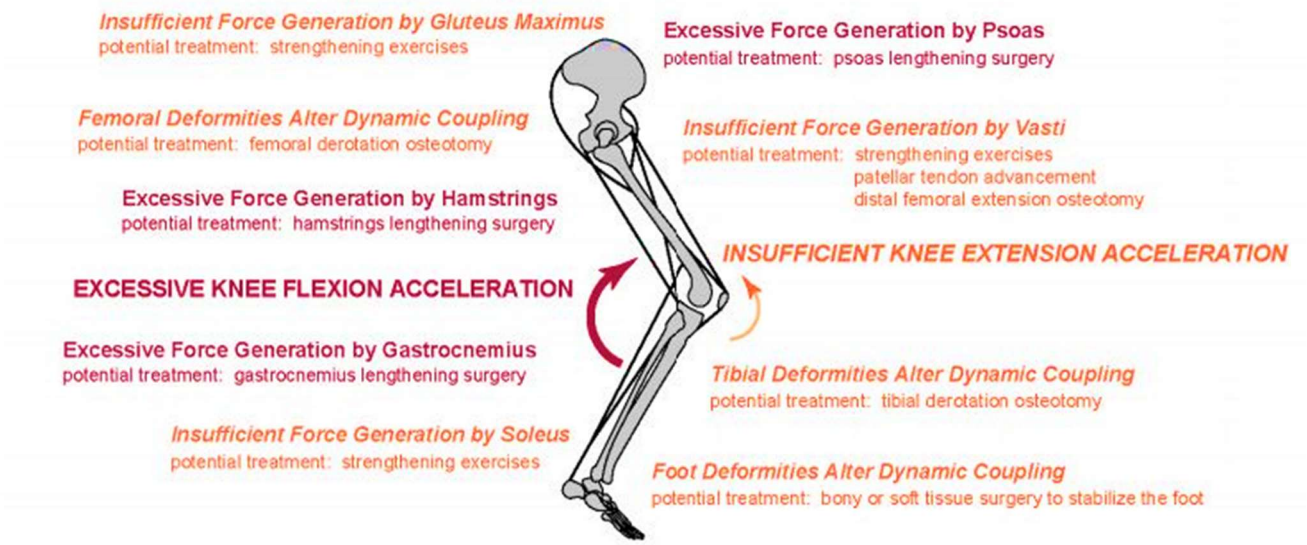

Figure 4. Several possible biomechanical causes of crouch gait. Adapted from (Hicks, 2010).

Several prior investigations have examined the potential factors that contribute to the development of this abnormal gait, and figure 4 references the most relevant. The cause for crouch gait development is normally multifactorial and it is highly dependent on each patient, so the treatment should be tailored to meet the individual's musculoskeletal deficits. To determine the appropriate treatment for each case, it is required a very careful assessment with three-dimensional gait analysis and identification of all the pathologic features which require correction. The accuracy level of the gait analyses and physical exams performed before treatment can determine its success.

The usual mild crouch can be initially managed with spasticity procedures, which normally include medication or intramuscular injections, muscle strength training, and foot orthoses. However, moderate, and severe crouch gait usually require more complicated approaches as surgical interventions, which, due to the progressive nature of CG over time, are more tolerated and effective.

Orthopaedic surgeries

A recent systematic review on the management of crouch gait (Galey et al., 2017) indicates that orthopaedic surgery remains the dominant intervention to treat crouch in cerebral palsy, with hamstring lengthening being the most common approach. The scientific evidence on this matter supports some general surgical recommendations but it does not define which procedure is the most effective in improving the gait nor predict functional changes or long-term effects.

Initially, a patient with crouch tends to walk with increased sagittal plane knee flexion due to hamstrings or psoas spasticity, which, with time, can lead to a static contracture of the muscle (Herring, 2013). In this stage, muscle lengthening is the dominant intervention and it aims mainly to decrease knee flexion. A possible side effect of this approach is the development of limited postoperative knee flexion during swing phase, commonly known as stiff-knee gait. Some studies have investigated the role of rectus femoris transfer to the medial hamstrings, in cases like these, and they reported significant improvements after the surgery (Saw et al., 2003; Moreau et al., 2005; Dreher et al., 2012). The distal femoral extension osteotomy and improving quadriceps extensor function through patellar tendon advance have been widely considered as alternatives to the hamstring lengthening (Beals, 2001; Stout et al., 2008). Although these procedures offer a promising alternative, their positive and negative effects are yet to be clarified.

Another surgical procedure often considered is related to the conversion of bi-articular to mono-articular muscles, such as the hamstring transfer to the femoral condyles. This approach not only have biomechanical benefits, but also improve neural control in cerebral palsy, as mono-articular muscles require less complex control strategies (Prilutsky, 2000).

Bone deformities are often identified in children with cerebral palsy, and the only effective approach known is orthopaedic surgery. These anatomical malfunctions include *pes planovalgus*, femoral anteversion and external tibial torsion, which may decrease the ability of multiple muscles to extend the hip and knee joints, commonly known as lever-arm dysfunction. Rotational osteotomy is the preferred surgical approach to correct femoral anteversion and external tibial torsion, even though the effects of these interventions were not yet discernible (Galey et al., 2017).

In conclusion, surgical procedures to treat crouch gait are based on correction of joint contractures, improvement of lever arm dysfunctions, and restoration of muscle length. These methods are normally addressed simultaneously, in a single multilevel surgery, that has become the standard of care in ambulatory patients with CP.

Physical Therapy

Physical therapy is another treatment which, since it is not invasive, is often preferred as the first approach to prevent worse anatomical deformities, even though its role in treating this type of gait is not completely clear. While some studies have found that strengthening exercises may lead to functional improvements in patients with crouch gait, Scianni et al. (Scianni et al., 2009) concluded that strengthening interventions had no effect on strength, walking speed, or activity level in children with CP. Furthermore, Steele et al. (Steele, Damiano, et al., 2012) suggested that selected patients might benefit from progressive resistance strengthening program, whereas in others, such as individuals with hamstrings spasticity, crouch may worsen following such therapy. Muscle strengthening is a strong component of physical therapy in cases like crouch gait, and it is focused on the main lower limb extensor muscles. It may also be utilized in a post-operative recovery program in order to optimize surgical outcomes.

Orthoses

Ankle foot orthoses (AFOs) are highly prescribed in children with cerebral palsy to provide support and stability during walking. Solid ankle–foot orthoses and ground reaction ankle–foot orthoses are often recommended to reduce excessive knee flexion for crouch gait (Ries and Schwartz, 2018). Despite their differences in terms of structure, both apply a corrective internal plantarflexion moment to the ankle to prevent ankle dorsiflexion. They are often used in combination with other treatment interventions, commonly as a post-surgery recommendation to maintain the surgical corrections. Lerner et al. (Lerner et al., 2017) investigated for the first time the impact of the use of a robotic exoskeleton for the treatment of crouch gait. They concluded that the use of the powered lower limb exoskeleton improved the subject's gait, which may indicate an initial feasibility of robotic exoskeletons for treatment of crouch gait.

Galey et al. (Galey et al., 2017) highlighted that there is very little kinematic evidence to support non-surgical interventions, and the effects of these approaches are far from being clear. Therefore, future research should focus on evaluating the effectiveness of these less invasive options to treat crouch gait.

3.2 OpenSim

OpenSim is an open-source software system that enables the creation of highly accurate models of humans to understand and simulate movement. The framework of musculoskeletal modelling was introduced by Delp and Loan (Delp and Loan, 2000) in the early 1990s with the development of SIMM, which is another widely used software system for modelling the musculoskeletal system. This was the first software that aimed to develop and evaluate anatomical models of several musculoskeletal structures. It enabled a lot of biomechanical researchers to create dynamic simulations and investigate human locomotion. However, SIMM still has relatively limited tools for computing muscle excitations that produce coordinated movement and for analysing the results of dynamic simulations. These complementary capabilities are provided by OpenSim.

Most of the models used nowadays are generic based on cadaver data, like the model created by Delp when creating SIMM. This first model was based on the study of 5 cadaver subjects (Friederich, 1990). After that, Klein Horsman et al. (Klein Horsman et al., 2007) created a model with all parameters drawn from a single cadaver subject. While this model is self-consistent, it is unclear how well this single subject represents other subjects. It was recently updated by Carbone et al.

(Carbone et al., 2014) using a new dataset consisting of computed tomography and magnetic resonance images. Though, it is still based on a single cadaver, which is not indicated to scale a wide range of subjects. In 2010, Arnold et al. (Arnold et al., 2010) created a generic lower limb model using a comprehensive set of muscle architecture data from 21 cadaver subjects. It is still being widely used.

The software that was used to create the musculoskeletal models and perform the simulations of this dissertation was OpenSim 4.1. The OpenSim team, along with researchers in the wider community, have created computer models of many different musculoskeletal structures. The following are the most used these days to analyse gait, from those included with the OpenSim distribution and supported by the OpenSim team (SimTK Confluence, n.d.):

1) Gait2392_simbody: primarily lower extremity model with two legs and a lumped torso segment. Includes 23 degrees of freedom and 92 muscle-tendon actuators. It was created to simulate and analyse human movement that is dominated by lower extremity muscles. Results may be inaccurate during motions with high degrees of knee flexion. The model can be used for both kinematics and dynamics analyses.

2) Gait2354_simbody: very similar and intended for the same use as the previous model, but only has 54 muscle-tendon actuators. The number of muscles in the model was reduced to speed simulation time for education and initial simulation prototyping.

3.3 Muscle – Tendon system

The articulation of body segments to generate motion is accomplished through the functional integration of two different complex systems, nervous and musculoskeletal. The nervous system is responsible to control the various bodily activities, by generating and transmitting the signals, to the muscles, according to the information it receives from the brain. The musculoskeletal system receives that information and generate forces through its lever system, formed by muscles, tendons, and bones, which are linked through joints and ligaments. All the components from both systems work together to provide body stability and articulated body movements. Any dysfunction in either part of these systems may compromise the intended motion.

Muscle tissue is characterized by its capacity to generate force, through contraction. It is composed of excitable cells that act in response to nervous stimulus, and it is classified into three categories according to structure and function: skeletal, cardiac, and smooth. Muscles can shorten in a way to create motion, but they can only pull, never push. This chapter will only focus on the skeletal muscles, which are responsible for voluntary movements in addition to providing support and stability to the body.

Modelling the musculoskeletal system is quite challenging due to its complexity. In a muscle model, mathematical equations are used to predict the muscle forces generated in response to muscle activation and external loading. It is now commonly used to investigate and understand the muscle contribution to the control of movement and posture. These models represent the musculoskeletal structure, muscle-tendon dynamics, and multibody dynamics transformations, that generate simulated motion.

3.3.1 Structure

Muscles are attached to bones at two or more points, depending on the muscle. If the point of connection remains immobile during the muscle's action, it represents an origin. On the other hand, if the attachment is on the bone that moves during the action, the point is called insertion. At the ends of each muscle fiber, there is a membrane that contains numerous thin collagen fibrils, *sarcolemma*, and fuses with the tendon fiber. The tendons are formed by fibrous connective tissue, organised into bundles of tendon fibers, and they are responsible to connect the muscles to bones. This connection is what enables muscle forces to generate body movements. Additionally, the bones that move in relation to each other have to be linked through a joint that permits the motion.

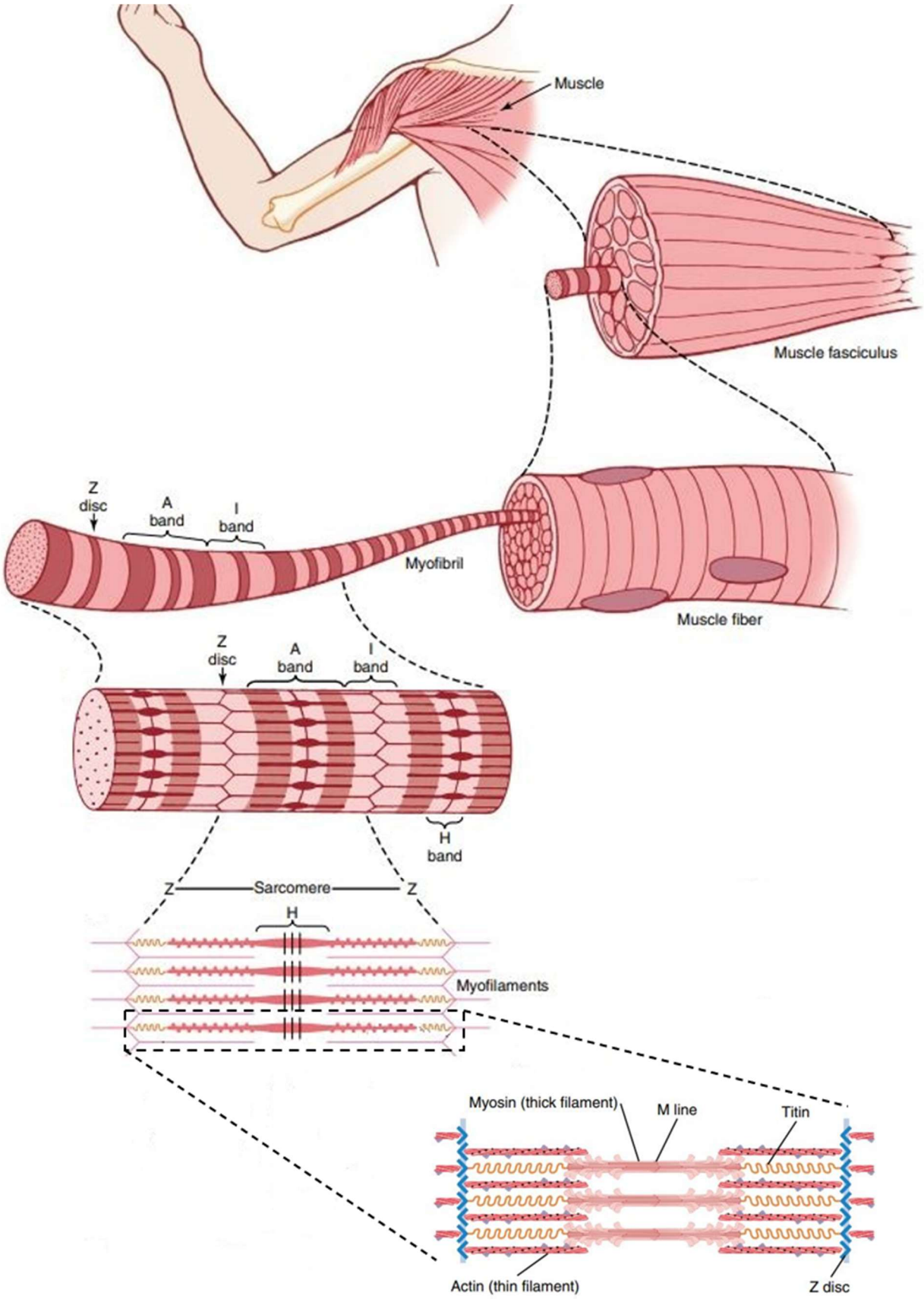

Figure 5. Organization of skeletal muscle, from gross to the molecular level. Adapted from (Hall, 2015).

Muscles can be classified according to the number of joints they can span. In this functional classification, they are divided into uniarticular and biarticular - e.g soleus is classified as a uniarticular muscle as it only actively participates in the ankle extension, while the hamstrings can participate in both knee flexion and hip extension, thus it is classified as a biarticular muscle.

The muscle tissue is characterized by four main properties related to its ability to produce force: irritability, which refers to its capacity to respond to either chemical, electrical or mechanical stimuli, contractility, the ability to contract and develop tension as a consequence of muscle shortening, extensibility, that is related with the tissue's capacity to be passively stretched beyond it normal resting length, and elasticity, which enables the muscle to return to its original length following stretching or contraction.

The skeletal muscle is a highly organized tissue that contains several bundles of muscle fibers, which are called muscle fascicles. Normally, each fiber extends the entire length of the muscles and it is innervated by only one nerve ending, near to the middle of the fiber. Then, each muscle fiber contains several hundred to several thousand *myofibrils*, that run parallel to each other and represent the muscle cells. These are made up of adjacent *myosin* and *actin* filaments (illustrated in figure 5), which are large polymerized protein molecules that are responsible for the actual muscle contraction. The *actin* (thin filaments) have Z disks attached to its end. These filamentous proteins connect *myofibrils* to one another all the way across the muscle fiber. Finally, the portion of the *myofibril* that lies between two successive Z disks, is called a *sarcomere*. The *myosin* filaments (thick filaments) are anchored to the centre of the *sarcomere*, called the M line. However, they are also connected to filamentous molecules of a protein called *titin*. These molecules act as a framework that holds the thick and thin filaments in place ensuring that the contractile mechanism works. The muscle contraction depends on the relative position of the *actin* and *myosin* filaments. They slide along each other and change the length of the *sarcomere* enabling contraction.

A classical anatomical observation is that muscles can vary in architecture and that this architecture reflects their function (Wilson & Lichtwark, 2011). There are two types of architectures for skeletal muscles (figure 6): parallel and pennate. In the first type, the fibres run along the muscle length and in the direction of force transmission. The angle between the orientation of the muscle fibres and the axis along which the force is achieved (same axis as tendon orientation) is called pennation angle, α. The second type is characterized by a pennation angle different from zero. The pennate muscles, due to its fibres' arrangement, are capable of producing greater forces than parallel muscles, which are more responsible for fast movements.

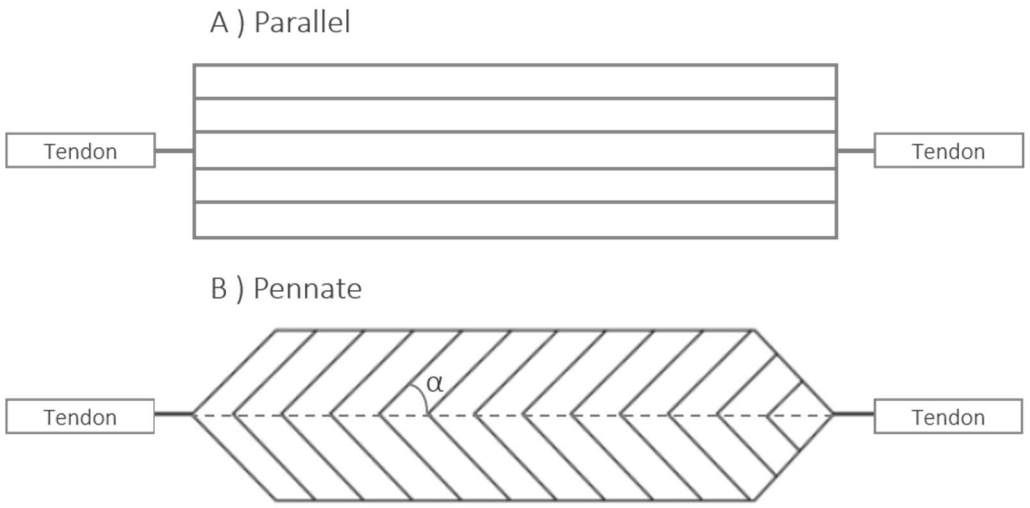

Figure 6. Representation of two muscle architectures. The pennation angle is identified by α.

The musculoskeletal system depends on the nervous system to operate. Every muscle needs to receive a nerve signal to begin the contraction mechanism. The motor neurons are the nerve cells responsible for controlling all of our muscle movements. They are inserted in the spinal cord and they transmit signals from there to the muscle fibres. This lot of skeletal muscle fibres and the respective motor neuron constitute a motor unit. A motor neuron can innervate more than one muscle fibre, but a muscle fibre can only be connected to one motor neuron. Small neurons can only innervate relatively few muscle fibers, though they form motor units that generate small forces, whereas large motor neurons innervate more powerful motor units (Purves et al., 2001). The simultaneous effort of several motor units results in the voluntary contraction of the respective skeletal muscle.

The interface between the nervous system and the musculoskeletal system is called the neuromuscular junction. Each muscle fibre has one, and it is where the neuron axon terminals connect with the muscle. The axons do not interact physically with the muscle fibres thus they are separated by a thin space called the synaptic cleft. This is where the signal transmission occurs, leading to muscle contraction.

3.3.2 Physiology

As it was mentioned before, the skeletal muscle is only capable of producing voluntary contractions, though it needs a nervous stimulus to contract. This process begins when the central nervous system creates electrical impulses that aim to trigger skeletal muscles. This electrical signal sets off an action potential that travels along the motor nerve to its endings on the neuromuscular junction. In turn, the axon terminals have a lot of synaptic vesicles containing a neurotransmitter substance called *acetylcholine*. By the time the signal reaches the end of the neuron, the axon releases this neurotransmitter into the synaptic cleft. The *acetylcholine* connects to its protein receptors and stimulates the opening of the *acetylcholine-gated* channels in the muscle membrane, which allow large quantities of sodium ions to diffuse to the interior of the muscle fibre membrane. This causes a local depolarization that in turn leads to the opening of voltage-gated sodium channels, which initiates an action potential at the membrane (Hall, 2015). Then, an enzyme in the synaptic cleft called *acetylcholinesterase* breaks the *acetylcholine* to force the closing of the ion channels, preventing further muscle contraction until another nerve impulse arrives. However, the action potential will continue to travel along the muscle fibre and depolarizes it. This causes the *sarcoplasmic reticulum* to release large quantities of calcium ions that have been stored within the reticulum. The calcium stimulates the actin and myosin interaction which starts the contractile process. All this process occurs in a fraction of a second.

The *myosin* molecules are made of polypeptide chains that wrap spirally around each other forming a double helix. At the end of each molecule, there are two globular polypeptide structures called *myosin* heads, that are arranged in such a way to point outwards. The *actin* filament contains *tropomyosin*, which is a protein that wraps spirally around the filaments. When the muscle is relaxed, these spiralling strands lie on top of the active sites of the *actin*, blocking the interaction between the *actin* and *myosin* filaments needed to cause contraction.

When the calcium ions are present in the sarcoplasm, which is the cytoplasm of the muscle cell, the *tropomyosin* changes its configuration, leaving the *myosin* binding sites exposed. Then, the *myosin* heads will interact with the binding sites on the *actin* subunits, forming what is called the cross-bridges. When this connection is complete, the *myosin* heads use ATP to change conformation and repeatedly pull on the thin filaments towards the centre of the *sarcomere*, thus pulling the Z discs towards the M line, so the muscle will shorten to cause contraction. As the calcium levels deplete, *tropomyosin* returns to its original position and it blocks the thin binding sites once more, while the muscle fibre relaxes.

3.3.3 Modelling

Computational human modelling requires a realistic reproduction of the complex anatomical structures and the relevant biological and physiological functions, by using mathematical formulations to achieve reliable outputs from the muscle model. The complexity of the model should be adequate to what is to be studied, so the choice of the model must consider the purpose of the research.

Musculoskeletal modelling is a current promising engineering solution to estimate some physical quantities, impossible to measure using non-invasive methods, which can be very useful for clinical use. Since the first classic model of Hill developed in the late thirties (Hill, 1938, 1949), a broad range of other models have been put forward for simulating human movement. From a purely structural viewpoint, the types of models fall into three broad categories, according to Winters and Stark (Winters and Stark, 1987): the simple second-order models, the Hill-based lumped-parameter model, and the Huxley-based distributed-parameter models. The simple second-order models treat the muscle joint system as a "black box" in which the contents can be approximated by a second-order linear. These models still have a lot of limitations when used to study human movement. The Hill-based lumped-parameter model is the most widely used, due to its capacity to represent the important features of the muscle mechanics. The Huxley-based distributed-parameter models attempt to correctly explain the mechanism of contraction with great accuracy, but at a high computational effort. These models are based on Huxley's model (Huxley and Simmons, 1971), which entails a direct relationship between the metabolic and mechanical behaviour, by modeling the dynamics of the cross-bridges cycling.

The underlying mechanisms behind the analysis employed in this dissertation are based on the dynamic system developed by Thelen (Thelen, 2003), which in turn uses the standard Hill muscle model as a reference. In this classic model, the dynamic behaviour of the contractile element can be expressed in terms of two nonlinear differential equations, used to describe activation and muscle-tendon contraction dynamics (figure 7).

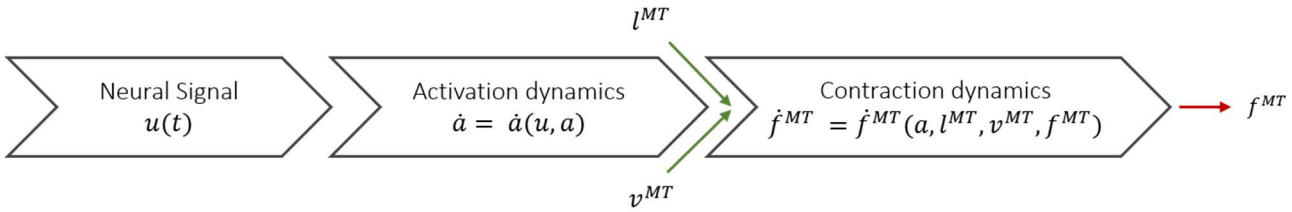

Figure 7. Schematic representation of muscle dynamics, with inputs and outputs. Where $u(t)$ represents the muscle excitation signal, a is the muscular activation, l^{MT} and v^{MT} refers to the length and shortening velocity of the musculoskeletal unit, and f^{MT} represents the force produced by the musculoskeletal unit.

3.3.3.1 Activation Dynamics

The muscle contraction as a result of the neural excitation is not an instantaneous process, nor is it the end of the neural excitation and following muscle relaxation. These time lags have to be considered when simulating muscle mechanics.

The activation dynamics corresponds to the transformation of the neural excitation signal into the activation of the contractile unit. This first stage is modelled as a unidirectional process with first-order dynamics, where the muscle excitation signal, $u(t)$, is a dimensionless quantity between 0 and 1, used as the input, and the muscular activation, a, is the output. The activation level is defined by a unit-less value that varies continuously from 0 to 1, as the muscle excitation. The relation between the neural excitation and muscle activation used in this work is described by the following nonlinear first-order differential equation (Thelen, 2003):

$$\frac{da}{dt} = \frac{u - a}{\tau_a(a,u)} \tag{1}$$

$$\tau_a(a,u) = \begin{cases} \tau_{act}\,(0{,}5 + 1{,}5a); & u > a \\ \tau_{deact}\,/(0{,}5 + 1{,}5a); & u \leq a \end{cases} \tag{2}$$

where $\tau_a(a,u)$ represents a time constant that varies with the activation level (Eq. 2), τ_{act} is the activation time constant, and the τ_{deact} is the deactivation time constant. This relation predicts that as the muscle becomes more activated, the dynamic process slows due to less efficient calcium release and diffusion (Winters, 1995). In contrast, deactivation slows with the decrease of the muscle activation level, because of the lack of calcium availability for uptake by the sarcoplasmic reticulum.

3.3.3.2 Contraction Dynamics

This step takes place once neural excitation is transformed into muscle activation, and it represents the relation between that activation and the force generated by the muscle-tendon actuator. Contraction dynamics have to account for the interaction of the force-length-velocity properties of the muscle, and the elastic properties of the tendon (Thelen, 2003). As it was previously stated, the Hill muscle model is the one that represents the muscle-tendon unit on which this work is based, and so, it also incorporates the muscle and tendon's properties.

The Hill-type muscle model is a purely mechanical representation of the muscle–tendon dynamic, which consists of three major components: the series element (SE), the parallel element (PE), and the contractile element (CE) (Lee et al., 2011). The SE represents the elasticity of connective elements within the muscle-tendon unit, such as the tendon, aponeurosis, and other structures. The PE accounts for the passive elasticity of the muscle in resisting against stretching, due to external forces that are being applied to the inactive muscle. In short, it represents the elasticity of the surrounding tissues, such as fascia and epimysium. Both these two components can be modelled as non-linear springs, due to the nonlinearity of their elastic behaviour. The contractile element is the main component, and it represents the contractile properties of the muscle.

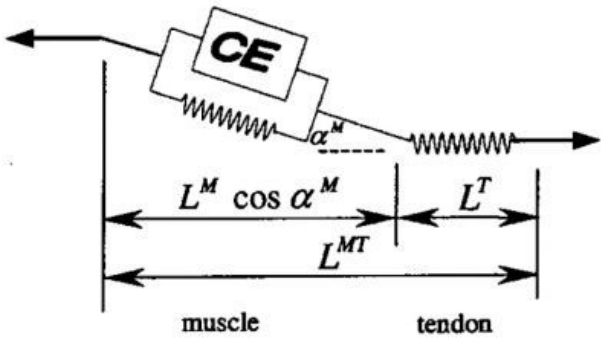

Figure 8. Hill muscle model to represent contraction dynamics. Adapted from (Thelen, 2003).

Muscle fibers are not necessarily aligned with the series elastic element, forming an angle between each other called the pennation angle, α^M. This misalignment influences the force-generation capacity and the force-length-velocity relationship of the muscle, by permitting a large number of muscle's fibres per cross-sectional area. According to Zajac's model (Zajac, 1989), the relationship between muscle and muscle-tendon lengths is given by the following equation:

$$l^{MT} = l^M \cos(\alpha^M) + l^T \qquad (3)$$

where l^{MT} is the length of the musculoskeletal unit, while l^M and l^T represent the muscle length and tendon length, respectively.

Thelen's model is a highly regarded model to describe muscle force production and so, it has been implemented widely in used and validated open source softwares, such as OpenSim. Nonetheless, it has some limitations that should be accounted for when selecting the appropriate model to use. For example, this model does not consider the muscle's physiological mechanisms, being the contractile element's functioning based on the force-length and force-velocity relationships of the muscle.

Force-length property

This functional property is associated with muscle capacity to generate force throughout a range of lengths. Without activation, the muscle only develops passive restoration force against increased stretching. When activated, the muscle produces active forces which results in its contraction. The curve that represents this property results from the summation of both types of force, resulting in the total muscle force, plotted against the length of the muscle (Lee et al., 2011).

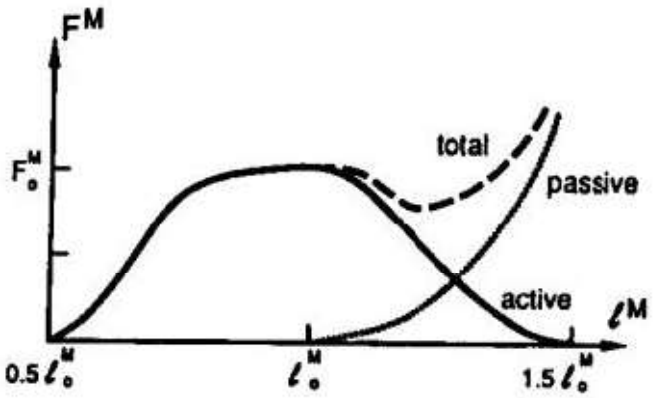

Figure 9. Force-length relationship of a muscle. Adapted from (Zajac, 1989).

By analysing the figure 9, it can be perceived that at the optimal fibre length, l_0^M, the contractile element attains its maximum isometric strength. This point is reached when the muscle has the maximum number of cross-bridges attached in each *sarcomere*. Below the optimal length, the active muscle force is entirely responsible for the generation of force, and it decreases with length reduction. Furthermore, in the case of stretching beyond the optimal fibre length, the active force weakens, and the passive force is generated as a resistance against elongation, which increase with the lengthening.

Force-velocity property

The force-velocity property represents the relationship between the velocity of muscle contraction and the amount of force it produces. In order to quantify this relationship, a fully activated muscle is subjected to constant tension. From figure 10, it is possible to state that the generation of muscle force and shortening speed are inversely related.

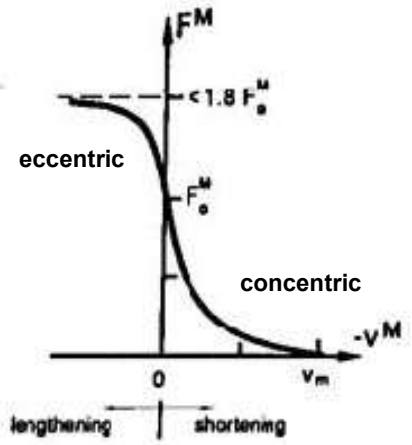

Figure 10. Force-velocity relationship for a fully activated muscle. Adapted from (Zajac, 1989).

In the figure above, F_0^M represents the force experienced at the optimal muscle length. When considering muscle lengths below the optimal length, the shortening velocity increases with the decrease of generated muscle force. The maximum velocity of shortening is experienced when there is no load on the muscle, although this condition is very difficult to achieve. On the other hand, as the external loads increase, the velocity of shortening decreases. The maximum isometric force is reached at the lowest shortening speed. As illustrated in figure 10, force values higher than F_0^M are associated with eccentric contraction, whereas positive shortening speed values are related to concentric contractions.

3.3.3.3 Tendon modelling and properties

Tendons are composed of a portion internal to the muscle and another external to the muscle, although both parts are assumed to have the same material properties and to experience the same strain throughout the tendon (Zajac, 1989). Additionally, tendon strain is defined as the amount of tendon stretch relative to its resting length, which is also called slack length and it is considered to be the length on elongation at which tendon begins to develop force. Despite the complexity of

tendon properties, they are assumed to be purely elastic in most coordination studies, as they are much simpler to model.

The most relevant parameters that should be considered in tendon modelling, according to Zajac (Zajac, 1989), are the peak isometric force, F_0^M, and the tendon slack length, l_S^T, which relationship defines the generic force-strain curve. These two parameters are specific to each muscle-tendon actuator. Tendon strain, ε^T, is directly related to the tendon length through the following equation:

$$\varepsilon^T = \frac{l^T - l_S^T}{l_S^T} \qquad (4)$$

where l^T refers to the tendon length. By considering the generic curve represented in figure 11, it is possible to obtain l^T using this equation.

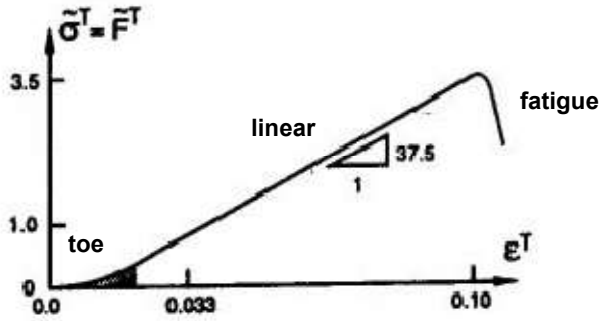

Figure 11. Generic tendon force-strain curve. Adapted from (Zajac, 1989).

The force-strain relationship is represented in three distinct regions. The toe region presents an exponential potential function, which represents the stretching of the tendon fibrils, out of their original setting, in response to the mechanical loading. The region that follows is defined by a linear function that describes the elastic behaviour of the tendon. Lastly, the fatigue stage is related to the stretching beyond the tendon limit and so, the tendon starts to undergo plastic deformations (Pandy and Barr, 2004). This final stage is not included in Thelen's model (Thelen, 2003), because the tendons are considered to be compliant and in equilibrium with the muscles, so the tendon stays in the linear region.

3.3.3.4 Muscle-tendon Actuator

Models, such as the one presented by Darryl G. Thelen (Thelen, 2003), integrate activation and contraction dynamics, which are described by all the relationships mentioned above, to provide the most realistic representation of a muscle-tendon structure possible. This chapter will describe the musculoskeletal actuator's parameters adopted in the generic model used in this dissertation.

Both tendons and muscles have their own properties and so can be studied individually, although it is their integrated function that defines the properties of the muscle-tendon actuator. Not only muscle and tendon work together as an actuator, but they represent the interface that converts muscle activation into muscle force. In the muscle-tendon unit, the tendon has no interaction with the muscle activation process, so it interacts with only the contractile process of the muscle tissue (Zajac, 1989). An individual muscle-tendon complex is characterized by four parameters: peak isometric force, F_0^M, optimal muscle fiber length, l_0^M, pennation angle at optimum fiber length, α_0, and tendon slack length, l_S^T. When a generic model is scaled by these four parameters, the force-length relation of each muscle-tendon actuator can be computed (Delp, 1990).

The first three parameters can be estimated using the following equations:

$$F_0^M = \sigma_0^M \times PCSA \qquad (5)$$

$$l_0^M = (l_0^S / l^S) \times l^M \qquad (6)$$

$$\alpha = \sin^{-1}\left(\frac{l_0^M}{l^M}\sin\alpha_0\right),\ 0 < \frac{l_0^M}{l^M}\sin\alpha_0 < 1 \qquad (7)$$

where σ_0^M represents the muscle's specific tension, $PCSA$ refers to its physiological cross-sectional area, l^S indicates the sarcomere length, whereas l_0^S represents the optimal sarcomere length, and l^M refers to the muscle's fibre length.

Most of the values needed for these estimations come from measurements on cadavers. The PCSA values were taken from both the works of Wickiewicz (Wickiewicz et al., 1983) and Friederich (Friederich, 1990), due to differences in their anatomical specimens. The values considered for the optimal fiber lengths were the same as reported from Wickiewicz (Wickiewicz et al., 1983), but scaled by a factor of 2,8 / 2,2. The maximum isometric forces were depicted by Anderson and Pandy (Anderson and Pandy, 1999). The estimation of optimal fibre length values (Eq.(6)) considers optimal *sarcomere* lengths given by experiment results (Friederich, 1990; Ward et al. 2009). Regarding the pennation angle, its estimation (Eq.(7)) is based on the assumption that this

parameter changes with the muscle's fibre length and that the muscle's volume remains constant (Lloyd and Besier, 2003). Therefore, the values for the pennation angle are taken, once again, from the works of Wickiewicz (Wickiewicz et al., 1983) and Friederich (Friederich, 1990).

Finally, the values that represent the tendon slack length are difficult to measure directly, so, this parameter's data used in this model is mostly based on results from numerical methods (Delp et al., 1990). Tendon slack length includes both the length of the free tendon and the length of the tendon internal to the muscle belly. In addition, this parameter's values were specified according to two assumptions: passive muscle force is only generated when the muscle fibres are longer than the optimal muscle fiber length, and tendon slack length values were adjusted so that the joint angles, at which maximum active joint moments occur, could best match the measurements of joint moments obtained *in vivo* (Delp et al., 1990).

Apart from these four parameters that characterize each muscle-tendon unit, there are others that define the muscle-tendon actuators. However, these parameters are set constants that are included in all actuators, and they are used to define the force-length and force-velocity relationships of the muscles. These constants are presented in the table below.

Table 2. Muscle-tendon model constant parameters.

Parameter	Value
$\boldsymbol{\varepsilon_0^M}$ – Passive muscle strain during maximum isometric force	0,6
$\boldsymbol{\varepsilon_0^T}$ – Tendon strain at maximum isometric force	0,033
$\boldsymbol{\varepsilon_{toe}^T}$ – Tendon strain above which tendon force behaves linearly with tendon strain	0,609 ε_0^T
$\boldsymbol{k_{toe}}$ – Exponential shape factor for the force – strain relation of the tendon	3
$\boldsymbol{k_{lin}}$ – Linear shape factor for the force – strain property of the tendon	1,712 / ε_0^T
$\boldsymbol{k^{PE}}$ – Exponential shape factor in the passive force-length property of the muscle	4
$\boldsymbol{\overline{F}_{toe}^T}$ – Normalized tendon force at tendon strain ε_{toe}^T	0,333
$\boldsymbol{\overline{F}_{len}^M}$ – Maximum normalized tendon force	1,8
$\boldsymbol{V_{max}^M}$ – Maximum contraction velocity in the fibers, in optimal fiber lengths/second	10
$\boldsymbol{A_f}$ – Shape factor related to the force-velocity relation of the muscle	0,3
$\boldsymbol{\Upsilon}$ – Shape factor for the active force-length Gaussian curve of the muscle	0,5

4. Methodology

4.1 Subjects

Three children with spastic diplegic CP were selected for this study. All subjects walked in crouch gait, with excess knee and hip flexion, and with at least 5 degrees of ankle dorsiflexion during stance. According to Steele's crouch severity classification (Steele, DeMers, et al., 2012), these subjects were classified as presenting a severe crouch pattern, because all had a minimum knee flexion angle greater than 50º. Regarding the typically developing children group, six subjects were chosen as most representative as possible of the age and structure of the CP children selected. These subjects performed both simulated crouch gait and their normal walking pattern. They were clinically analysed, and it was concluded that they did not present any neurological dysfunction.

Table 3. Subject characteristics.

	N	Age (years)	Height (cm)	Weight (kg)
TD children	6	8 ± 1	127 ± 5	25 ± 3
CP children	3	12 ± 3	139 ± 18	35 ± 9

4.2 Data Acquisition

Firstly, each child was submitted to a clinical exam done by a health professional. A sequence of measures was performed on each subject that aimed to evaluate bone and joint deformities, muscle length, selective motor control, and spasticity. The second part consisted of the gait analysis. The healthy children performed the simulated crouch wearing AFOs. It was intended to assess the acute modifications that occur at the lower limb joint kinematics in children without pathology, only by having that constraint at the ankle joint. Motion capture collected with Qualisys Track Manager software (Qualisys Inc., Gothenburg, Sweden), version 2.9, operating on an optoelectronic system of 14 Qualisys cameras (Qualisys Oqus 300, Qualisys AB, Gothenburg, Sweden) at a frequency rate of 100 Hz. Ground reaction forces were collected with three Bertec and one Kistler force plates. Each subject had 25 reflective markers and 4 marker clusters placed on specific anatomic places, according to CAST (calibrated anatomical systems technique) protocol and CODA pelvis, used to reconstruct 8 body segments. Plantar pressure data was recorded with an EMED pedography platform and in the AFOs condition it was used a pedar insole system. The gait analysis started with

the recording of a static trial barefoot in the standing position. Afterward, the child was instructed to walk along a 10m corridor, at a self-selected speed. The dynamic trials ended when the child successfully achieved a minimum of 10 good kinetic walking cycles for each side, considering the natural variability in kinematic and kinetic gait parameters.

4.3 Visual3D Implementation

The data processing and inverse kinematics was performed using the Visual3D software. It provides tools for signal processing and filtering, and inverse kinematics. The variables were filtered using a 4^{th} order Butterworth filter at 8Hz. Visual3D models are based on a linked set of rigid segments, which are treated as independent parts of the body and have their local coordinate systems. The motion that defines the interaction between the segments is given by tracking a set of markers, that is linked to the real segments. Each joint was modelled with 6 degrees of freedom, enabling the model to simulate the motion as accurately as possible. In this software, the inverse kinematics problem is solved as a global optimization problem, which means that the pose of the model is computed to best match the data from the motion capture in terms of global criterion. This optimization approach is based on the method developed by Lu and O'Connor (Lu and O'Connor, 1999). On the other hand, the default segment masses defined in the software are determined according to Dempster (Dempster, 1955), whereas the inertial properties of each model segment are computed based on Hanavan (Hanavan, 1964).

4.4 OpenSim Implementation

The musculoskeletal modeling was mostly developed using OpenSim (Delp et al., 2007; Ajay et al., 2011), which is an open-source software for musculoskeletal modelling. The output files used from Visual3D were only the inverse kinematics and ground reaction force data. In this software, a musculoskeletal model consists of rigid body segments connected by joints and articulated by actuators (representing muscles). Muscles span these joints and generate forces and motion. The steps that describe the modeling done in OpenSim are represented in the figure below.

Figure 12. Pipeline of the work in OpenSim. RRA refers to the Residual Reduction Algorithm, CMC to the Computed Muscle Control tool and IAA to the induced accelerations analysis, available in OpenSim 4.1.

4.4.1 Generic Musculoskeletal Model

The musculoskeletal model used in this work is the Gait2392 model, based on the models created by Darryl Thelen, and Ajay Seth, Frank C. Anderson, and Scott L. Delp. This is a 23-degree-of-freedom computer model of the human musculoskeletal system in three-dimensions. It features 92 muscle-tendon actuators to represent 76 muscles in the lower extremities and torso. This model represents a subject that is about 1.8 m tall and has a mass of 75.16 kg.

4.4.1.1 Bones and Joint Geometry

Every bone of the lower limbs and the torso are represented. The surface data for the pelvis and thigh are obtained by a three-dimensional digitizer, which determines the coordinates of the vertices. For the shank and foot, it was acquired from the work of Stredney (Stredney, 1982). Each body segment has a reference frame associated.

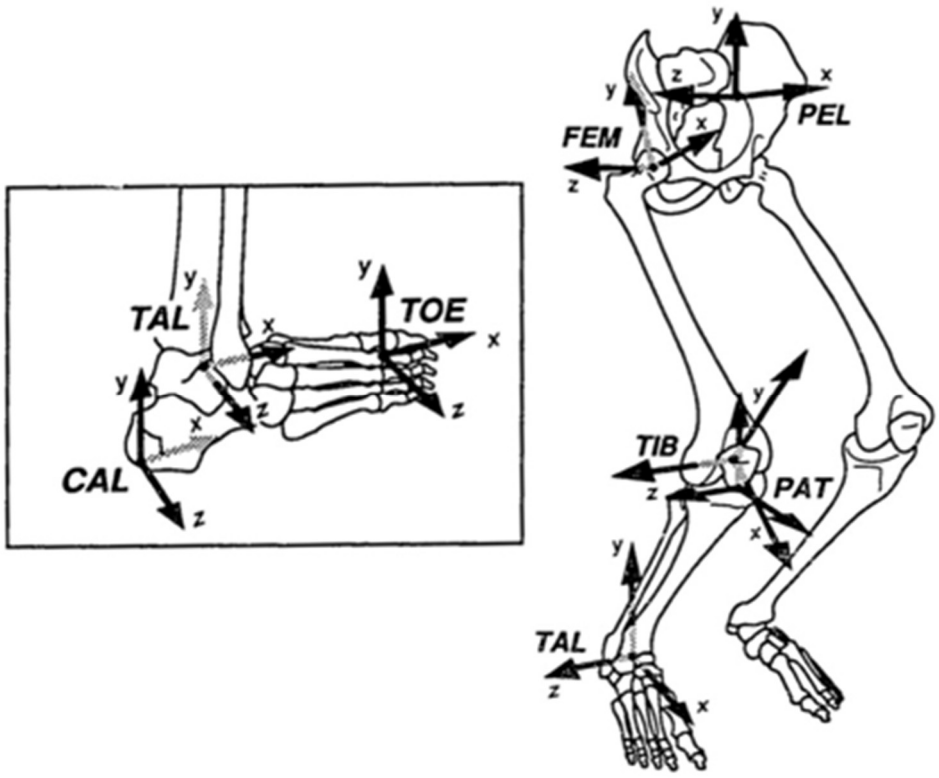

Figure 13. Location of the body-segmental reference frames. Adapted from (Delp, 1990).

The exact location description of each frame is more accurately described below:

- Pelvis: The pelvic reference frame is fixed at the midpoint of the line connecting the two anterior superior iliac spines.
- Femur: The femoral frame is fixed at the centre of the femoral head.
- Tibia: The tibial frame is located at the midpoint of the line between the medial and lateral femoral epicondyles.
- Patella: The patellar frame is located at the most distal point of the patella.
- Talus: The talar frame is located at the midpoint of the line between the apices of the medical and lateral malleoli.
- Calcaneus: The calcaneal frame is located at the most interior, lateral point on the posterior surface of the calcaneus.
- Toe: The toe frame is located at the base of the second metatarsal.

Because of its three-bone, multi-ligament structure, the knee joint presents a challenge for the determination of the moment arm of the quadriceps muscles. Yamaguchi (Yamaguchi et al., 1989) developed a simplified knee model with a single degree of freedom for the kinematics of both the tibiofemoral joint and the patellofemoral joint in the sagittal plane. This was adopted in the Gait2392 model, where the femoral condyles are represented as ellipses, and the tibial plateau is represented as a line segment. The tibiofemoral contact point depends on the knee angle and is specified according to data reported by Nisell (Nisell et al., 1986). In order to avoid kinematic constraints, the patella was removed from the initial Delp model by Ajay Seth.

The locations and orientations for each foot joint follow the descriptions provided by Inman (Inman, 1976). The ankle, subtalar, and metatarsophalangeal joints were modelled as frictionless revolute joints, which restricts five degrees of freedom, allowing only rotation about one axis. Furthermore, it was noticed an exhibited unrealistic motion at the metatarsophalangeal joint. In order to fix it, the joint was rotated by 8° on a right-handed vertical axis rotation to minimize joint disarticulation, as stated by Delp (Delp, 1990).

4.4.1.2 Muscle Geometry

The muscle-tendon actuators are represented by a series of line segments with origin and insertion landmarks defined on the bone surface models. These two landmarks are sufficient for

describing the muscle path for most of the muscles, but others wrap around other muscles or bones and so need more points to have a more accurate representation (Delp, 1990). Despite the effort to define each muscle with precision, there are muscles in the lower limb that pass through the bones or deeper muscles with extreme hip flexion and extension, and those can generate unrealistic moment arms.

4.4.1.3 Inertial Properties

The inertial parameters for the body segments were adapted from the model developed by Anderson and Pandy (Anderson and Pandy, 1999). Both mass and inertial properties of the segments, apart from the hindfeet and toes, are based on data attained from five subjects (age 26 ± 3 years, height 177 ± 3 cm, and weight 70.1 ± 7.8 kg). However, the lengths used in the model are taken from the Delp model (Delp, 1990). Regarding the hindfeet and toes, the parameters are found by setting the volumes of the segments as a set of connected vertices.

All the inertial properties for the body segments are summarized in the table below. These values were scaled by a factor of 1.05626 from those reported by Anderson and Pandy (Anderson and Pandy, 1999).

Table 4. Inertial parameters for the body segments included in the model.

		Moments of inertia			Centre of mass		
Body Segment	Mass (Kg)	xx	yy	zz	x	y	z
Torso	34,2366	1,4745	0,7555	1,4314	-0,03	0,32	0
Pelvis	11,7770	0,1028	0,0871	0,0579	-0,0707	0	0
Right femur	9,3014	0,1339	0,0351	0,1412	0	-0,17	0
Right tibia	3,7075	0,0504	0,0051	0,0511	0	-0,1867	0
Right talus	0,1000	0,0010	0,0010	0,0010	0	0	0
Right calcaneus	1,2500	0,0014	0,0039	0,0041	0,1	0,03	0
Right toe	0,2166	0,0001	0,0002	0,0010	0,0346	0,006	-0,0175
Left femur	9,3014	0,1339	0,0351	0,1412	0	-0,17	0
Left tibia	3,7075	0,0504	0,0051	0,0511	0	-0,1867	0
Left talus	0,1000	0,0010	0,0010	0,0010	0	0	0
Left calcaneus	1,2500	0,0014	0,0039	0,0041	0,1	0,03	0
Left toe	0,2166	0,0001	0,0002	0,0010	0,0346	0,006	0,0175

4.4.2 Scaling

The first part of musculoskeletal modeling should begin with scaling the generic model, which is the starting point. The OpenSim (Delp et al., 2007; Ajay et al., 2011) provides a scale tool that enables the user to alter the anthropometry of a model, so that it is possible to match to a specific subject as closely as possible.

In this work, it was only used manual scaling, so, the size and inertial properties of all segments were adjusted according to the scale factors obtained from the pre-processing done in Visual3D. Logically, all the insertion points of the actuators are also adjusted, as well as joint frame locations. This tool also allows scaling the mass of each segment, using the scale factors and the input target mass of the subject. This approach ensures that mass distribution is preserved and that the total scaled model mass corresponds to the input target mass.

The muscle and ligament scaling includes the adjustment of length-dependent parameters as optimal fibre length and tendon slack length, which is based on scale factors defined as the ratio of the fibre or tendon length before and after scaling. These values depend on the actuators' parameters, so this scaling step ensures that they stay with the same respective proportion of the actuators' lengths.

Regarding the muscle function, these models usually describe the force-generating properties of muscles using the five-parameter 'Hill-type' muscle-tendon unit (Zajac, 1989). When studying muscle function, it is important to consider strength, which is one of the five parameters, and it is defined as peak isometric muscle force. This value represents the contractile force produced by a fully activated muscle when it is held at its maximum fibre length. In generic models as Gait2392, this parameter is obtained from cadavers of adult donors, and it is not automatically scaled (Rajagopal et al., 2016). So, peak isometric force should be determined on a subject-specific basis, particularly in studies involving children.

Muscle strength for individual muscles cannot be determined in vivo using dynamometers measurements (Correa and Pandy, 2011). Also, maximum voluntary contractions are difficult to elicit even from healthy subjects, let alone for those affected by neurologic conditions such as cerebral palsy. It is possible to estimate the peak isometric force of each muscle on basis of muscle size, and all measurements needed can be taken using magnetic resonance imaging. This is commonly done by multiplying the muscle's physiological cross-sectional area by the muscle-specific tension (σ) (Zajac, 1989; Delp et al., 1990; Garner and Pandy, 2003). Nowadays, there is still a significant cost associated with obtaining magnetic resonance scans, which makes this

approach difficult to apply. Moreover, for some muscles in the lower limb, parameters like pennation angles and fibre lengths are still very challenging to determine, so the values measured can be highly subjective.

To overcome these limitations, Correa and Pandy (Correa and Pandy, 2011) developed an alternative scaling procedure which includes the mass of the subject and individual muscle-tendon lengths (l_{MT}) of both generic and scaled model (Eq. (8)). Whereas, van der Krogt et al. (van der Krogt et al., 2016) scaled maximum isometric muscle forces in children, using just the subject's body mass (Eq. (9)).

$$F_{max}^{scaled} = F_{max}^{generic} \times \frac{M^{scaled}}{M^{generic}} \times \frac{l_{MT}^{generic}}{l_{MT}^{scaled}} \quad (8)$$

$$F_{max}^{scaled} = F_{max}^{generic} \times \left(\frac{M^{scaled}}{M^{generic}}\right)^{\frac{2}{3}} \quad (9)$$

Kainz et al. (Kainz et al., 2018) aimed to evaluate if these methods could be used to scale maximum isometric muscle forces (MIMF) in musculoskeletal models of children with CP by comparing them with the hand-held-dynamometer scaling method. They concluded that these approaches didn't differ much between them and both formulas could be used to scale MIMF as they led to successful simulations.

In this work, Correa and Pandy's scaling approach was employed (Eq. (8)) because they consider more musculoskeletal parameters of the subject which may represent a model more adjusted to the child. Therefore, the peak isometric force of all the muscles of all subjects were scaled individually using this method.

Before going to the next stage, the subtalar and metatarsophalangeal joints were locked in a neutral position because it is a normal procedure in cases where the foot segments with a small mass, compared to the other segments, were too sensitive against errors in the muscle force estimation (Trinler, 2016).

4.4.3 Inverse Dynamics

The main goal of the inverse dynamics (ID) tool provided by the OpenSim is to determine the generalized forces at each joint responsible for a given movement. The output joint angles from the inverse kinematics done in Visual3D with ground reaction force data are used by the inverse dynamics analysis to compute joint moments, as it is represented in the scheme below.

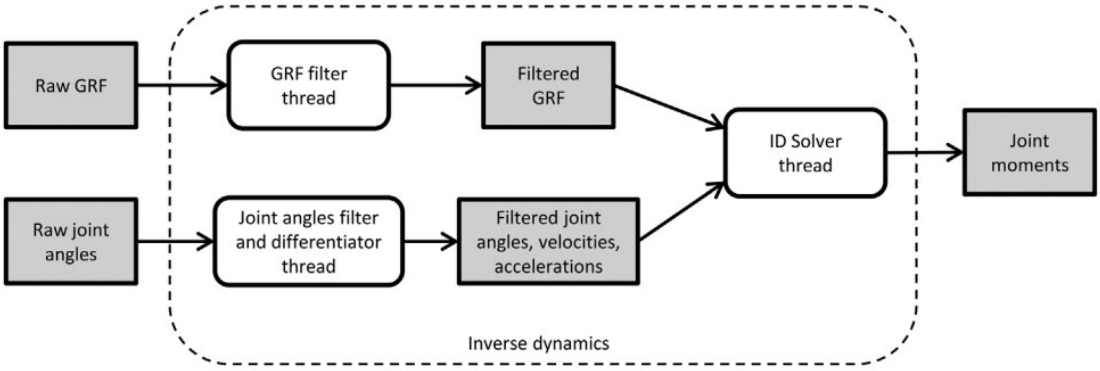

Figure 14. Real-time implementation of inverse kinematics

The inverse dynamics analysis implemented in the Inverse Dynamics Solver thread solves the dynamic equation of motion:

$$M(q)\ddot{q} + C(q,\dot{q}) + G(q) = \tau \qquad (10)$$

where q, $\dot{q}$, $\ddot{q}$ are the position, velocity, and acceleration of the generalised coordinates. M, C, G are the mass, centrifugal and Coriolis, and gravitational forces matrices, respectively, whereas τ is the vector of unknown joint moments (Pizzolato et al., 2017). All the terms from the left hand-side of the equation are completely known, so the tool uses this known motion to calculate the unknown generalized forces.

4.4.4 Residual Reduction Algorithm

To analyse movement using musculoskeletal models, it is needed the respective in vivo kinematic data. This collected information usually carries dynamic inconsistencies between experimental kinematics and ground reaction forces, normally related to inaccuracies in mass distribution and experimental errors. As the model follows physical laws to simulate the intended movement, it creates non-physical compensatory forces that account for these inconsistencies, called residuals. The OpenSim provides a tool that can be used to minimize these effects of modeling and marker data processing errors. The ground reaction forces and accelerations estimated from measured marker kinematics for a subject do not satisfy Newton's Second Law, so it needs to be reformulated:

$$F_{exp} + F_{residual} = \sum_{i=1}^{segments} m_i(a_i - g) \qquad (11)$$

where m_i denotes the mass of each body segment, a_i its acceleration and g the acceleration of gravity. The residual forces and moments created relate to the three translational (F_x, F_y, F_z) and three rotational (M_x, M_y, M_z) degrees of freedom between the pelvis and the ground. In reference to the musculoskeletal model, the x-axis represents the anterior/posterior direction, the y-axis denotes the axial direction and the medial-lateral direction is shown in the z-axis. The rotational degrees of freedom describe the pelvis list, pelvis rotation, and pelvis tilt motions, respectively.

The residual reduction is a form of forward dynamics simulation that utilizes tracking controllers to follow the model kinematics. The residual reduction algorithm (RRA) used the kinematics output file from the inverse dynamics tool and these values were filtered at 6 Hz. The analysis begins by setting the values of the model's generalized coordinates to the values computed by the inverse dynamics tool for the defined initial time. Then, RRA steps forward in time (with each time step of 0.001 s) until the end of the task length. During this process, force values are computed for all of the model's actuators which take the model from the current profile to the one coveted in the next instant in time, by minimizing the following objective function:

$$J = \sum_{i=1}^{nx} \left(\frac{f_{act\,i}}{f_{act\,i}^{opt}}\right)^2 + \sum_{i=1}^{nq} \omega_i \left(\ddot{q}_{des\,i}\,(t+T) - \ddot{q}_{rra\,i}\,(t)\right)^2 \qquad (12)$$

where $f_{act\,i}$ and $f_{act\,i}^{opt}$ represent the force and the optimal force of the actuator i, and ω_i the weight of the acceleration errors. The parcel of the summation minimizes and distributes loads across actuators, while the second part minimizes the error between the model accelerations and the desired accelerations. The algorithm tries to both reduce the residuals and adjust accelerations according to the original values. However, these two parameters vary inversely, since by drastically reducing the residuals, adjusted kinematics may differ from the original data.

To reduce the residual forces and moments, the residuals are computed and averaged over the duration of the movement. Then, the algorithm recommends changes in the model mass parameters, such as the location of the centre of mass of a chosen segment, which normally is the torso due to its dimensions and tendency to sustain estimation errors. The average value of F_y, the vertical residual force, is used to compute the recommended mass changes for all of the body segments, according to the expression:

$$dm = \frac{F_y}{g} \qquad (13)$$

The RRA reaches its final stage when the mass adjustments are determined, to reduce residuals even more. After the masses of all body segments were manually changed, RRA should be performed again, using the model with the adjusted torso, until the recommended adjustments are no longer significant.

4.4.5 Computed Muscle Control

Following the residual reduction algorithm step, the modified musculoskeletal model is used to compute a set of muscle excitations that will drive the dynamic musculoskeletal model to track a set of desired kinematics in the presence of applied external forces, in this case, ground reaction forces. The computed muscle control (CMC) does this by using, not only a static optimization step but also a proportional-derivate control to create a forward dynamic simulation that closely tracks the kinematics from the RRA (Delp et al., 2007). The CMC algorithm is divided into four stages and it is applied at each integration time step, T, during the forward dynamic simulation.

At the beginning of this process, a set of desired accelerations, $\ddot{\vec{q}}_{des}$, is computed, based on a set of experimental kinematics and the current kinematic state of the model. The algorithm will drive the model coordinates, $\vec{q}$, towards the experimental coordinates data, $\vec{q}_{exp}$, by following a proportional-derivate control law presented below:

$$\ddot{\vec{q}}_{des}(t+T) = \ddot{\vec{q}}_{exp}(t+T) + \overrightarrow{k_v}\left[\dot{\vec{q}}_{exp}(t) - \dot{\vec{q}}(t)\right] + \overrightarrow{k_p}\left[\vec{q}_{exp}(t) - \vec{q}(t)\right] \quad (14)$$

where $\overrightarrow{k_v}$ and $\overrightarrow{k_p}$ are the feedback gains on the velocity and position errors, respectively. If the desired kinematics are achieved, the velocity and position errors will be driven to zero and the respective gains follow the relation presented in Eq. (15).

$$\overrightarrow{k_v} = 2\sqrt{\overrightarrow{k_p}} \quad (15)$$

For musculoskeletal models, the error gains should drive any error to zero slowly, so normally the chosen values are $\overrightarrow{k_v} = 20$ and $\overrightarrow{k_p} = 100$ to cut down tracking errors (SimTK Opensim, 2012).

In the second stage, the set of actuator controls that will give rise to muscle forces is computed to produce the desired accelerations, obtained in the previous stage. Static optimization is used to guaranty the load distribution across synergistic actuators at any instant in time during the simulation. The CMC analysis performed in this work is called *the fast target* and it is formulated by the sum of squared controls extended by a set of equality constraints, $C_j = 0$, which requires the desired accelerations to be achieved within a set tolerance value, as expressed below.

$$J = \sum_{i=1}^{nx} x_i^2 \qquad C_j = \ddot{q}_j{}^* - \ddot{q}_j \quad (16)$$

The CMC tool can fail due to strength deficiencies in the muscles of the musculoskeletal model, which can be solved with the addition of reserve actuators that compensate for any lack of strength. These actuators have a very low strength thus require a much higher excitation value, which is a good indicator of how accurate the adjustments were previously performed.

The third step is responsible to compute the muscle excitations, which are estimated by inverting the dynamics of the muscle (Thelen and Anderson, 2006). When these values are determined, the algorithm reaches its final stage in which the muscle excitations are inputted into a standard forward dynamic simulation, advancing forward in determined time steps until the end of the task simulation.

4.4.6 Induced Acceleration Analysis

The induced acceleration analysis (IAA) is used to compute accelerations induced by individual forces acting on a model, like muscular forces. This tool is important to understand which muscles are responsible for each portion of the specific movement, especially regarding propulsion and weight-bearing stages. For this analysis, the states and controls obtained from CMC were used as inputs. The equation of motion that describes how this analysis works is given by:

$$[M]\ddot{q} = G(q) + V(q, \dot{q}) + S(q, \dot{q}) + [R]f \qquad (17)$$

where $[M]$ represents the mass matrix, $G(q)$ comprises the generalized forces resulting from the effect of gravity, $V(q, \dot{q})$ corresponds to the forces due to Coriolis and centrifugal effects, $S(q, \dot{q})$ is the resulting generalized force due to contact elements and $[R]$ translates the force transmission matrix containing the muscles moment arms, which transforms the applied force, f, into a generalized force.

When analysing the contribution of muscle forces for the mass centre acceleration, it is being considered the effect of the reaction forces with the environment caused by these forces, and not the internal muscle forces themselves. They do not accelerate the centre of mass directly. So, the algorithm must decompose the external reaction force in order to include only the induced contribution of each internal force to the external reaction force and the acceleration of the system. Thus, from manipulating the previous expression, the acceleration induced by a single element is:

$$\ddot{q}_i = [M]^{-1}\{F_i + S_i\} \qquad (18)$$

where F_i is the force of interest to be analysed and S_i represents the contributions resulting from the interaction of the musculoskeletal model with the environment, which in this work it is restricted to ground reaction forces. None of these variables is known, so the OpenSim software replaces the contribution of contact with appropriate kinematic constraints. The constraint reaction forces are solved simultaneously with the following equations of motion:

$$[M]\ddot{q} = G(q) + V(q, \dot{q}) + [R]f + [C]^T\lambda \qquad [C]\ddot{q} = B(t, q, \dot{q}) \qquad (19)$$

where $[C]$ represents the constraint matrix, λ corresponds to constraint reaction forces and $B(t, q, \dot{q})$ describes the position and velocities of the constraint equations described as a function of time.

Several constraint types can be supported with an IAA. In this case, it was used a “RollingOnSurface” that described a constraint on both toes that are in contact with a plane defined on another body, the ground. The following equations describe the kinematic behaviour of this constraint type, known as pure rolling:

$$\rho_y\,(q) = 0 \tag{20}$$

$$\dot{\rho_x}\,(q, \dot{q}) = 0 \tag{21}$$

$$\dot{\rho_z}\,(q, \dot{q}) = 0 \tag{22}$$

$$\omega_y\,(q, \dot{q}) = 0 \tag{23}$$

These four conditions represent a non-penetrating constraint, an anterior/posterior no–slip constraint, a mediolateral no–slip constraint and a no – twist constraint, respectively (Hamner et al., 2010).

5. Results

5.1 Joint kinematics and moments

The first step was to compute the joint kinematics and moments. In figures 15 and 16, these results are shown for the hip flexion, knee flexion, and ankle dorsiflexion, because these are the joints that define crouch gait in the sagittal plane. For the CP children, the results are presented individually, and each plot shows the several trials that were performed. Regarding the simulated crouch and the unimpaired gait, all subjects' results are shown in the same plot when considering the same parameter, due to a greater consistency of data. These parameters were obtained mainly to validate the assumptions related to the gait patterns performed by each group, as they have all been analysed in previous studies.

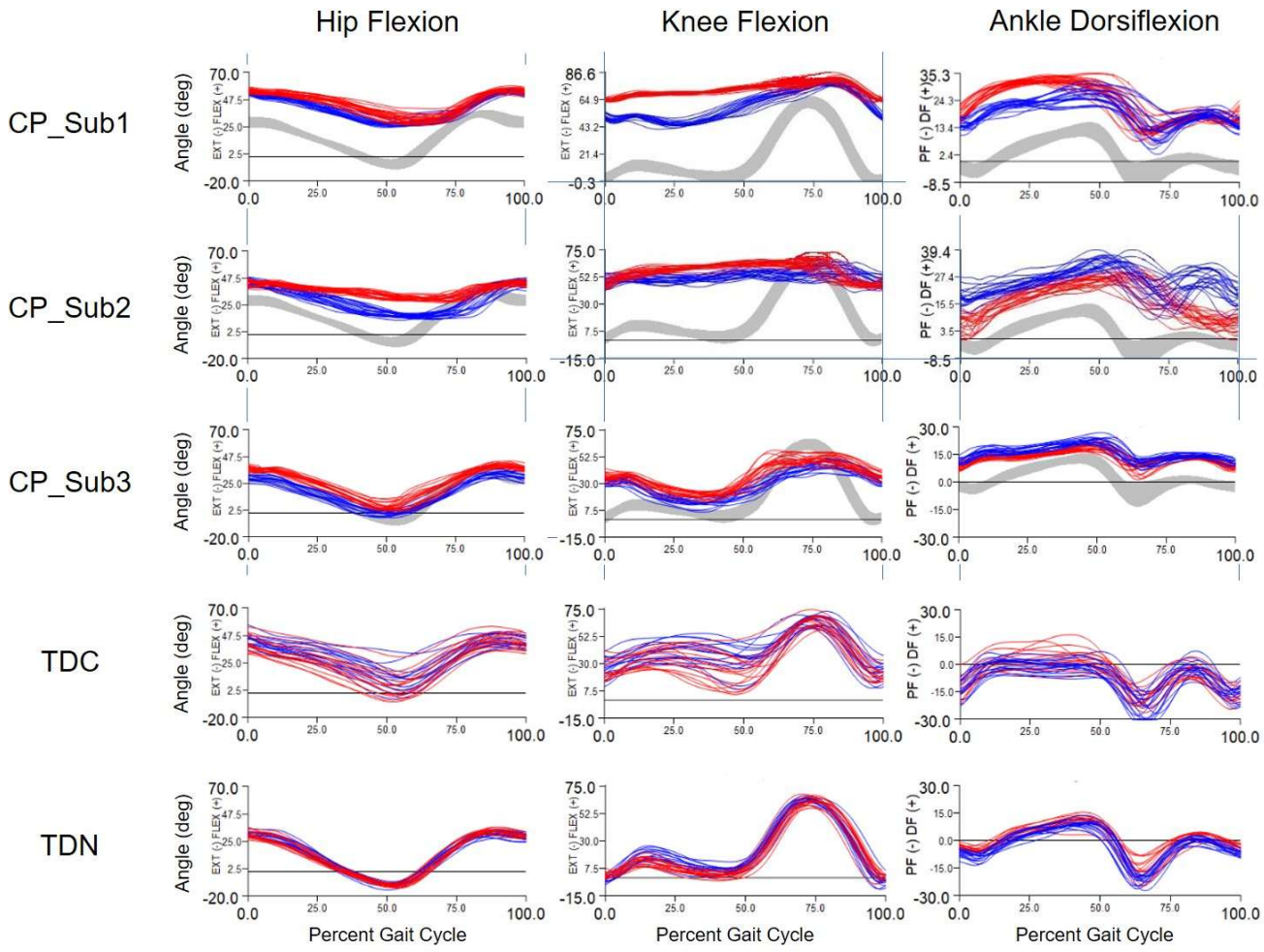

Figure 15. Hip, knee, and ankle flexion angles during simulated and real crouch gait, and unimpaired gait. TDC refers to the average values of the typically developing children performing CG, and TDN represents the same subjects in normal walking. The grey area indicates the standard value range for unimpaired gait.

The results show that the children with cerebral palsy have a very similar gait pattern when considering these three joints' flexion. However, CP_Sub3 seems to have a slightly higher capacity to extend the joints which may suggest a lesser degree of crouch severity, although all have been clinically diagnosed with severe crouch gait. When simulating crouch gait, the TD children showed an excessive flexion of the hip and knee, characteristic of this abnormal gait, but a reduced capacity in imitating the increased ankle dorsiflexion, also widely seen in this pathological gait. As it was expected, the healthy children in normal walking presented a gait pattern in accordance with the standard value ranges that define unimpaired gait (grey area).

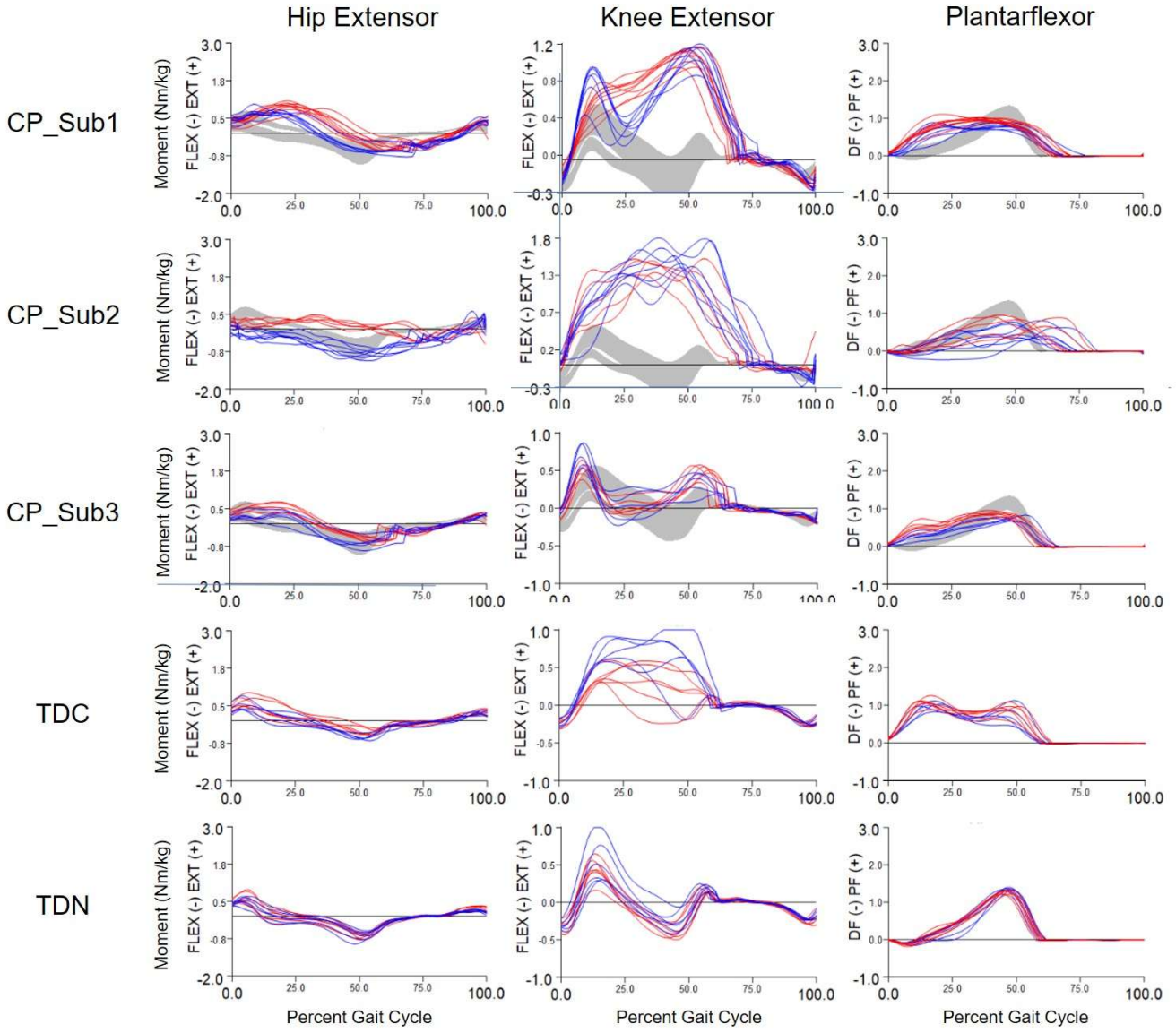

Figure 16. Hip, knee, and ankle flexion moments during simulated and real crouch gait, and unimpaired gait. TDC refers to the average values of the typically developing children performing CG, and TDN represents the same subjects in normal walking. The grey area indicates the standard value range for unimpaired gait.

Regarding joint moments, the results obtained for the neurologically intact children performing their normal walking are once again according with what was expected. These same children simulating crouch gait presented hip flexion moments very similar with the ones normally seen in unimpaired gait. On the other hand, both knee and ankle flexion moments are more in line with what was estimated in the CP children. At last, the results of the real crouch gaits are consistent and represent once again what is expected in this type of abnormal gait. As it was previously observed regarding the joint angles, the CP_Sub3 presented slightly lower values for the joint moments, when compared to the other two subjects, which confirms a possible lesser degree of crouch severity.

The joint kinematics displayed are the results obtained from the Visual3D analysis, and so they were used to validate the resultant joint moments obtained from the residual reduction algorithm.

5.2 Residual Reduction Algorithm

As it was explained before, the residual reduction algorithm tool was implemented to reduce residual forces and moments related to kinematic inconsistencies and model assumptions. This algorithm uses, apart from the ground reaction forces data and the kinematic data outputs from the previous step, three other input files with several parameters that can be adjusted according to the type of movement to be analysed. Before the implementation of this tool, both tasks and actuators' files were carefully edited and adjusted to obtain more appropriate results for each simulation. These documents are available with the software and present default values that define the coordinates to track and the corresponding weights, and the residual and reserve actuators' parameters, used to replace muscles. At least two passages for each case had to be done until it was ensured that the mass centre adjustments were small enough to show no significant differences and to reach steady values for the average residuals.

The OpenSim provides guidelines to evaluate the results of the algorithm implementation, where some of the computed parameters should meet the threshold values recommended. In addition to this, a significant reduction in the peak residual forces and moments should be verified in the RRA results, compared to those from the inverse dynamics analysis. As it is displayed in table 5, the peak residual forces suffered significative reductions for the CP children simulations. Considering the fore-aft direction (FX), the highest reduction suffered was 66% in the Sub3, while Sub1 and Sub2 registered reductions of 54% and 43%, respectively. Along the medio-lateral direction (FZ), the reductions were 74%, 72%, and 56%, where the smallest value corresponds to Sub2, and the higher to Sub3.

Table 5. Value ranges of the residual forces obtained from RRA and Inverse Dynamics, in analysing the CP children with crouch gait. Root mean square (RMS) values on the results from RRA.

		Residual Forces / N		
Subjects – crouch gait		FX	FY	FZ
CP_Sub1	Range $_{ID}$	[-18,64 ; 18,11]	[-16,99 ; 76,87]	[-35,48 ; 23,98]
	Range $_{RRA}$	[-2,57 ; 10,65]	[-10,92 ; 12,54]	[-5,62 ; 9,76]
	RMS	5,74	5,74	5,87
CP_Sub2	Range $_{ID}$	[-20,43 ; 26,35]	[-85,25 ; 46,85]	[-32,72 ; 27,12]
	Range $_{RRA}$	[-3,44 ; 12,22]	[-29,55 ; 22,22]	[-11,70 ; 14,47]
	RMS	6,24	13,82	8,75
CP_Sub3	Range $_{ID}$	[-29,62 ; 17,62]	[-81,17 ; 73,81]	[-27,47 ; 35,58]
	Range $_{RRA}$	[-10,04 ; 9,35]	[-8,07 ; 10,31]	[-2,52 ; 9,29]
	RMS	5,05	4,47	5,65

The most significant reductions were registered in the vertical direction (FY), with values ranging from 87% to 65%, and once again Sub3 has the higher value, while Sub1 also registered a high reduction of 84%. Although the reduction for Sub2 has been significant (65%), the peak residual force value surpasses the threshold, defined by OpenSim as being 25N.

Table 5 also presents the root mean square (RMS) values for all directions, and, according to the threshold values recommended by OpenSim, these are considered acceptable from 0 to 10N. The results obtained showed values within this range, apart from Sub2 which presents a slightly higher RMS value in the vertical direction.

The peak residual moments were much more difficult to reduce, and even impossible in most of the cases. Sub3 was the only one who showed a reduction of the peak residual moments, in both medio-lateral and vertical directions, of 22% and 31%, respectively. In the fore-aft direction, the values increased significantly for Sub2 and Sub3, but the highest increase was obtained in the medio-lateral direction, for Sub1. However, this subject registered no significant changes in the peak residual moments, from the ID to the RRA analysis, in both vertical and fore-aft directions. Despite the fact that none of the subjects presented an acceptable reduction of the peak residual moments with the RRA implementation, the respective RMS values are all within the expected interval (0-30 Nm). In addition to this, every peak residual moment is smaller than 75 Nm, which is considered to be the highest value accepted.

Table 6. Value ranges of the residual moments obtained from RRA and Inverse Dynamics, in analysing the CP children with crouch gait. Root mean square (RMS) values on the results from RRA.

		Residual Moments / Nm		
Subjects – crouch gait		MX	MY	MZ
CP_Sub1	Range $_{ID}$	[-25,78 ; 2,93]	[-5,94 ; 7,25]	[-11,78 ; 15,82]
	Range $_{RRA}$	[-27,43 ; 0,63]	[-7,67 ; 1,18]	[1,53 ; 35,01]
	RMS	14,62	3,99	15,03
CP_Sub2	Range $_{ID}$	[-21,69 ; 26,98]	[-12,93 ; 12,28]	[-39,21 ; 6,83]
	Range $_{RRA}$	[-42,20 ; 4,35]	[-12,55 ; 18,33]	[-52,90 ; 7,04]
	RMS	15,01	7,27	29,61
CP_Sub3	Range $_{ID}$	[-8,15 ; 13,33]	[-11,41 ; 5,95]	[-24,09 ; 8,70]
	Range $_{RRA}$	[-23,38 ; 0,97]	[-7,91 ; 7,03]	[-18,80 ; 2,64]
	RMS	14,49	3,68	9,09

Table 7 presents the residual force parameters of the healthy children, when simulating crouch gait. For this group, the reductions in the peak residual forces were much more significant when

compared with the previous group. Along the for-aft direction, the reductions ranged from 92% to 60% (Sub1 – 60%; Sub2 – 78%; Sub3 – 85%; Sub4 – 73%; Sub5 – 92%; Sub6 – 79%). In the vertical direction, the reductions were slightly higher, from 74% to 91% (Sub1 – 82%; Sub2 – 85%; Sub3 – 74%; Sub4 – 75%; Sub5 – 85%; Sub6 – 91%). Regarding the medio-lateral direction, the reductions were also significative and ranged from 69% to 93% (Sub1 – 75%; Sub2 – 74%; Sub3 – 69%; Sub4 – 83%; Sub5 – 82%; Sub6 – 93%).

The RMS values for the fore-aft and medio-lateral directions are all within the acceptance interval, as well as the peak residual force values. On the other hand, along the vertical direction, the residual forces and the respective RMS have considerably exceeded the defined thresholds. As all the experimental trials were performed under the same circumstances, these increased values for the residuals may have occurred to compensate for possible inconsistencies between the ground reaction force data and the kinematic data. These abnormal residual values along the vertical direction may also be related to errors in defining the relative position of the force plate and foot's reference frames.

Table 7. Value ranges of the residual forces obtained from RRA and Inverse Dynamics, in analysing the TD children simulating crouch gait. Root mean square (RMS) values on the results from RRA.

		Residual Forces / N		
Subjects – crouch gait		FX	FY	FZ
TD_Sub1	Range $_{ID}$	[-37,76 ; 20,12]	[-11,59 ; 196,04]	[-7,46 ; 13,34]
	Range $_{RRA}$	[-14,76 ; 3,37]	[-19,80 ; 35,02]	[-0,49 ; 3,27]
	RMS	8,70	17,61	1,04
TD_Sub2	Range $_{ID}$	[-37,10 ; 26,22]	[-51,52 ; 194,47]	[-18,90 ; 11,60]
	Range $_{RRA}$	[-6,27 ; 8,43]	[-20,49 ; 28,88]	[-2,58 ; 5,00]
	RMS	4,53	11,73	2,93
TD_Sub3	Range $_{ID}$	[-19,50 ; 55,95]	[-97,08 ; 206,27]	[-5,02 ; 15,61]
	Range $_{RRA}$	[-4,89 ; 8,52]	[-38,70 ; 53,30]	[-1,64 ; 5,15]
	RMS	2,92	24,71	3,19
TD_Sub4	Range $_{ID}$	[-18,72 ; 32,69]	[-55,79 ; 237,02]	[-11,14 ; 22,96]
	Range $_{RRA}$	[-2,60 ; 8,96]	[-47,82 ; 60,25]	[-1,24 ; 4,29]
	RMS	5,24	29,22	1,86
TD_Sub5	Range $_{ID}$	[-52,50 ; 44,26]	[-69,80 ; 229,11]	[-10,76 ; 7,18]
	Range $_{RRA}$	[-4,59 ; -0,07]	[-24,32 ; 34,51]	[0,29 ; 2,19]
	RMS	2,69	13,19	1,17
TD_Sub6	Range $_{ID}$	[-38,23 ; 21,52]	[-20,20 ; 246,85]	[-8,38 ; 28,00]
	Range $_{RRA}$	[-8,02 ; 2,28]	[-9,29 ; 20,68]	[-2,16 ; -0,33]
	RMS	5,69	9,18	1,65

Regarding the residual moments, it was possible to obtain good reductions along both vertical and medio-lateral directions (MY: Sub1 – 28%; Sub2 – 52%; Sub3 – 36%; Sub4 – 5%; Sub5 – 42%; Sub6 – 15% / MZ: Sub1 – 68%; Sub2 – 17%; Sub3 – 17%; Sub4 – 55%; Sub5 – 26%; Sub6 – 48%). In the fore-aft direction, there has been an increase in the peak residual moments for all subjects in this group, yet these values are still much smaller than 50Nm, which is the first threshold considered to evaluate this parameter. Additionally, the RMS values are all considered as very acceptable values.

Table 8. Value ranges of the residual moments obtained from RRA and Inverse Dynamics, in analysing the TD children simulating crouch gait. Root mean square (RMS) values on the results from RRA.

		Residual Moments / Nm		
Subjects – crouch gait		MX	MY	MZ
TD_Sub1	Range $_{ID}$	[-7,25 ; 2,74]	[-2,34 ; 2,52]	[-19,06 ; -1,32]
	Range $_{RRA}$	[-13,69 ; 2,21]	[-1,81 ; 1,67]	[-0,91 ; 6,44]
	RMS	9,07	1,11	3,75
TD_Sub2	Range $_{ID}$	[-4,10 ; 7,56]	[-5,90 ; 1,20]	[-12,78 ; -4,23]
	Range $_{RRA}$	[-25,16 ; -0,015]	[-2,85 ; 1,10]	[-10,51 ; 3,38]
	RMS	16,42	1,26	4,71
TD_Sub3	Range $_{ID}$	[-4,25 ; 2,90]	[-3,55 ; 3,28]	[-0,99 ; 26,46]
	Range $_{RRA}$	[-15,02 ; -3,83]	[-1,85 ; 2,26]	[-3,69 ; 22,06]
	RMS	10,73	1,16	10,03
TD_Sub4	Range $_{ID}$	[-1,99 ; 4,96]	[-4,97 ; 3,09]	[3,61 ; 21,67]
	Range $_{RRA}$	[-22,95 ; -3,96]	[-3,33 ; 4,70]	[-2,38 ; 9,75]
	RMS	17,25	2,41	5,38
TD_Sub5	Range $_{ID}$	[-1,85 ; 6,58]	[-6,21 ; 2,15]	[-17,35 ; 1,99]
	Range $_{RRA}$	[-30,07 ; -1,66]	[-3,63 ; 3,19]	[-12,83 ; 2,24]
	RMS	18,79	2,35	7,09
TD_Sub6	Range $_{ID}$	[-9,15 ; -1,75]	[-0,13 ; 7,02]	[-23,81 ; -3,76]
	Range $_{RRA}$	[-28,09 ; -0,96]	[-4,13 ; 5,94]	[-3,48 ; 12,43]
	RMS	17,86	3,07	5,89

Finally, the peak residual forces and moments of the healthy children performing their normal gait patterns are given in tables 9 and 10. The residual forces were quite simple to reduce and it was possible to get significant reductions for all subjects, in every direction (FX: Sub1 – 73%; Sub2 – 83%; Sub3 – 90%; Sub4 – 87%; Sub5 – 79%; Sub6 – 66% / FY: Sub1 – 74%; Sub2 – 73%; Sub3 – 73%; Sub4 – 73%; Sub5 – 80%; Sub6 – 69% / FZ: Sub1 – 93%; Sub2 – 72%; Sub3 – 64%; Sub4 – 64%; Sub5 – 71%; Sub6 – 68%). Furthermore, in the fore-aft and medio-lateral direction, the RMS values and the peak forces are all within the acceptance interval. However, along the vertical

direction, the peak residual forces increased considerably with the RRA Implementation, for all subjects. Consequently, the RMS values and those peak values significantly exceed the reference thresholds. A similar increase in the same direction was identified in the previous group, which included the same subjects but performing a different gait pattern. So, the causes for these unwanted forces may be related to what was previously explained.

Table 9. Value ranges of the residual forces obtained from RRA and Inverse Dynamics, in analysing the TD children performing their normal gait. Root mean square (RMS) values on the results from RRA.

		Residual Forces / N		
Subjects – normal gait		FX	FY	FZ
TD_Sub1	Range ID	[-32,91 ; 22,17]	[-12,77 ; 192,53]	[-27,94 ; 18,82]
	Range RRA	[-8,82 ; 0,28]	[-27,93 ; 49,55]	[-1,94 ; 0,60]
	RMS	5,81	25,43	0,96
TD_Sub2	Range ID	[-8,03 ; 23,53]	[-14,28 ; 191,85]	[-15,04 ; 25,18]
	Range RRA	[0,25 ; 4,52]	[-35,97 ; 52,25]	[-0,54 ; 7,24]
	RMS	2,75	28,01	4,44
TD_Sub3	Range ID	[-20,31 ; 19,92]	[-23,80 ; 198,96]	[-18,76 ; 24,96]
	Range RRA	[-2,05 ; 0,32]	[-36,32 ; 54,07]	[-1,37 ; 8,72]
	RMS	1,12	24,57	5,96
TD_Sub4	Range ID	[-30,76 ; 21,55]	[-16,38 ; 234,31]	[-14,96 ; 33,03]
	Range RRA	[-3,10 ; 4,19]	[-39,17 ; 61,62]	[-1,46 ; 11,58]
	RMS	2,65	30,22	7,87
TD_Sub5	Range ID	[-31,00 ; 25,48]	[-10,74 ; 241,60]	[-14,79 ; 27,98]
	Range RRA	[-6,49 ; 0,58]	[-33,38 ; 49,52]	[-0,34 ; 8,24]
	RMS	4,25	24,80	5,10
TD_Sub6	Range ID	[-33,48 ; 13,93]	[-14,26 ; 260,49]	[-7,22 ; 24,88]
	Range RRA	[-11,28 ; 0,18]	[-45,97 ; 81,07]	[-0,37 ; 8,13]
	RMS	7,06	39,78	4,47

Once again, the peak residual moments were much more difficult to reduce. Along the fore-aft direction, Sub3 and Sub4 registered considerable reductions of 53% and 64%, respectively. The other subjects increased significantly the peak residual values with the RRA implementation. Regarding the vertical direction, most of the subjects registered reductions in the peak moments (Sub1 – 17%; Sub2 – 23%; Sub3 – 30%; Sub4 – 39%), while Sub5 and Sub6 had their values increased. Along the medio-lateral direction, the peak values were also reduced for the majority of the subjects (Sub1 – 40%; Sub2 – 72%; Sub5 – 43%; Sub6 – 44%), but Sub3 and Sub4 registered significant increases. Despite the variations identified in the peak residual moments from the inverse dynamics output values to the RRA final results, all of the RMS values are smaller than the

threshold defined to evaluate this parameter, as well as the peak residual values for all subjects and in all directions.

Table 10. Value ranges of the residual moments obtained from RRA and Inverse Dynamics, in analysing the TD children performing their normal gait. Root mean square (RMS) values on the results from RRA.

		Residual Moments / Nm		
Subjects – unimpaired gait		MX	MY	MZ
TD_Sub1	Range $_{ID}$	[-10,80 ; 7,27]	[-5,06 ; 3,78]	[-24,57 ; -2,17]
	Range $_{RRA}$	[-16,93 ; -1,28]	[-4,03 ; 4,20]	[-14,77 ; 6,28]
	RMS	9,65	2,11	6,87
TD_Sub2	Range $_{ID}$	[-6,15 ; 4,40]	[-2,79 ; 2,28]	[1,63 ; 25,22]
	Range $_{RRA}$	[-21,62 ; -4,85]	[-2,14 ; 1,70]	[-3,13 ; 6,92]
	RMS	11,64	0,78	3,42
TD_Sub3	Range $_{ID}$	[-31,65 ; 1,82]	[-7,79 ; 7,80]	[-7,82 ; 7,83]
	Range $_{RRA}$	[-14,85 ; 4,99]	[-5,43 ; 3,05]	[-11,86 ; 5,53]
	RMS	6,03	2,47	5,73
TD_Sub4	Range $_{ID}$	[-29,39 ; 0,37]	[-6,43 ; 4,10]	[-8,95 ; 6,29]
	Range $_{RRA}$	[-10,73 ; 2,20]	[-3,93 ; 1,29]	[-13,16 ; 9,84]
	RMS	6,43	1,31	4,29
TD_Sub5	Range $_{ID}$	[-5,61 ; 5,45]	[-2,80 ; 1,82]	[-28,28 ; -4,75]
	Range $_{RRA}$	[-26,22 ; -5,49]	[-5,24 ; 4,94]	[-16,01 ; 6,26]
	RMS	17,58	2,66	9,43
TD_Sub6	Range $_{ID}$	[-10,72 ; 7,98]	[-4,02 ; 4,62]	[-33,33 ; -2,27]
	Range $_{RRA}$	[-31,95 ; -4,64]	[-5,58 ; 6,80]	[-18,66 ; 3,61]
	RMS	21,26	2,34	8,16

The position errors for the pelvis and all of the joint degrees of freedom are given in the appendix tables A - F. By analysing these tables, the values regarding the pelvis are all within the acceptable values, although, along the vertical direction, most of the translational errors were higher than expected due to the nature of the tasks performed. The position errors related to the joint degrees of freedom are also considerably smaller than the threshold considered, but some peak values regarding the ankle are higher than expected, but all within the accepted values. This effect was mainly identified for healthy children.

5.3 Computed Muscle Control

Muscle forces were estimated using a forward-dynamics optimization method called computed muscle control, previously explained. Apart from the residuals, reserve actuators are appended to the model to compensate for any possible muscle deficiency during the simulation, for every joint degree of freedom. These fictitious actuators are characterized by a low optimal force and high maximum and minimum excitation, to prevent the optimizer from trying to use those forces when it is not needed. The optimal forces for the residual actuators and the tracking task implemented in the CMC were the same as the ones set for the RRA implementation. All the simulations ran successfully, and, once again, the reserves actuators role in the results was carefully evaluated. These results are given in tables 11,12 and 13, one for each research group.

Table 11. Value ranges of the reserve actuators, given in Nm, for each joint degree of freedom obtained from CMC, in analysing the CP children with crouch gait. Root mean square (RMS) values on these results.

		Subjects – crouch gait		
Reserve Actuators		CP_Sub1	CP_Sub2	CP_Sub3
Right hip flexion	Range	[-0,0110 ; 0,0405]	[-0,0062 ; 0,0310]	[-0,0159 ; 0,0217]
	RMS	0,0151	0,0150	0,0106
Right hip adduction	Range	[0,0014 ; 0,0694]	[-0,0244 ; 0,0067]	[-0,0605 ; 0,0180]
	RMS	0,0354	0,0105	0,0403
Right hip rotation	Range	[-0,2190 ; 0,0297]	[-0,0573 ; 0,1000]	[-0,0485 ; 0,0423]
	RMS	0,0849	0,0347	0,0254
Right knee	Range	[-0,0893 ; 0,0272]	[-0,0366 ; 0,0174]	[-0,0341 ; 0,0145]
	RMS	0,0154	0,0191	0,0080
Right ankle	Range	[-0,0199 ; 4,4581]	[-0,0335 ; 5,5700]	[-0,0245 ; 2,2014]
	RMS	1,1705	0,7877	0,3450
Left hip flexion	Range	[-0,0390 ; 0,1007]	[-0,0146 ; 0,0107]	[-0,0233 ; 0,0380]
	RMS	0,0445	0,0057	0,0187
Left hip adduction	Range	[-0,0641 ; 0,0064]	[-0,0058 ; 0,0224]	[-0,0451 ; 0,0149]
	RMS	0,0274	0,0119	0,0116
Left hip rotation	Range	[-0,1385 ; 0,0262]	[-0,0284 ; 0,1364]	[-0,0402 ; 0,3854]
	RMS	0,0465	0,0828	0,1387
Left knee	Range	[-0,2025 ; 0,0306]	[-0,0251 ; 0,0235]	[-0,0298 ; 0,0195]
	RMS	0,0638	0,0175	0,0153
Left ankle	Range	[-0,0323 ; 3,1717]	[-0,0136 ; 5,4236]	[-0,0200 ; 15,3048]
	RMS	0,5310	0,6331	3,4380
Lumbar extension	Range	[-0,0129 ; 0,0181]	[-7,8942 ; -0,0219]	[-0,0517 ; 0,0042]
	RMS	0,0092	3,9019	0,0310
Lumbar bending	Range	[-0,0268 ; 0,0037]	[-0,0634 ; 9,1031]	[-0,0459 ; 0,0319]
	RMS	0,0091	4,4693	0,0208
Lumbar rotation	Range	[-0,0394 ; 0,0677]	[-0,5373 ; 19,3959]	[-0,1098 ; 0,0772]
	RMS	0,0270	9,1396	0,0554

Table 12. Value ranges of the reserve actuators, given in Nm, for each joint degree of freedom obtained from CMC, in analysing the TD children simulating crouch gait. Root mean square (RMS) values on these results.

		Subjects – crouch gait					
Reserve Actuators		TD_Sub1	TD_Sub2	TD_Sub3	TD_Sub4	TD_Sub5	TD_Sub6
Right hip flexion	Range	[-0,0203 ; 0,0558]	[-0,1499 ; 0,0220]	[-0,0797 ; 0,1006]	[-0,0181 ; 0,0153]	[-0,3254 ; 0,0161]	[-0,0334 ; 0,0634]
	RMS	0,0311	0,0631	0,0595	0,0127	0,1413	0,0371
Right hip adduction	Range	[-0,0968 ; 0,0168]	[-0,4877 ; -0,0485]	[-0,0791 ; 0,0131]	[-0,0828 ; -0,0001]	[-0,8446 ; -0,0253]	[-0,0689 ; -0,0025]
	RMS	0,0271	0,2162	0,0328	0,0598	0,3533	0,0364
Right hip rotation	Range	[-0,01071 ; 0,0172]	[-0,1441 ; -0,0415]	[-0,1010 ; 0,0241]	[-0,0107 ; 0,0364]	[-0,3444 ; -0,0238]	[-0,1668 ; 0,0061]
	RMS	0,0427	0,0689	0,0559	0,0129	0,1323	0,0757
Right knee	Range	[-0,0972 ; 0,0094]	[-0,1046 ; 0,0542]	[-0,1480 ; 0,0134]	[-0,0385 ; 0,0151]	[-0,0656 ; 0,0415]	[-0,1155 ; 0,0060]
	RMS	0,0455	0,0383	0,0811	0,0126	0,0267	0,0653
Right ankle	Range	[-0,0054 ; 1,1195]	[-0,0355 ; 0,0095]	[-0,0027 ; 3,3272]	[-0,0151 ; -0,0004]	[-0,0112 ; 0,0030]	[-0,0034 ; 0,0697]
	RMS	0,2543	0,0165	0,3916	0,0101	0,0076	0,0316
Left hip flexion	Range	[-0,0275 ; 0,0571]	[-0,0521 ; 0,0761]	[-0,0621 ; 0,0175]	[-0,0207 ; 0,0351]	[-0,3920 ; 0,1056]	[-0,0275 ; 0,0155]
	RMS	0,0253	0,0500	0,0402	0,0235	0,0862	0,0154
Left hip adduction	Range	[-0,2106 ; 0,0106]	[-0,2214 ; 0,0178]	[-0,2237 ; 0,0024]	[-0,0568 ; 0,0092]	[-0,7419 ; -0,0019]	[-0,0602 ; 0,0004]
	RMS	0,1613	0,0845	0,1376	0,0212	0,0854	0,0415
Left hip rotation	Range	[-0,1776 ; 0,1680]	[-0,3197 ; -0,0006]	[-0,0587 ; 0,0300]	[-0,0451 ; 0,0236]	[-0,4026 ; -0,0161]	[-0,0306 ; 0,0321]
	RMS	0,1051	0,1381	0,0270	0,0271	0,1468	0,0187
Left knee	Range	[-0,1244 ; 0,0008]	[-0,1422 ; 0,0003]	[-0,0419 ; 0,0183]	[-0,0636 ; 0,0134]	[-0,2135 ; 0,0030]	[-0,0438 ; 0,0226]
	RMS	0,0414	0,0752	0,0133	0,0369	0,1201	0,0175
Left ankle	Range	[-0,0661 ; 0,0129]	[-0,0022 ; 0,1299]	[-0,0122 ; 0,0037]	[-0,0089 ; 0,3187]	[-0,0274 ; 0,0716]	[-0,0733 ; 0,0197]
	RMS	0,0196	0,0532	0,0064	0,0919	0,0296	0,0277
Lumbar extension	Range	[0,0032 ; 0,0115]	[-0,1220 ; 0,0087]	[-0,0288 ; 0,0113]	[-0,0311 ; 0,0106]	[-0,0083 ; -0,0012]	[-0,0024 ; 0,0130]
	RMS	0,0080	0,0634	0,0134	0,0165	0,0048	0,0071
Lumbar bending	Range	[0,0029 ; 0,0142]	[-0,0100 ; 0,1689]	[-0,0255 ; 0,0022]	[-0,0244 ; 0,0186]	[0,0047 ; 0,0174]	[0,0061 ; 0,0180]
	RMS	0,0117	0,0756	0,0119	0,0174	0,0117	0,0118
Lumbar rotation	Range	[-0,0656 ; -0,0119]	[0,0408 ; 0,5030]	[-0,0517 ; 0,0540]	[-0,0085 ; 0,1365]	[0,0094 ; 0,0797]	[-0,0799 ; 0,0110]
	RMS	0,0476	0,2024	0,0307	0,0859	0,0366	0,0457

Table 13. Value ranges of the reserve actuators, given in Nm, for each joint degree of freedom obtained from CMC, in analysing the TD children performing their normal gait. Root mean square (RMS) values on these results.

		Subjects – unimpaired gait					
Reserve Actuators		TD_Sub1	TD_Sub2	TD_Sub1	TD_Sub1	TD_Sub1	TD_Sub1
Right hip flexion	Range	[-0,0233 ; 0,0662]	[-0,0212 ; 0,0636]	[-0,0436 ; 0,1042]	[-0,0353 ; 0,0385]	[-0,0138 ; 0,0503]	[-0,0074 ; 0,0396]
	RMS	0,0299	0,0341	0,0505	0,0236	0,0186	0,0164
Right hip adduction	Range	[-0,1058 ; 0,0175]	[-0,0990 ; 0,0110]	[-0,1515 ; 0,0138]	[-0,1361 ; 0,0037]	[-0,1342 ; 0,0038]	[-0,0770 ; 0,0012]
	RMS	0,0517	0,0336	0,0509	0,0780	0,0777	0,0549
Right hip rotation	Range	[-0,2717 ; 0,0705]	[-0,1143 ; 0,0087]	[-0,5200 ; 0,0556]	[-0,0769 ; 0,0553]	[-0,0934 ; 0,0796]	[-0,0575 ; 0,0388]
	RMS	0,1166	0,0484	0,2051	0,0400	0,0514	0,0319
Right knee	Range	[-0,1333 ; 0,0097]	[-0,0857 ; 0,0071]	[-0,3003 ; 0,0121]	[-0,0789 ; 0,0108]	[-0,1289 ; 0,0027]	[-0,1045 ; 0,0023]
	RMS	0,0427	0,0445	0,0818	0,0371	0,0521	0,0551
Right ankle	Range	[-0,0036 ; 2,4682]	[-0,0045 ; 0,4891]	[-0,0025 ; 1,6233]	[-0,0834 ; 0,0284]	[-0,0467 ; 0,0687]	[-0,0180 ; 0,0309]
	RMS	0,5903	0,1277	0,3390	0,0309	0,0188	0,0099
Left hip flexion	Range	[-0,0192 ; 0,0783]	[-0,0246 ; 0,0707]	[-0,0407 ; 0,0568]	[-0,0200 ; 0,0506]	[-0,0172 ; 0,0402]	[-0,0022 ; 0,0381]
	RMS	0,0297	0,0306	0,0271	0,0266	0,0201	0,0203
Left hip adduction	Range	[-0,1611 ; 0,0157]	[-0,2489 ; 0,0084]	[-0,2240 ; -0,0007]	[-0,0767 ; 0,0127]	[-0,0659 ; 0,0094]	[-0,0926 ; 0,0067]
	RMS	0,1018	0,1377	0,1409	0,0272	0,0198	0,0344
Left hip rotation	Range	[-0,0782 ; 0,5959]	[-0,1786 ; 0,0787]	[-0,0173 ; 0,4514]	[-0,1895 ; 0,0130]	[-0,0674 ; 0,0155]	[-0,1609 ; 0,0189]
	RMS	0,1981	0,0860	0,1323	0,0694	0,0290	0,0638
Left knee	Range	[-0,1908 ; 0,0032]	[-0,1750 ; 0,0029]	[-0,1529 ; 0,0221]	[-0,1629 ; 0,0071]	[-0,0672 ; 0,0038]	[-0,0631 ; 0,0016]
	RMS	0,0677	0,0892	0,0629	0,0469	0,0301	0,0356
Left ankle	Range	[-0,1821 ; 0,0463]	[-0,0620 ; 0,0382]	[-0,2720 ; 0,0398]	[-0,0058 ; 2,3376]	[-0,0009 ; 0,1836]	[-0,0013 ; 0,2146]
	RMS	0,0562	0,0277	0,0604	0,5050	0,0515	0,0498
Lumbar extension	Range	[-0,0182 ; 0,0103]	[-0,0215 ; 0,0124]	[-0,0672 ; 0,0319]	[-0,0252 ; 0,0063]	[-0,0119 ; 0,0044]	[-0,0135 ; 0,0055]
	RMS	0,0091	0,0094	0,0330	0,0154	0,0077	0,0061
Lumbar bending	Range	[-0,0086 ; 0,0275]	[-0,0192 ; 0,0239]	[-0,0214 ; 0,0440]	[-0,0299 ; 0,0118]	[-0,0106 ; 0,0175]	[-0,0061 ; 0,0138]
	RMS	0,0157	0,0128	0,0153	0,0128	0,0100	0,0082
Lumbar rotation	Range	[-0,0849 ; 0,0311]	[-0,0328 ; 0,0740]	[-0,1057 ; 0,1308]	[-0,0635 ; 0,0555]	[-0,0316 ; 0,0354]	[-0,0350 ; 0,0453]
	RMS	0,0506	0,0410	0,0549	0,0316	0,0216	0,0210

The acceptance interval to evaluate the reserve actuators presented by OpenSim is, preferably, from 0 to 25 Nm, although values until 50 Nm can be accepted. The maximum reserve actuator values registered, and the respective RMS values were all validated, considering the OpenSim defined thresholds.

As in RRA, CMC also returns the values for the position errors of the joint degrees of freedom. These values are given in the appendix tables G-I for all research groups. By analysing these results attentively, it was verified that they are all within the acceptable limit of 0 to 5 degrees, which is an additional indicator that CMC ran successfully in every simulation.

After the results shown above have been validated, the muscle forces obtained by CMC can then be analysed. The muscle's behaviour during the gait cycle is represented in figures 17, 19, and 21 for the CP children, and in figures 18, 20, and 22 for one representative healthy subject of each gait pattern performed. The plots showing the results of TD children, do not show muscle forces in the period of initial double support, which represents the first 10% of the gait cycle, because it was not possible to obtain experimental data for that period. The muscle results will be only analysed and discussed during the stance phase of the gait cycle, as it is the period of interest for this work. The results are shown for the muscle groups that mainly contribute to the task performed.

Table 14. Description of the muscle groups considered.

Muscle Groups	Description
Gastrocnemius	Includes two musculoskeletal actuators representing the medial and lateral muscle's components.
Soleus	Refers to the soleus muscle, which is represented by only one actuator.
Vasti	Represents three muscle-tendon actuators, the vastus medials, vastus intermedius, and vastus lateralis.
Rectus Femoris	Refers to the rectus femoris muscle, which is represented by one actuator.
Hamstrings	Includes three muscle-tendon actuators representing the bi-articular hamstrings including the biceps femoris long head, semimembranosus, and semitendinosus.
Iliopsoas	Represents both Iliacus and psoas, each modelled by a single actuator.
Gluteus Maximus	Refers to three muscle-tendon actuators representing the medial, intermediate, and lateral components of the muscle.
Ankle Dorsiflexors	Muscle-tendon actuators representing the anterior tibialis, extensor digitorum, extensor hallus longus, and peroneus tertius.
Hip Abductors	Includes the gluteus medius and gluteus minimus, each modelled as three muscle-tendon actuators representing the anterior, intermediate, and posterior components of the muscle.

The crouch gait subjects showed similar muscle contributions, throughout the stance phase, for the gastrocnemius and soleus, with an identified increase during terminal stance and pre-swing. The healthy children in performing both the abnormal gait pattern and unimpaired gait had similar behaviours for these two muscle groups, but with much higher forces produced. Additionally, normal gait required more strength of these muscles than the simulated crouch. Regarding the vasti, the CP children showed different muscle behaviours among them. While the Sub1 and Sub2 display a high and constant request of this muscle's strength, Sub3 only showed muscle demand during the mid-stance, and no significant muscle force during the rest of the stance. The TD children results simulating the crouch gait, for this muscle group, displayed a much higher demand on the muscles compared to unimpaired gait, but a behaviour similar to the ones seen in CP_Sub1 and CP_Sub2.

The CP children did not show significant changes in the iliopsoas behaviour among them. However, the crouch gait, compared with the simulated crouch, required more muscle forces during the stance and compared with the normal gait, it showed a reduced muscle demand during the terminal stance and pre-swing. Regarding the hamstrings, for the CP children, they were mostly required during early stance and the beginning of the mid-stance, apart from the CP_Sub1 who showed a peak muscle force during the mid-stance which was not identified in the other CP patients. The simulated crouch and the unimpaired gait required this muscle's strength mainly during the beginning of the mid-stance and an increase in the muscle force in the end of terminal stance. In crouch gait, the rectus femoris was mostly required at the beginning of the stance but it also showed some significant activity during terminal stance in all of the CP children. In both simulated crouch and unimpaired gait, the rectus femoris showed higher forces during mid-stance.

The hip abductors had a major force required during the mid-stance compared with terminal stance, for the CP children, and their behaviour was similar among the subjects. On the other hand, in simulated crouch and unimpaired gait, these muscles showed significant strength requirement in both mid-stance and terminal stance. Regarding the ankle dorsiflexors, crouch gait demanded muscle activity mainly in early stance, but also during pre-swing, although CP_Sub1 did not show significant muscle force in this final part of the stance. The results related to normal gait and simulated crouch also indicate major force during the beginning of the stance, and the simulated abnormal gait also suggest muscle activity during the terminal stance. Finally, the gluteus maximus was most in demand during the initial double support and the mid-stance phases, for the CP children. The simulated crouch showed a different behaviour, regarding this muscle group, where the peak force occurred in mid-stance and the muscle activity was considerably high throughout the stance phase. In normal gait, the gluteus maximus was mainly required during mid-stance, not having a significant role during terminal stance.

EMG Validation

It was possible to obtain the surface electromyography (EMG) signals for all of the CP children and healthy subjects, from the medial gastrocnemius, tibialis anterior, gluteus medius, and rectus femoris. As the first three muscles are the major contributors to force production of the muscle groups in which they are included, their EMG data were considered to validate their muscle group behaviour. The signal was sampled at 1000Hz and high-pass filtered with a cut-off frequency of 30Hz.

These results are shown in the figures B - I of the appendix. Regarding the healthy children, the EMG signal describes fairly well the muscles' behaviour for both simulated and normal gaits, mainly during the stance phase. For the children with cerebral palsy, the tibialis anterior and gluteus medius stimulations are shown to be consistent with the muscle forces estimated for the ankle dorsiflexors and hip abductors, respectively, during stance. However, regarding the medial gastrocnemius and the rectus femoris, the respective EMG signal do not match the muscle force behaviour so well. There are some peaks in the muscle force curves that do not have a corresponding EMG peak.

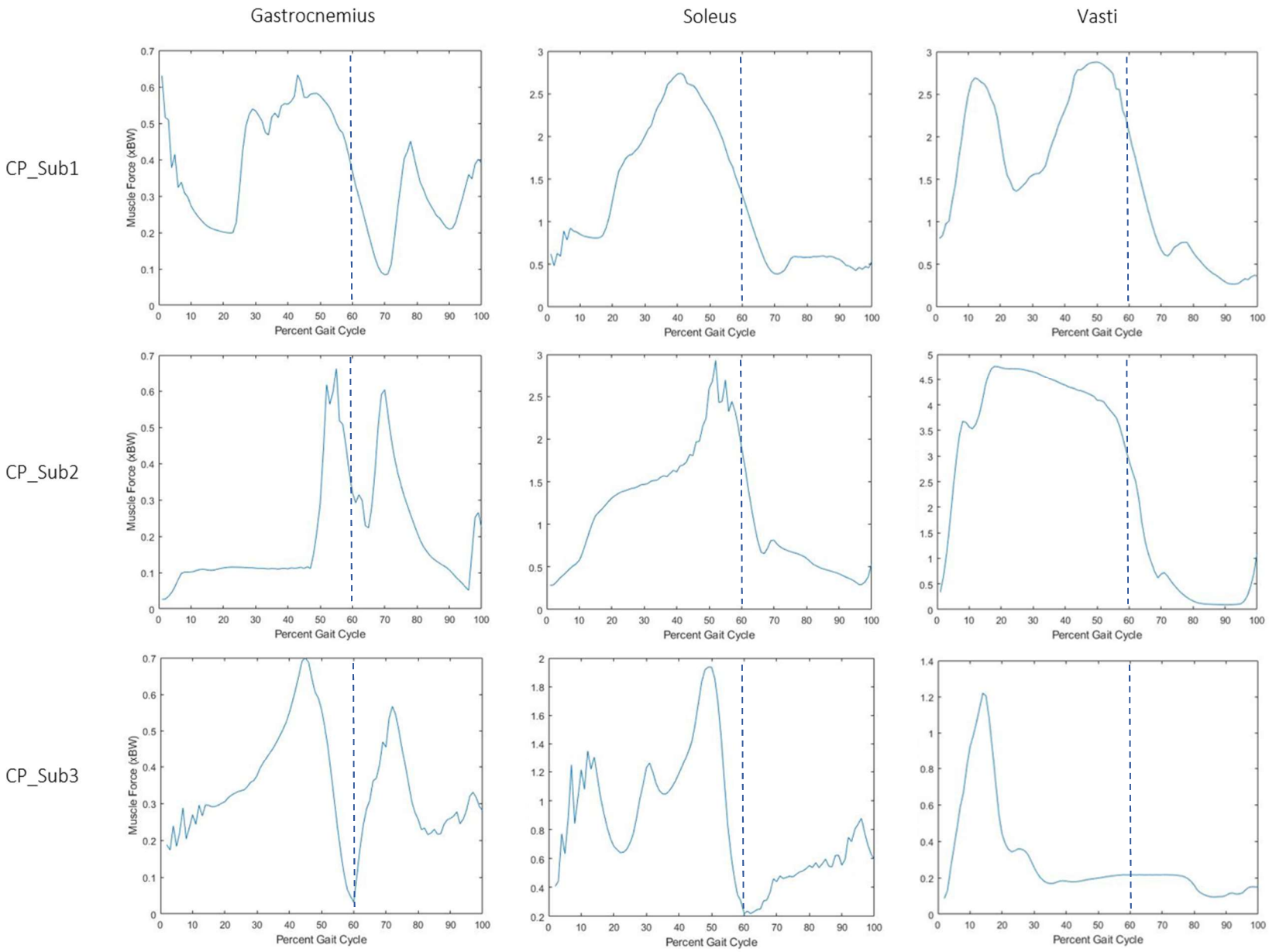

Figure 17. Resulting gastrocnemius, soleus and vasti forces normalized by bodyweight (BW) obtained from CMC, for all CP children.

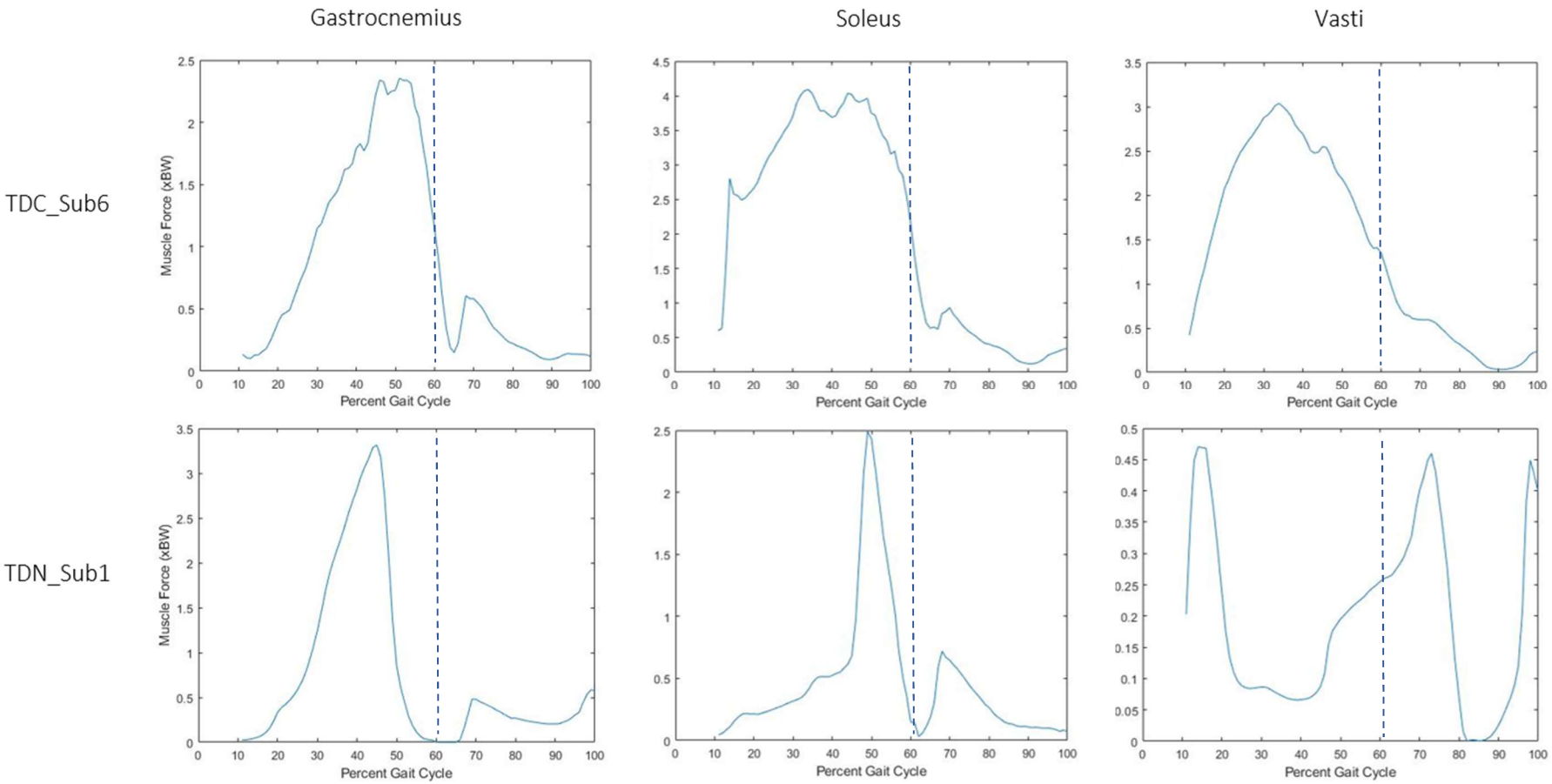

Figure 18. Resulting gastrocnemius, soleus and hip vasti forces normalized by bodyweight (BW) obtained from CMC, for the subject TD_Sub6 simulating crouch gait and the subject TD_Sub1 performing normal gait.

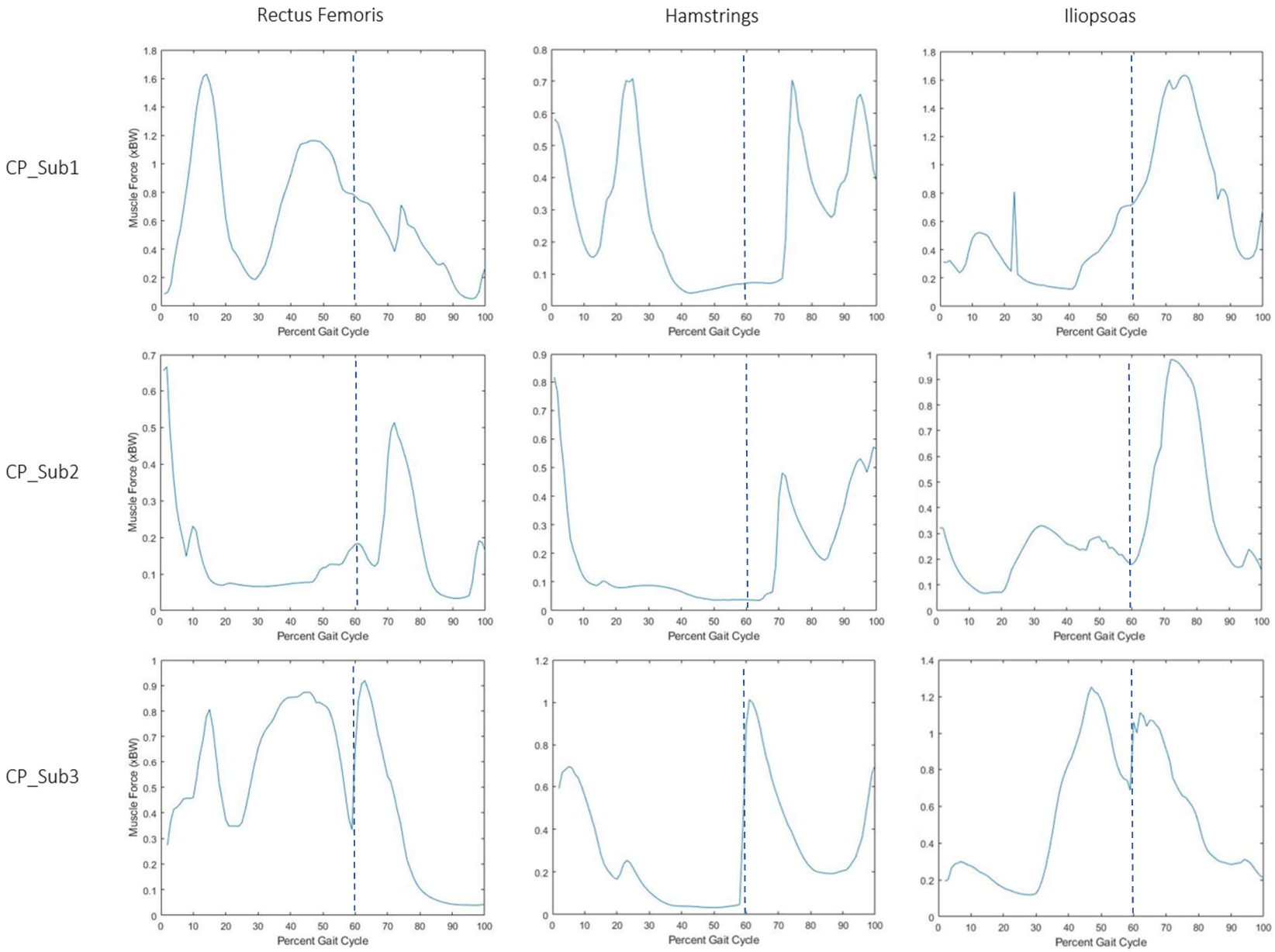

Figure 19. Resulting rectus femoris, hamstrings and iliopsoas forces normalized by bodyweight (BW) obtained from CMC, for all CP children.

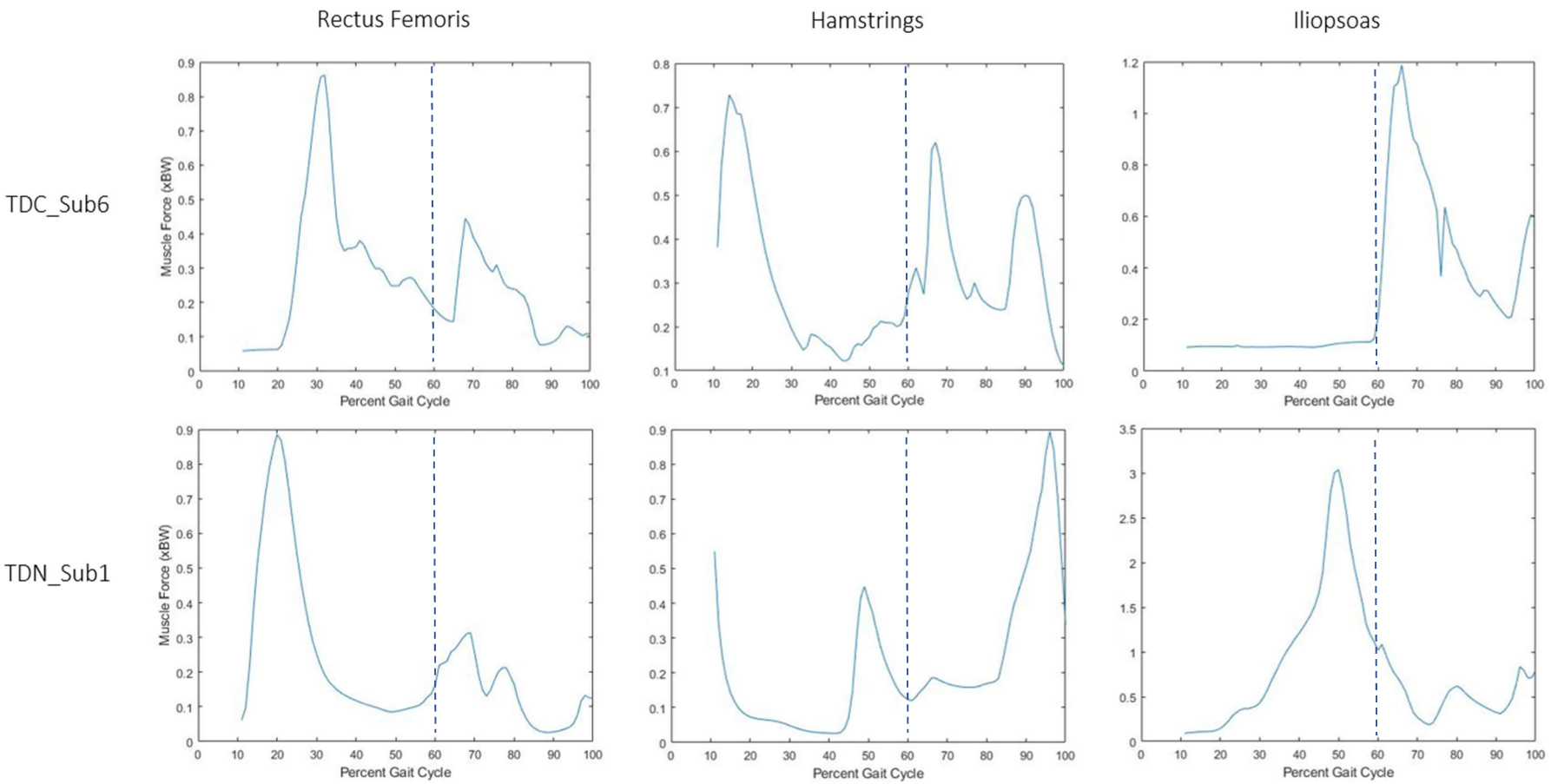

Figure 20. Resulting rectus femoris, hamstrings and iliopsoas forces normalized by bodyweight (BW) obtained from CMC, for the subject TD_Sub6 simulating crouch gait and the subject TD_Sub1 performing normal gait.

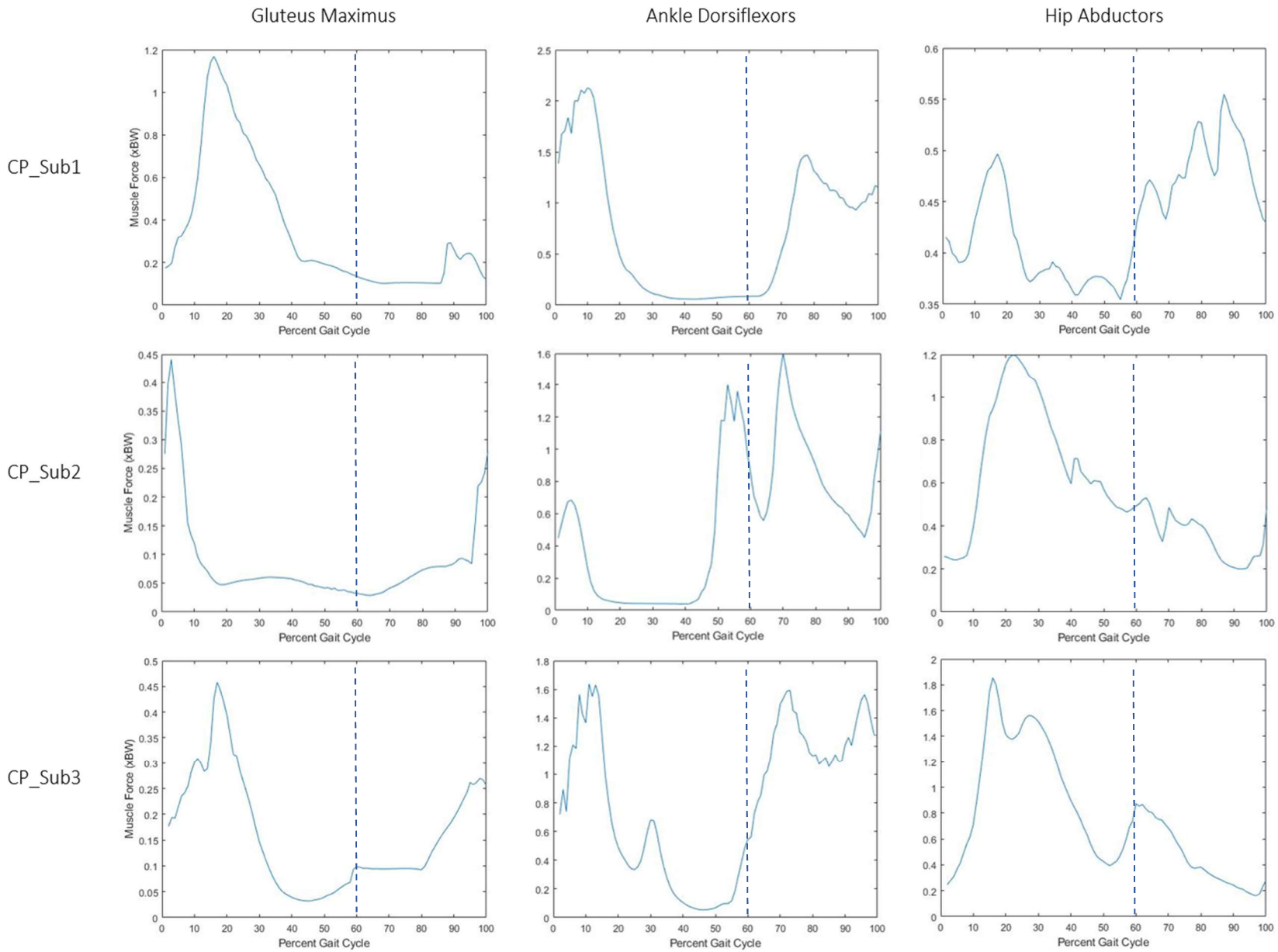

Figure 21. Resulting gluteus maximus, ankle dorsiflexors and hip abductors forces normalized by bodyweight (BW) obtained from CMC, for all CP children.

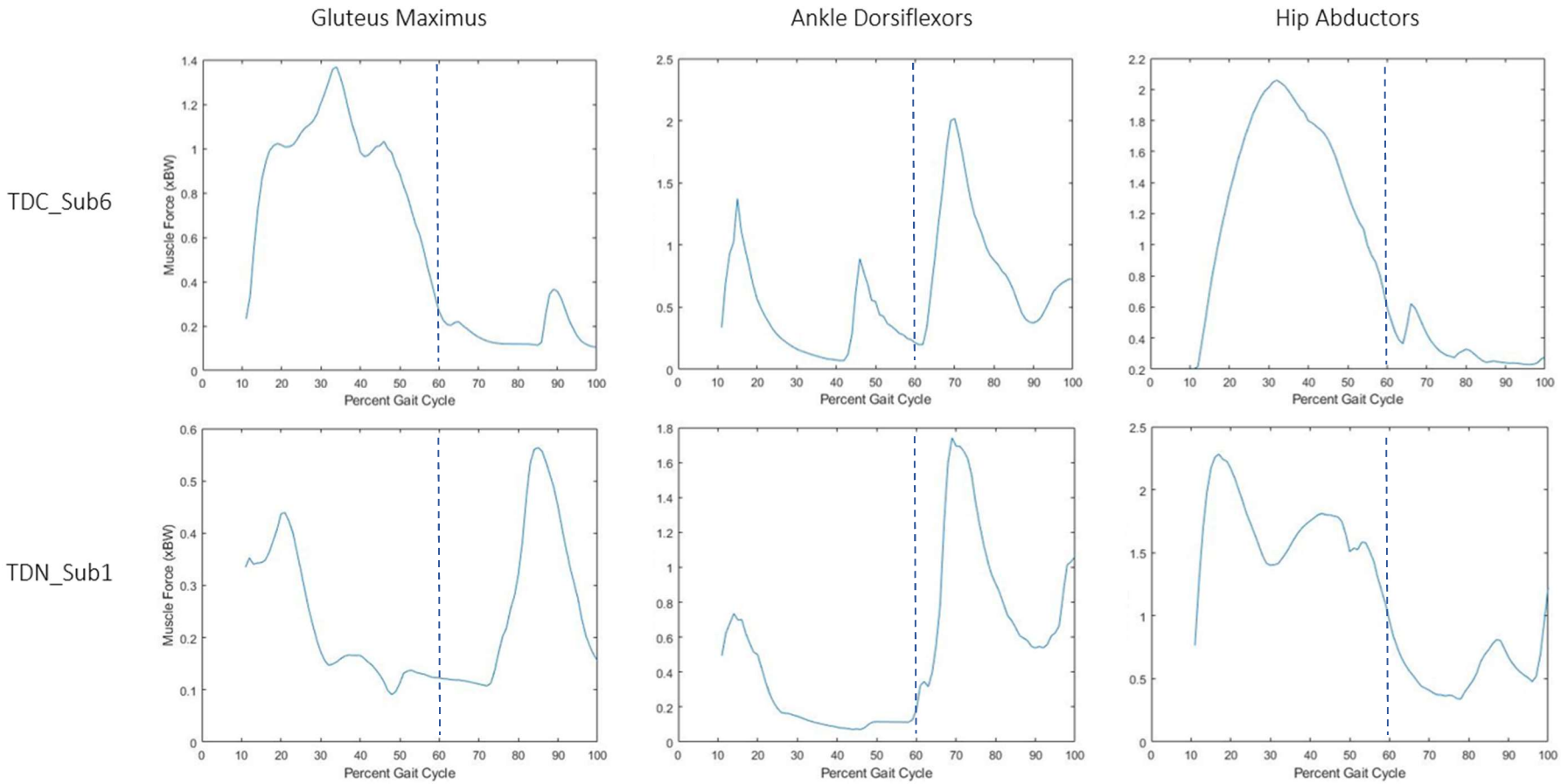

Figure 22. Resulting gluteus maximus, ankle dorsiflexors and hip abductors forces normalized by bodyweight (BW) obtained from CMC, for the subject TD_Sub6 simulating crouch gait and the subject TD_Sub1 performing normal gait.

To better analyse the magnitude of muscle contributions during stance and compare it between the groups, the average muscle results for each different gait pattern are represented in the figure below.

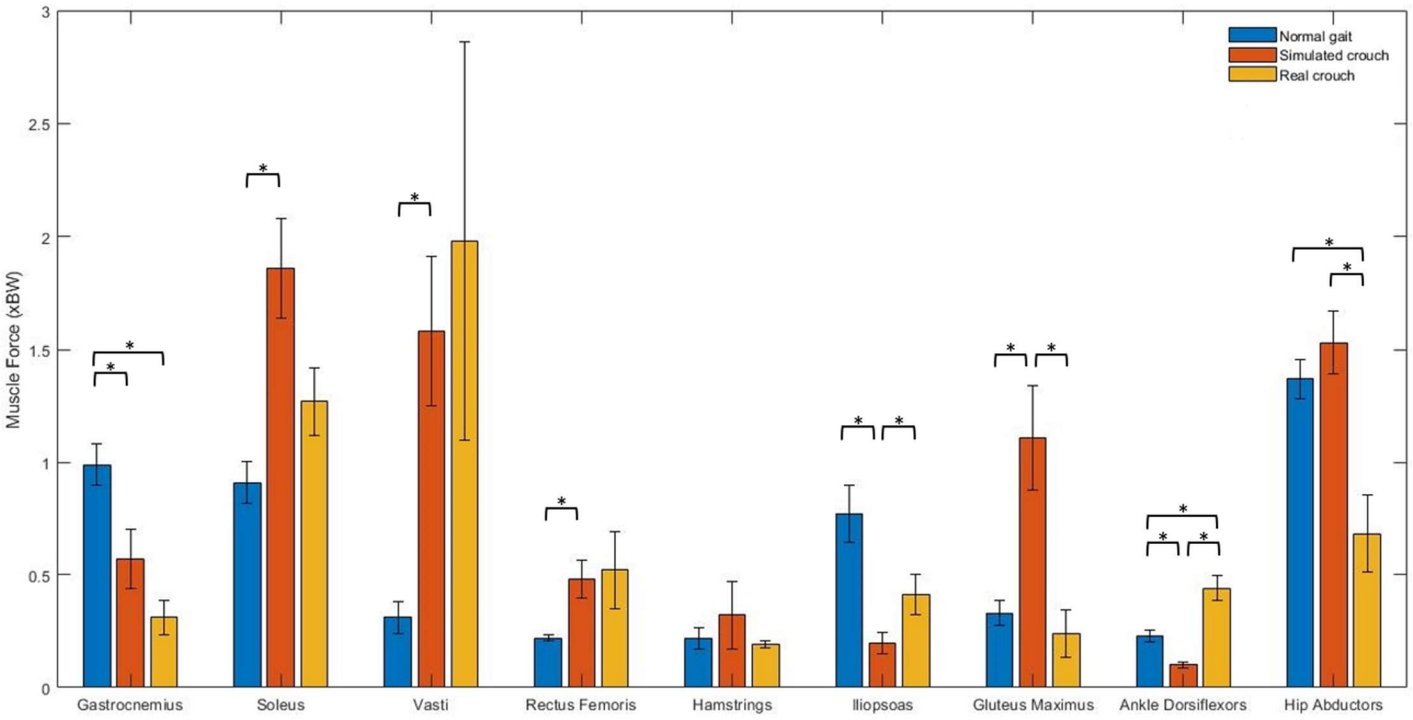

Figure 23. The average muscle force during stance normalized by bodyweight (BW). Error bars are ±1 standard error.

The muscle groups that mostly contributed during stance in unimpaired gait were the gastrocnemius, soleus, iliopsoas, and hip adductors, which was the group with the highest contribution. In the simulated crouch, the most significant forces produced came from the soleus, vasti, gluteus maximus and hip abductors. The crouch gait relied mostly on the vasti, soleus, and hip abductors' forces during stance.

Regarding the healthy children simulating crouch gait and performing unimpaired gait, the muscle forces were only considered not to be significantly different when comparing the hamstrings and the hip abductors. The forces produced by soleus, vasti, rectus femoris, and gluteus maximus were far superior in the simulated crouch. On the other hand, the gastrocnemius, iliopsoas, and ankle dorsiflexors showed higher force values during normal gait stance.

When comparing the average muscle forces results of the simulated crouch with the real crouch gait, only four of the muscle groups considered reported statistically significant differences. In this case, the gluteus maximus and the hip abductors required much more muscle strength during

simulated crouch, while iliopsoas and ankle dorsiflexors showed slightly higher demand during unimpaired gait.

Finally, by analysing the normal gait and crouch gait, the results indicate that the only significant differences in the muscle forces between these groups were found in the gastrocnemius, ankle dorsiflexors, and hip abductors. The unimpaired gait required greater muscle forces from the gastrocnemius and hip abductor, but less strength from the ankle dorsiflexors.

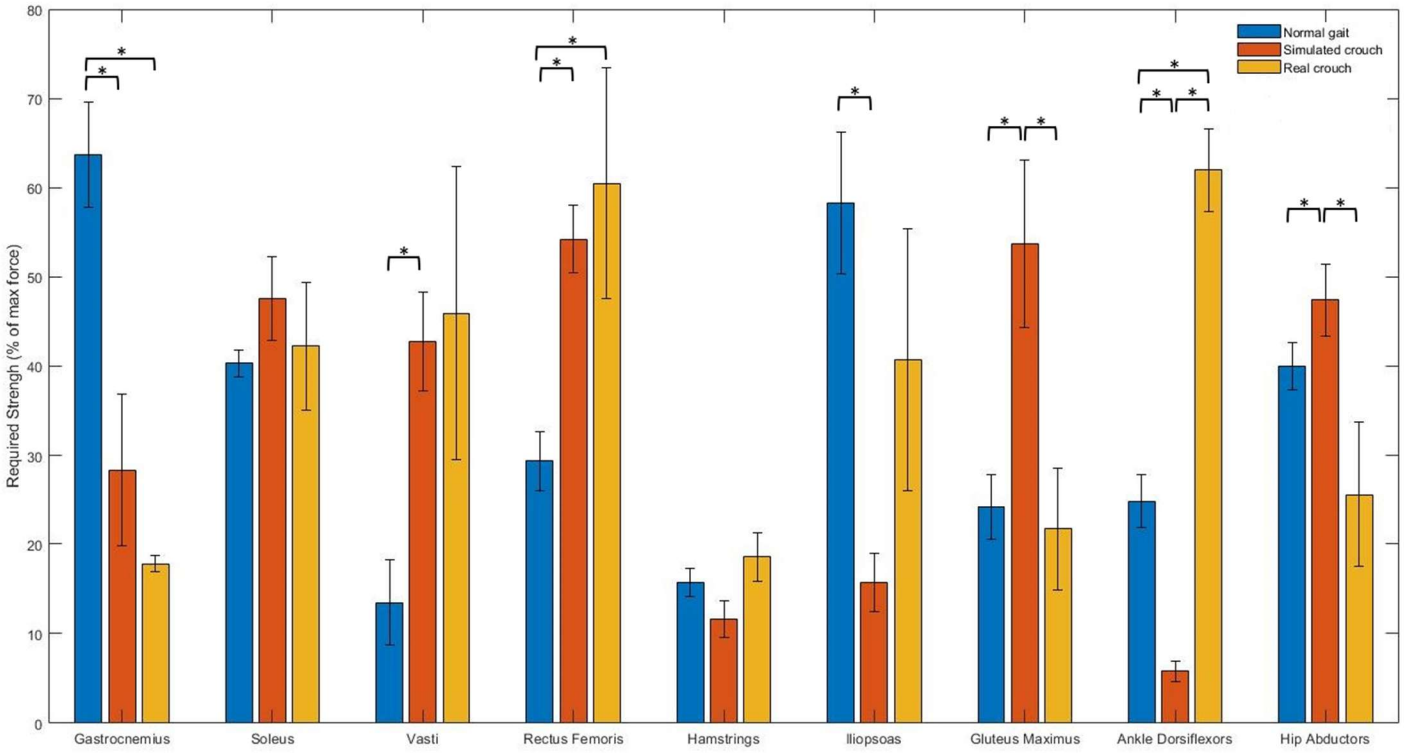

Figure 24. Required strength for each muscle group expressed as percent of the maximum isometric force. Error bars are ±1 standard error.

The force-generating capacity can be an important parameter when comparing crouch gait with unimpaired gait. It may provide insight into individual muscle weakness, which is one of the most common causes of these gait disturbances. The figure above presents the required strength for each muscle group, expressed as percent of the maximum isometric force. The results show that crouch gait required much less gastrocnemius' force than unimpaired gait, while ankle dorsiflexors and rectus femoris were much more required in the abnormal gait. Additionally, simulated crouch demanded more from the gluteus maximus and hip abductors than real crouch, whereas the ankle dorsiflexors proved to be much more in demand during real crouch.

5.4 Induced Acceleration Analysis

The final step of this work was to calculate the acceleration of the mass centre generated by individual muscles, which can provide insight into how each muscle contributes to support and progression during stance. The muscle groups considered in this analysis are the same as in CMC.

In figure 25, the muscle contributions for the vertical and fore-aft accelerations of the mass centre are displayed throughout the stance phase, for the CP children. From these results, it is possible to notice that the vasti mostly contributes to upward accelerations of the mass centre in the first 30% of the stance, and after that, the major contribution comes from the soleus. Considering the same direction, the gastrocnemius also contributes upwards, but more steadily throughout this gait phase. The ankle dorsiflexors are the major responsible for the downward acceleration and in slowing the forward progression. They appear to always contribute at the beginning of the stance phase, although it is unclear if they also contribute during the rest of the stance in crouch gait. The forward acceleration of the mass centre is mostly guaranteed at the end of the stance phase by the soleus and gastrocnemius. The gastrocnemius contributes to the progression only at the end of this gait period, while the soleus' contribution is constant during the stance. Finally, the vasti and rectus femoris also have a significant role in slowing the forward acceleration of the body, but the part of the stance in which they contribute the most it is not clear in these results concerning crouch gait.

Regarding the simulated crouch and unimpaired gait performed by the healthy children, the results of one representative subject of each gait pattern can be seen in figure 26. In simulated crouch, for the major muscle contributors of both vertical and for-aft accelerations, the periods of greatest contributions are uncertain during the gait cycle. However, it is possible to state that soleus and gastrocnemius still being those which provide the greatest contribution to progression and support, while the ankle dorsiflexors act to oppose the upward acceleration, and the vasti is the greatest opponent to the forward acceleration. In unimpaired gait, the results showed that soleus and gastrocnemius produce greater forward and vertical acceleration of the mass centre mainly during terminal stance. Additionally, the hip abductors are the major contributors to support and to slow the forward acceleration in early stance, although this same muscle group act at the end of the stance contributing to downward and forward accelerations. The ankle dorsiflexors start by contributing to the vertical acceleration, but in mid-stance change their behaviour to contribute significantly to the downward acceleration. The greatest opposition to forward acceleration occurs throughout the mid-stance, and the major contributors are rectus femoris and ankle dorsiflexors. At last, the iliopsoas contributes to the forward and backward accelerations during terminal stance.

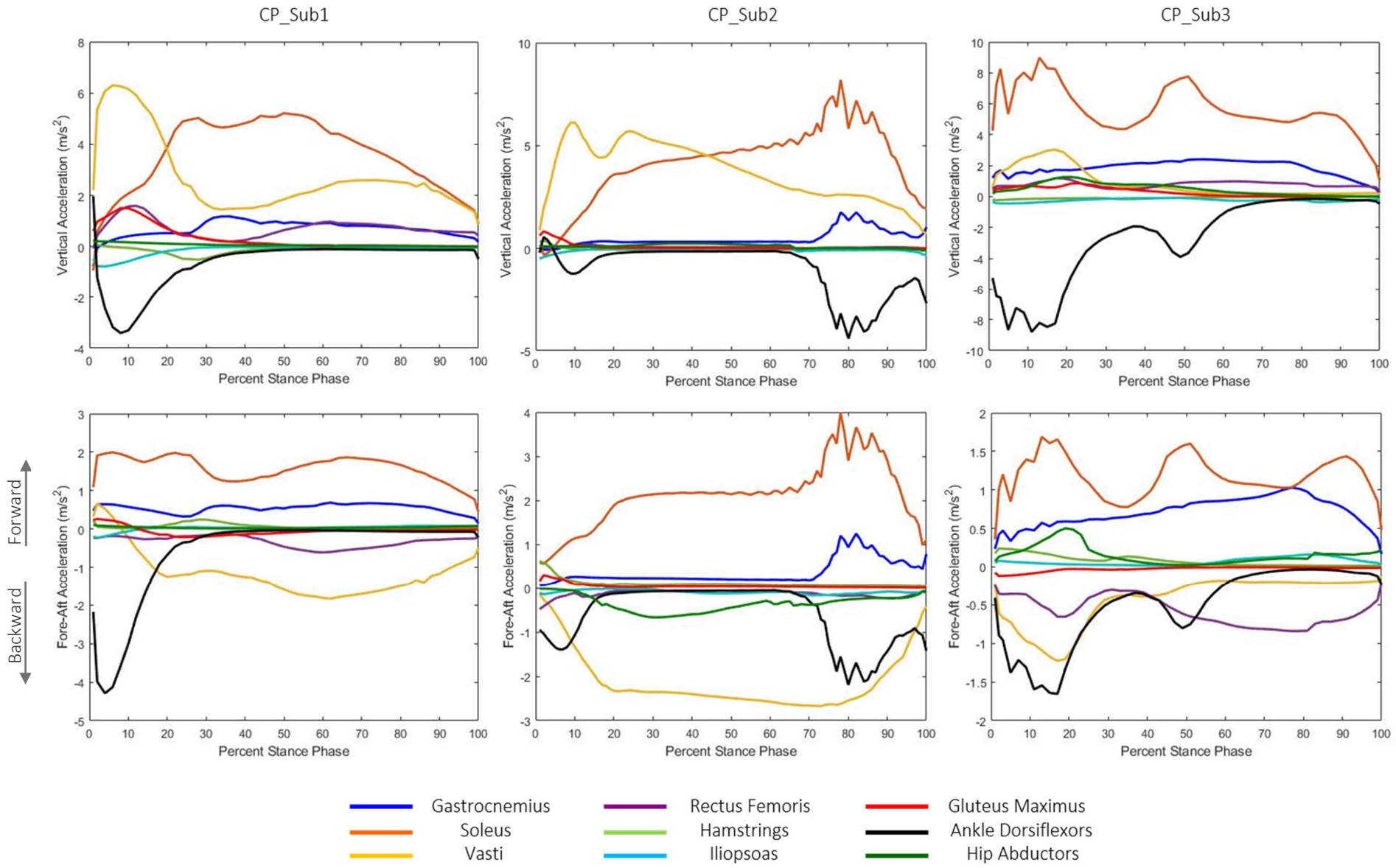

Figure 25. Contributions of each muscle group to the accelerations of the body's centre of mass, along the vertical and fore-aft directions. These contributions refer to the CP children group.

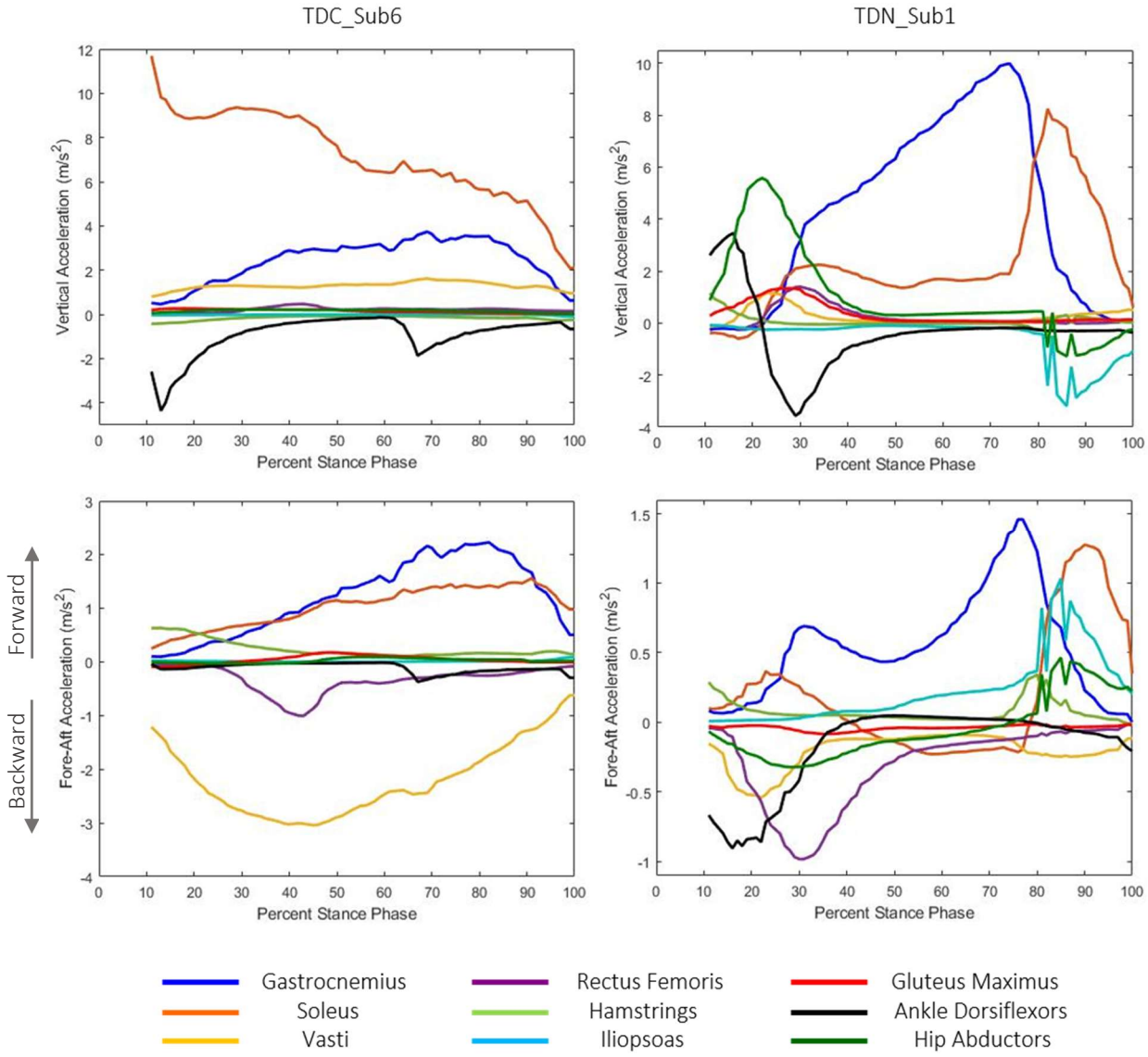

Figure 26. Contributions of each muscle group to the accelerations of the body's centre of mass, along the vertical and fore-aft directions. These contributions refer to one of the TD children simulating crouch gait, and another performing normal walking, TDC_Sub6, and TDN_Sub1 respectively.

To better understand how much each muscle contributes to the mass centre accelerations, the average values were calculated and represented in the bar plots present in figures 27 and 28. This way to display the acceleration values helps to compare the different gait patterns performed.

In both unimpaired gait and simulated crouch, the soleus and the gastrocnemius appear to be the muscle groups that contribute the most to the upward acceleration of the mass centre. On the other hand, in crouch gait, the major contributors to support are the vasti and the soleus, although the gastrocnemius still have a significant contribution. The upward acceleration produced by soleus was greater during simulated crouch than normal gait and real crouch, while the contribution of the gastrocnemius, was greater during unimpaired gait than simulated and real crouch gait.

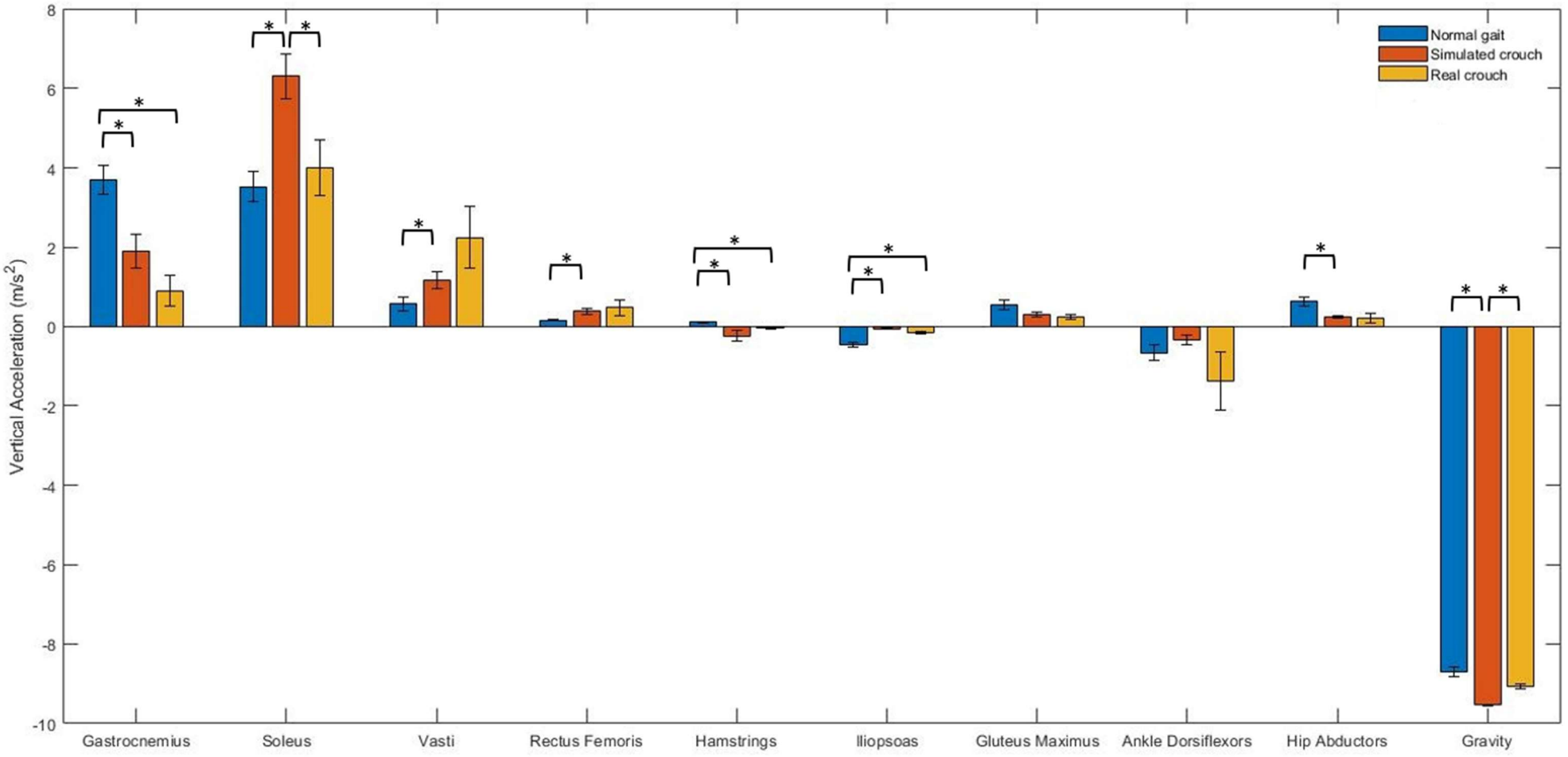

Figure 27. The average vertical accelerations of the mass centre during stance produced by each muscle. Gravity indicates the acceleration of the mass centre when only gravity is applied. Error bars are ±1 standard error.

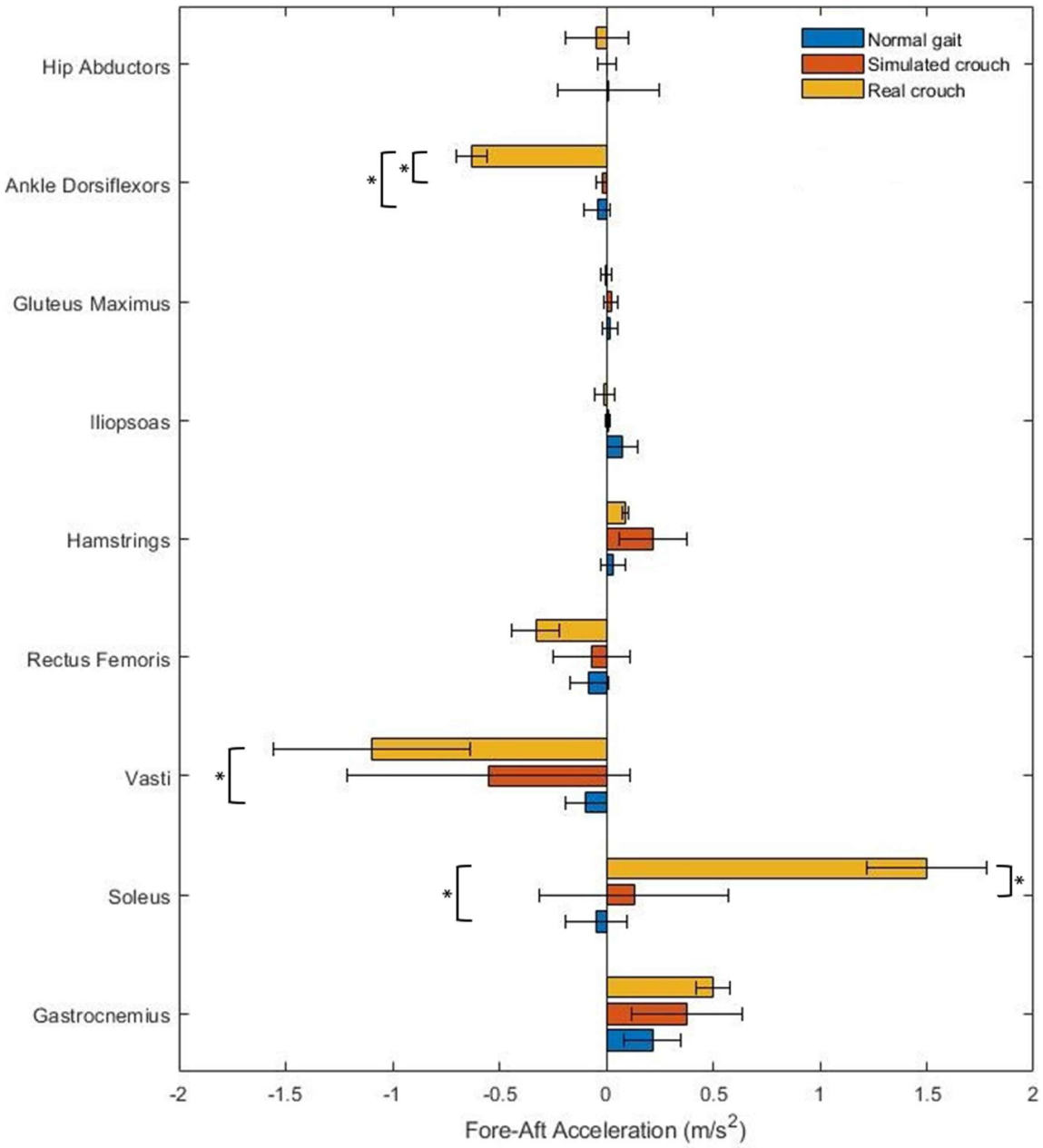

Figure 28. The average for-aft accelerations of the mass centre during stance produced by each muscle. Error bars are ±1 standard error.

The ankle dorsiflexors produced the greatest downward acceleration in all of the gait patterns performed. The positive contributions of the vasti and rectus femoris to vertical acceleration was greater in simulated crouch than normal gait. In contrast, the same contribution from the hip abductors was greater during unimpaired gait when compared with simulated crouch. In both real and simulated crouch, the hamstrings produced downward accelerations, but in normal gait, this muscle group contributed to upward acceleration. The downward acceleration produced by the iliopsoas was significantly greater in normal gait than simulate and real crouch gait.

Regarding fore-aft accelerations, the results were more similar between the research groups. The hamstrings and gastrocnemius produced significant contributions to forward acceleration of the mass centre, while the rectus femoris contributed in the opposite direction, in all of the gait patterns performed. The vasti produced backward acceleration in all of the gait patterns, but the acceleration produced in real crouch was significantly greater than in normal gait. The soleus contributed to progression in simulated and real crouch, although the forward acceleration was greater in real crouch gait. In unimpaired gait, this muscle produced accelerations in the opposite direction. Finally, the ankle dorsiflexors barely contributed to the acceleration of the mass centre, considering the fore-aft direction, in normal gait and simulated crouch, but in real crouch, they presented a significant contribution to backward acceleration.

5.5 Statistical tests used for group comparison

In order to test statistically significant differences between the groups, two different statistical tests were applied. Both are non-parametric tests due to the small number of samples considered and, consequently, to the impossibility of testing the normality of each distribution. Since the typically developing children are performing two different gait patterns, there are different group results for the same subjects, which have to be considered as paired samples. When comparing the results of the CP children with any results of the healthy children, they are considered independent samples, so the mean results from each group had to be compared two by two. The Mann-Whitney test was used to compare the group means of children with cerebral palsy performing crouch gait with healthy children, both simulating the pathological gait and performing unimpaired gait. To differentiate the group means obtained from TD children's results, walking in these different gait patterns, it was used the Wilcoxon Signed-Rank Test, as they consist of paired samples. Both statistical tests were performed using the IBM SPSS Statistics software, and the conclusions were taken based on the p-values obtained, considering a 95% confidence interval.

6. Discussion

This dissertation aimed to estimate and compare muscle forces in simulated and real crouch gait, investigate the individual muscle contributions to vertical and fore-aft acceleration of the mass centre in both gait performances, and evaluate the capacity of neurologically intact children to imitate crouch gait.

The crouch gait subjects produced joint angles and moments in accordance with previous studies (Steele et al., 2010, 2012, 2013), which classify the gait performed as severe crouch gait. They presented excessive hip and knee flexion, and increased ankle dorsiflexion, throughout the entire gait cycle. The results obtained for the hip and knee joints' parameters during simulated crouch followed the same trend, but with a slightly higher capacity to extend these joints. The healthy children showed some difficulty in simulating the characteristic ankle dorsiflexion commonly seen in crouch gait. For normal gait, it was comparable to that observed in the literature, as both joint moments and angles followed the expected pattern.

The muscle forces were computed using CMC and the instants during the stance phase, at which each muscle had its maximum force generation, were analysed. The gastrocnemius and soleus are considered to be the main muscles responsible for the ankle plantarflexion, which in normal gait begins in early single support and continues all along the stance phase into the pre-swing (Neptune et al., 2001). In this study, the healthy subjects showed peak forces from these plantarflexors during terminal stance and pre-swing, for both gait patterns performed, although simulated crouch required more strength from these muscles throughout the stance phase. In these final stages of the stance, the ankle dorsiflexors are responsible for counteracting the weight of the body to accelerate the leg into swing. Real crouch displayed a similar behaviour to simulated crouch concerning the force-generating extent of these plantarflexors during the stance. The gastrocnemius produced more force during unimpaired gait compared with both simulated and real crouch. In turn, the soleus only showed statistically significant differences in this parameter when comparing normal gait and simulated crouch, having unimpaired gait showed lower muscle forces.

The force-generating capacity is related to the percentage of maximum isometric muscle force that was required during the gait phase that is being studied. Regarding this parameter, simulated and real crouch required less gastrocnemius strength than normal gait. It was previously suggested that weakness of the gastrocnemius could contribute to crouch gait (Steele, van der Krogt, et al., 2012), and from the results obtained it is possible to support this hypothesis. Furthermore, by comparing the TD children simulating crouch with the CP children, the results indicate that the

diminished capacity to generate force from the gastrocnemius may be more related to the posture adopted in crouch gait than muscle weakness.

Considering the stance phase in normal walking, the quadriceps, which include the rectus femoris and the three vasti muscles, are the major responsible for knee extension and, logically, for the deceleration of knee flexion (Zajac et al., 2003). The muscle forces from this muscle group are expected mainly during mid-stance (Anderson & Pandy, 2003), which is what is observed in the results from the TD children performing unimpaired gait. On the other hand, in simulated and real crouch gait, the quadriceps have a much more continuous action throughout the stance phase, as was expected based on Steele's work (Steele, DeMers, et al., 2012). Furthermore, the results indicate that the forces produced by vasti and rectus femoris were significantly greater in simulated crouch than in unimpaired gait. This was also expected by comparing real crouch gait with normal gait (Perry et al., 1975; Hsu et al., 1993; Steele et al., 2013). Even though the force values were higher in real crouch gait, this difference could not be considered statistically significant due to the high variance of this parameter among the CP children. Regarding the force-generating capacity of the vasti and rectus femoris, simulated and real crouch gait required more strength than unimpaired gait, which indicates that weakness of the quadriceps is not a likely contributor to crouch gait (Steele, van der Krogt, et al., 2012). Once again, both the magnitude of the forces produced by the rectus femoris and vasti and the force-generating capacity of these muscles do not differ from simulated to real crouch gait, which may suggest that the overload on these muscles is necessary to maintain the crouch posture.

The hamstrings are the agonist muscles of knee flexion. According to Anderson and Pandy (Anderson and Pandy, 2003), the hamstrings are expected to generate force mostly during early stance, when considering just the stance phase. However, during pre-swing, there is also some activity from this muscle group due to a characteristic slight bending of the knee. This behaviour throughout the stance can be verified in the muscle forces obtained for the neurologically intact children in normal gait, whereas in both simulated and real crouch the muscles did not show significant force production during pre-swing. Additionally, in these two abnormal gait performances, the hamstrings mostly generated force during early stance but also mid-stance. Despite these differences, the forces produced by the hamstrings were approximately the same for all of the research groups, as well as the required strength from this muscle group, as expected (Steele, van der Krogt, et al., 2012).

The main muscle group responsible for hip flexion is the iliopsoas. Iliopsoas normally develops its highest amount of force during terminal stance (Anderson and Pandy, 2003), which can be

observed in the results estimated for the healthy children. Simulated crouch gait and the crouch performed by CP_Sub1 and CP_Sub2 did not show significant force values during stance, whereas CP_Sub3 displayed a considerable amount of force in terminal stance, although significantly less than that generated during the same period in unimpaired gait. This is related to the similarity found when analysing hip flexion angles for this subject with respect to the TD children performing normal walking. As it was verified in a previous study (Steele, van der Krogt, et al., 2012), normal gait and crouch gait required approximately the same iliopsoas' strength during stance.

The primary function of the gluteus maximus is hip extension. In unimpaired gait, the muscle forces produced by this muscle reached the highest values during mid-stance, while during the rest of the stance, the values decreased substantially. This was expected because the most upright position is adopted in mid-stance. Regarding the children with cerebral palsy, gluteus maximus had its highest force production during early stance or mid-stance, presenting low values of muscle force during terminal stance and pre-swing. However, simulated gait showed a continuous production of muscle strength throughout the stance, with values significantly higher than the other two gait patterns performed. Simulated crouch required a greater demand on the gluteus maximus than unimpaired gait and real crouch gait. The TD children performing this abnormal gait showed a higher capacity in extending the hip compared with the CP children, so it was expected a higher demand on this muscle.

According to previous studies (Steele, van der Krogt, et al., 2012; Steele et al., 2013), no differences were expected in the strength requirement for the ankle dorsiflexors, when comparing normal walking with crouch gait. However, the forces produced by these muscles were significantly greater in CG than in unimpaired gait. Additionally, simulated crouch presented the lowest force values of the three groups. A previous study (Balzer et al., 2013) had also come to this result by comparing simulated crouch with normal gait.

The hip abductors strength required was significantly less during stance in real crouch gait and unimpaired gait than simulated crouch. Differences between normal walking the real abnormal gait were not identified, contrary to the results from Steele's work (Steele, van der Krogt, et al., 2012).

Muscles are responsible to oppose the effect of gravity in the skeletal, enabling the vertical and forward propulsion of the body, so analysing individual muscle contributions to the mass centre accelerations affords further insight into how support and progression works during gait. In early stance (approximately the first 17% of stance phase), the ankle dorsiflexors are expected to be the main contributors to support, promoting the upwards mass centre acceleration, in unimpaired gait (Mochon and McMahon, 1980; Winter, 1980; Kepple et al., 1997; Anderson and Pandy, 2003). Their

function during this stage is to resist the fall of the forefoot because of the weight acceptance, characteristic of this phase before the foot-flat moment. The results of this study are consistent with the assumptions for the normal gait regarding this muscle group in early stance, whereas in simulated and crouch gait these muscles only contributed to the downward acceleration of the mass centre, having a negative effect in supporting the body. As this behaviour is observed in both simulated and real performances of crouch gait, it may be related to the crouch posture adopted, and probably not with any muscular disfunction of the ankle dorsiflexors. Due to this lack of support during early stance by this muscle group, the vasti and soleus are activated earlier to compensate for the downward acceleration generated. This is observed in simulated and real crouch gait, which suggests that these two muscles are crucial in supporting the body throughout this gait phase. In this first stage of the stance, the vertical acceleration of the mass centre is much more relevant than the fore-aft acceleration, although this is still significant. In normal walking and real crouch, the major contributors to backward acceleration of the mass centre are the ankle dorsiflexors and vasti, while in simulated crouch gait, the dorsiflexors do not affect fore-aft accelerations, being the quadriceps the sole muscles responsible.

Regarding the mid-stance phase (approximately between 17% and 50% of the stance phase) in unimpaired gait, the gluteus maximus, vasti and rectus femoris are expected to produce the bulk of the contributions to support, yet the posterior components of hip abductors generate relevant upwards acceleration during this period (Mochon and McMahon, 1980; Winter, 1980; Kepple et al., 1997; Anderson and Pandy, 2003; Zajac et al., 2003). These contributions were identified in the results of normal walking, with an additional substantial contribution of the ankle plantarflexors, which was not expected. In simulated and real crouch gait, the muscles that produced the most significant upwards accelerations were the ankle plantarflexors and vasti, while the hip abductors and gastrocnemius had no significant effect in either direction of the vertical mass centre acceleration, compared with normal walking. In order to compensate for the lack of these muscles' contributions to support, the soleus was much more required to act in both simulated and real crouch, and the vasti contributed significantly more in real crouch than unimpaired gait.

During terminal stance (approximately between 50% and 83% of the stance phase) of unimpaired gait, the upwards acceleration of the mass centre is still the most relevant, and it is ensured by the contributions of the soleus and gastrocnemius, as it was expected (Zajac et al, 2003; Neptune et al., 2001). During mid-stance, in both simulated and real crouch gaits, the contribution of the gastrocnemius along the vertical direction is much less compared to unimpaired gait. That lower muscle contribution to support is compensated by a larger upwards acceleration produced by the vasti.

Lastly, the stance phase ends with pre-swing (approximately between 83% and 100% of the stance phase). This period is characterized by a large component of progression, which is represented by a significant increase in the forward acceleration profile of the mass centre. In unimpaired gait, the support during pre-swing is mainly provided by the ankle plantarflexors, in which the soleus contributes approximately twice as much as gastrocnemius (Sutherland et al., 1980; Perry, 1992; Kepple et al., 1997; Neptune et al., 2001; Anderson and Pandy, 2003; Zajac et al., 2003). Furthermore, these muscles are also the main responsible for the forward progression during this phase. The results show that the ankle plantarflexors produced indeed the highest accelerations in both forward and upwards directions in normal walking, but also simulated and real crouch gait. Although the soleus and gastrocnemius are the major contributors, the vasti also produced a relevant vertical acceleration of the mass centre, in simulated and real abnormal gait performances.

The erect posture adopted in unimpaired gait supports the bodyweight better than crouch posture, so the gravity effect on downwards acceleration of the mass centre is expected to be higher during crouch gait (Steele et al., 2013). Additionally, the abnormal posture is characterized by an increased knee and hip extensor moments, which also difficult the upwards acceleration of the mass centre in CP children. This lack of skeletal support in simulated and real couch gait seems to lead to a constant activation of the major contributors to support throughout the stance, which are shown to be the same muscle groups (vasti, soleus and gastrocnemius) for all of the gaits performed. The results suggest that in simulated crouch, the child relies more on the soleus' contribution to upwards acceleration than in real crouch. On the other hand, the CP children seem to rely more on the upwards acceleration produced by the vasti, than the TD children simulating crouch gait. The results are not clear concerning this last assumption because, although the vasti produced greater upwards accelerations during real crouch than simulated crouch, this difference was not proven to be statistically significant due to the high variance of this parameter among the CP children.

In unimpaired gait, the ankle plantarflexors and quadriceps are expected to produce opposing fore-aft accelerations of the mass centre in different phases of the gait (Steele et al., 2013). The balance between the activation of these two muscle groups enables the subject to modulate gait speed. In both simulated and real crouch, these muscles also produced opposite accelerations in the for-aft direction, but they were almost constant throughout the stance phase, contrary to what was observed in normal walking. This explains the limitation in controlling the speed of walking, which is characteristic in children with cerebral palsy who present crouch gait. The major contributors to the fore-aft acceleration of the mass centre were shown to be the same for all the

gaits performed. However, the ankle dorsiflexors produced a significantly greater backward acceleration in real crouch than in simulated crouch and normal walking, which seems to be compensated by the higher contribution to forward acceleration by the soleus.

7. Conclusion

The main goals of this dissertation were to investigate the muscle forces and individual muscle contributions to vertical and fore-aft acceleration of the mass centre during stance in simulated crouch gait performed by neurologically intact children, and compare it with the same results from CP children with crouch gait. Furthermore, this work had also the purpose to evaluate the capacity of healthy children to imitate crouch gait, given that there is little literature using this approach. All the results were obtained using musculoskeletal modelling and, based on those results, it is possible to conclude that it was a valid and capable method to successfully compute the analyses carried out for this study.

The joint angles and moments for the simulated crouch gait showed a similar pattern to real abnormal gait, and significant differences when compared with unimpaired gait. This suggests that healthy children are capable to simulate crouch gait in a reproducible manner.

The results indicate that simulated and real crouch gait present a similar muscle behaviour throughout the stance phase, relying mostly on the same muscle groups. Thus, we can conclude that the most significant differences between this pathological gait and normal walking are more likely to be related to the crouch posture adopted than muscular dysfunctions. The individual muscle contributions to vertical and fore-aft acceleration of the mass centre showed that the major contributors to vertical acceleration are the same in all of the research groups, being the vasti, soleus and gastrocnemius very important in supporting the crouch posture.

7.1 Limitations

The results of this study should be taken in the context of the study's limitations.

Although the generic model used is widely recommended as indicated for gait analysis, it is still a simplified representation of the musculoskeletal system of the lower limbs. Furthermore, this generic model represents the musculoskeletal structure of an adult, not a child, which involves further errors in the scaling process. As it was explained before, the subtalar and metatarsophalangeal joints had to be locked, keeping the foot at a neutral position, and taking out two degrees of freedom concerning foot adduction/abduction and inversion/eversion. In addition, the simulations performed do not accounted for possible bone deformities, sometimes present in CP children walking in a

crouch gait. The muscle weakness is commonly considered to be one of the causes to crouch gait, but it is difficult to evaluate. Therefore, it was not considered in scaling the optimal muscle forces.

At last, the very small number of children with cerebral palsy analysed is one of the major limitations of this work, in addition to the fact that it was not possible to obtain ground reaction forces during early stance for the healthy children.

7.2 Future work

Firstly, it would be interesting to study more deeply the differences in muscle activity between the simulated crouch and the real pathological gait by considering a substantially larger sample of subjects for all of the research groups. Enlarging the samples can also make the results more robust.

Secondly, investigating the lengths and shortening velocities of the musculoskeletal units throughout the gait cycle would give an even greater insight on the muscle function in simulated and real crouch gait.

Finally, performing an intra-individual reproducibility study of all the parameters considered in this dissertation, would help to determine the acceptable variability in analysing the results obtained. All the subjects from all the research groups should be included.

8. References

Ajay, S. et al. (2011). OpenSim: a musculoskeletal modeling and simulation framework for in silico investigations and exchange. Procedia Iutam, 2, pp. 212–232. doi: 10.1177/0003122413519445.Are.

Anderson, F. C., & Pandy, M. G. (1999). A dynamic optimization solution for vertical jumping in three dimensions. Computer Methods in Biomechanics and Biomedical Engineering, 2(3), pp. 201–231. doi: 10.1080/10255849908907988.

Anderson, F. C., & Pandy, M. G. (2003). Individual muscle contributions to support in normal walking. *Gait and Posture*, *17*(2), 159–169. https://doi.org/10.1016/S0966-6362(02)00073-5.

Armand, S., Decoulon, G., Bonnefoy-Mazure, A. (2016). Gait analysis in children with cerebral palsy. EFORT Open Rev. 2016 Dec 22; 1(12):448-460. doi: 10.1302/2058-5241.1.000052. PMID: 28698802; PMCID: PMC5489760.

Arnold, A.S., Anderson, F.C., Pandy, M.G., Delp,S.L. (2005). Muscular contributions to hip and knee extension during the single limb stance phase of normal gait: a framework for investigating the causes of crouch gait. Journal of Biomechanics 38, 2181–2189.

Arnold, E.M., Ward, S.R., Lieber, R.L. et al. (2010). A Model of the Lower Limb for Analysis of Human Movement. Ann Biomed Eng 38; 269–279 https://doi.org/10.1007/s10439-009-9852-5.

Baker, R. (2007). The history of gait analysis before the advent of modern computers. *Gait and Posture*, *26*(3), 331–342. https://doi.org/10.1016/j.gaitpost.2006.10.014.

Balzer, J., Schelldorfer, S., Bauer, C., & van der Linden, M. L. (2013). Effects of simulated crouch gait on foot kinematics and kinetics in healthy children. *Gait and Posture*, *38*(4), 619–624. https://doi.org/10.1016/j.gaitpost.2013.02.009.

Beals, R.K. (2001). Treatment of knee contracture in cerebral palsy by hamstring lengthening, posterior capsulotomy, and quadriceps mechanism shortening. Dev. Med. Child Neurol. 43; 802–805, doi:http://dx.doi.org/10.1111/j.1469-8749.2001.tb00166.x.

Carbone, V., Fluit, R., Pellikaan, P., van der Krogt, M., Damsgaard, M., Vigneron, L., Koopman, B., Verdonschot, N. (2014). TLEM2.0: A new complete and consistent musculoskeletal geometry dataset for subject-specific Modelling of the Lower Extremity. Proceedings of the 7th World Congress of Biomechanics Boston. WCB, U.S.A.

Centers for Disease Control and Prevention (CDC). (2019). Cerebral Palsy (CP). Available at: https://www.cdc.gov/ncbddd/cp/index.html [Accessed June 2020].

Chimera, N. J., Warren, M., Bunn, P. dos S., Silva, E. B. da, Whittaker, J. L., Booysen, N., de la Motte, S., Dennett, L., Lewis, C. L., Wilson, D., McKay, C., Warner, M., Padua, D., Emery, C. A., Stokes, M., Guduru, R. K. R., & Domeika, A. (2017). How Important is Motion Capture to Find Kinematics Of Humans ?: A Review. *British Journal of Sports Medicine*, *51*(7), 26–28.

Correa, T. A., & Pandy, M. G. (2011). A mass-length scaling law for modeling muscle strength in the lower limb. *Journal of Biomechanics*, *44*(16), 2782–2789. https://doi.org/10.1016/j.jbiomech.2011.08.024.

Delp, S. (1990). Surgery simulation: A computer graphics system to analyse and design musculoskeletal reconstructions of the lower limb. [Unpublished Ph.D. dissertation]. Stanford University.

Delp, S. L. et al. (1990). An interactive graphics-based model of the lower extremity to study orthopedic surgical procedures. IEEE transactions on Biomedical Engineering. Stanford University. doi: 10.1109/10.102791.

Delp, S. L., & Loan J. P. (2000). A computational framework for simulating and analyzing human and animal movement. Computing in Science & Engineering, vol. 2, no. 5, pp. 46-55, Sept.-Oct. 2000, doi: 10.1109/5992.877394.

Delp, S. L., Anderson, F. C., Arnold, A. S., Loan, P., Habib, A., John, C. T., Guendelman, E., & Thelen, D. G. (2007). OpenSim: Open-source software to create and analyze dynamic simulations of movement. *IEEE Transactions on Biomedical Engineering*, *54*(11), 1940–1950. https://doi.org/10.1109/TBME.2007.901024.

Dempster, W. T. (1955). Space requirements of the seated operator : geometrical, kinematic, and mechanical aspects of the body, with special reference to the limbs. University of Michigan, East Lansing.

Dreher, T., Vegvari, D., Wolf, S.I., Geisbüsch, A., Gantz, S., Wenz, W., & Braatz, F. (2012) Development of knee function after hamstring lengthening as a part of multilevel surgery in children with spastic diplegia. J. Bone Jt. Surg. Am. 94 (2012) 121–130, doi:http://dx.doi.org/10.2106/JBJS.J.00890.

Friederich, J.A.J. (1990). Muscle fiber architecture in the human lower limb. Journal of Biomechanics, 23(1), pp. 91–95. doi: 10.1227/01.NEU.0000297048.04906.5B0.

Gage, J. R., & Novacheck, T. F. (2001). An update on the treatment of gait problems in cerebral palsy. *Journal of Pediatric Orthopaedics Part B*, *10*(4), 265–274. https://doi.org/10.1097/01202412-200110000-00001.

Gage, J. R., Schwartz, M. H., Koop, S. E., & Novacheck, T. F. (2009). The Identification and Treatment of Gait Problems in Cerebral Palsy (2nd ed.). Mac Keith Press.

Galey, S. A., Lerner, Z. F., Bulea, T. C., Zimbler, S., & Damiano, D. L. (2017). Effectiveness of surgical and non-surgical management of crouch gait in cerebral palsy: A systematic review. *Gait and Posture*, *54*, 93–105. https://doi.org/10.1016/j.gaitpost.2017.02.024.

Garner, B.A., Pandy, M.G. (2003). Estimation of muscle-tendon properties in the human upperlimb. Annals of Biomedical Engineering; 31(2), 207–220.

Hall, J.E. (2015). Guyton and Hall: Textbook of Medical Physiology (13th ed.). Elsevier.

Hamner, S. R., Seth, A., & Delp, S. L. (2010). Muscle contributions to propulsion and support during running. Journal of Biomechanics, 43(14), pp. 2709–2716. doi: 10.1016/j.jbiomech.2010.06.025.

Hanavan, E. P. (1964). A Mathematical Model of the human body', Aerospace Medical Rsearch Laboratories, pp. 1–149. Available: http://oai.dtic.mil/oai/oai?verb=getRecord&metadataPrefix=html&identifier=AD0608463.

Herring, J.A. (2013). Tachdjian's Pediatric Orthopaedics: From the Texas Scottish Rite Hospital for Children (5th ed.). Elsevier Health Sciences.

Hicks, J. L., Schwartz, M. H., Arnold, A. S., & Delp, S. L. (2008). Crouched postures reduce the capacity of muscles to extend the hip and knee during the single-limb stance phase of gait. *Journal of Biomechanics*, *41*(5), 960–967. https://doi.org/10.1016/j.jbiomech.2008.01.002.

Hicks, J.L. (2010). Biomechanical guidelines for the treatment of crouch gait in children with cerebral palsy [Unpublished Degree type thesis or dissertation]. Stanford, CA: Stanford University.

Hill, A. V. (1938). The Heat of Shortening and the Dynamic Constants of Muscle. Proceedings of the Royal Society B: Biological Sciences, 126(843), pp. 136–195. doi: 10.1098/rspb.1938.0050.

Hill, A. V. (1949). The abrupt transition from rest to activity in muscle. Proceedings of the Royal Society B: Biological Sciences, 136(884), pp. 399–420. doi: 10.1098/rspb.1949.0033.

Himmelmann, K., McManus, V., Hagberg, G., Uvebrant, P., Krägeloh-Mann, I., & Cans, C. (2009). Dyskinetic cerebral palsy in Europe: Trends in prevalence and severity. *Archives of Disease in Childhood*, *94*(12), 921–926. https://doi.org/10.1136/adc.2008.144014.

Hsu, A.T., Perry, J., Gronley, J.K., Hislop, H.J. (1993). Quadriceps force and myoelectric activity during flexed knee stance. Clinical Orthopaedics and Related Research, 254–262.

Huxley, A. F., & Simmons, R. M. (1971) Proposed mechanism of force generation in striated muscle, Nature, 233(5321), pp. 533–538. doi: 10.1038/233533a0.

Inman, V. T. (1976). The Joints of the Ankle. in Wilkins, B. W. & (ed.). Baltimore: Williams & Wilkins.

Jacobsson, B., & Hagberg, G. (2004). Antenatal risk factors for cerebral palsy. *Best Practice and Research: Clinical Obstetrics and Gynaecology*, *18*(3), 425–436. https://doi.org/10.1016/j.bpobgyn.2004.02.011.

Kainz, H., Goudriaan, M., Falisse, A., Huenaerts, C., Desloovere, K., De Groote, F., & Jonkers, I. (2018). The influence of maximum isometric muscle force scaling on estimated muscle forces from musculoskeletal models of children with cerebral palsy. *Gait and Posture*, *65*(July), 213–220. https://doi.org/10.1016/j.gaitpost.2018.07.172.

Kedem, P., & Scher, D. M. (2016). Evaluation and management of crouch gait. Curr. Opin. Pediatr. 28, 55–59. doi: 10.1097/MOP.0000000000000316.

Kepple, T.M., Siegel, K.L, Stanhope, S.J. (1997). Relative contributions of the lower extremity joint moments to forward progression and support during gait. Gait Posture 1997;6:1-8.

Kimmel, S. A., & Schwartz, M. H. (2006). A base line of dynamic muscle function during gait. Gait & Posture 23,211–221.

Khouri, N., & Desailly, E. (2017). Contribution of clinical gait analysis to single-event multi-level surgery in children with cerebral palsy. *Orthopaedics and Traumatology: Surgery and Research*, *103*(1), S105–S111. https://doi.org/10.1016/j.otsr.2016.11.004.

Klein Horsman, M.D., Koopman, H.F., van der Helm, F.C., Prosé, L.P., & Veeger, H.E. (2007). Morphological muscle and joint parameters for musculoskeletal modelling of the lower extremity. Clin Biomech (Bristol, Avon). 2007 Feb; 22(2):239-47. doi: 10.1016/j.clinbiomech.2006.10.003.

Krägeloh-Mann, I., & Cans, C. (2009). Cerebral palsy update. *Brain and Development*, *31*(7), 537–544. https://doi.org/10.1016/j.braindev.2009.03.009.

Lee, D., Glueck, M., Khan, A., Fiume, E., & Jackson, K. (2011). Modeling and simulation of skeletal muscle for computer graphics: A survey. In *Foundations and Trends in Computer Graphics and Vision* (Vol. 7, Issue 4). https://doi.org/10.1561/0600000036.

Lerner, Z. F., Damiano, D. L., Park, H. S., Gravunder, A. J., & Bulea, T. C. (2017). A Robotic Exoskeleton for Treatment of Crouch Gait in Children with Cerebral Palsy: Design and Initial Application. *IEEE Transactions on Neural Systems and Rehabilitation Engineering*, *25*(6), 650–659. https://doi.org/10.1109/TNSRE.2016.2595501.

Liu, M. Q., Anderson, F.C., Pandy, M. G., & Delp, S. L. (2006). Muscles that support the body also modulate forward progression during walking. Journal of Biomechanics 39, 2623–2630.

Liu, M. Q., Anderson, F.C., Schwartz, M.H., & Delp, S.L. (2008). Muscle contributions to support and progression over a range of walking speeds. Journal of Biomechanics; 41:3243–52.

Lloyd, D. G., & Besier, T. F. (2003). An EMG-driven musculoskeletal model to estimate muscle forces and knee joint moments in vivo. Journal of Biomechanics, 36(6), pp. 765–776. doi: 10.1016/S0021-9290(03)00010-1.

Lu, T.W., & O'Connor, J.J. (1999). Bone position estimation from skin marker coordinates using global optimization with joint constraints. J Biomech 32: 129-134.

Matjačić, Z., & Olenšek, A. (2007). Biomechanical characterization and clinical implications of artificially induced crouch walking: Differences between pure iliopsoas, pure hamstrings and combination of iliopsoas and hamstrings contractures. *Journal of Biomechanics*, *40*(3), 491–501. https://doi.org/10.1016/j.jbiomech.2006.02.018.

Mochon, S., & McMahon, T.A. (1980) Ballistic walking: an improved model. Math Biosci 1980; 52:241 /60.

Moreau, N., Tinsley, S., & Li, L. (2005). Progression of knee joint kinematics in children with cerebral palsy with and without rectus femoris transfers: a long-term follow up. Gait Posture 22, 132–137, doi:http://dx.doi.org/10.1016/j.gaitpost.2004.08.003.

Moster, D., Wilcox, A.J., Vollset, S.E., Markestad, T., & Lie, R.T. (2010). Cerebral palsy among term and postterm births. JAMA; 304(9):976–82. doi:10.1001/jama.2010.1271.

Neptune, R. R., Kautz, S. A., & Zajac, F. E. (2001). Contributions of the individual ankle plantar flexors to support, forward progression and swing initiation during walking. *Journal of Biomechanics*, *34*(11), 1387–1398. https://doi.org/10.1016/S0021-9290(01)00105-1.

Neptune, R. R., Zajac, F. E., & Kautz, S. A. (2004). Muscle mechanical work requirements during normal walking: the energetic cost of raising the body's center-of-mass is significant. J Biomech.; 37(6):817-25. doi: 10.1016/j.jbiomech.2003.11.001. PMID: 15111069.

NICE - National Institute for Health and Care Excellence. (2020). Cerebral palsy in children and young people [Quality standard - QS162]. NICE Guidance. https://www.nice.org.uk/guidance/qs162 [Accessed June 2020].

Nisell, R., Nemeth, G., & Ohlsen, H. (1986). Joint forces in exension of the knee - analysis of a mechanical model. Acta Orthopaedica Scandinavica, 57(1), pp. 41–46.

Nonnekes, J., Goselink, R. J. M., Růzicka, E., Fasano, A., Nutt, J. G., & Bloem, B. R. (2018). Neurological disorders of gait, balance and posture: A sign-based approach. *Nature Reviews Neurology*, *14*(3), 183–189. https://doi.org/10.1038/nrneurol.2017.178.

Palisano, R., Rosenbaum, P., Walter, S., Russell, D., Wood, E., & Galuppi, B. (1997). Development and reliability of a system to classify gross motor function in children with Cerebral Palsy. Developmental medicine and child neurology. 39; 214-23. 10.1111/dmcn.1997.39.issue-4.

Pandy, M. G. (2001). Computer Modelling and Simulation of Human Movement, Annual review of biomedical engineering, 3(1), pp. 245–273. doi: 10.1146/annurev.bioeng.3.1.245.

Pandy, M. G., & Barr, R. E. (2004). Biomechanics of the Musculoskeletal System, in McGraw-Hill (ed.) Standard Handbook of Biomedical Engineering and Design. McGraw-Hill, pp. 1–34. doi: 10.1.

Perry, J., Antonelli, D., & Ford, W. (1975). Analysis of knee-joint forces during flexed-knee stance. J Bone Joint Surg Am; 57:961–7.

Perry, J. (1992). Gait analysis: normal and pathological function. Journal of Pediatric Orthopaedics: November-December 1992 - Volume 12 - Issue 6 - p 815.

Pinzur, M. S. (1987). Gait patterns in spastic hemiplegia in children and young adults. The Journal of Bone and Joint Surgery: Oct 1987 - Volume 69 - Issue 8 - p 1304.

Pizzolato, C., Reggiani, M., Modenese, L., & Lloyd D. G. (2017). Real-time inverse kinematics and inverse dynamics for lower limb applications using OpenSim. Computer Methods in Biomechanics and Biomedical Engineering, 20:4, 436-445, DOI: 10.1080/10255842.2016.1240789.

Prilutsky, B.I. (2000). Coordination of two- and one-joint muscles: functional consequences and implications for motor control. Motor Control. 4; 1-44.

Purves, D., Augustine, G.J., Fitzpatrick, D., et al. (2001). Neuroscience (2nd ed.): The Motor Unit. Sunderland (MA): Sinauer Associates. Available: https://www.ncbi.nlm.nih.gov/books/NBK10874/ [Accessed October 2020].

Rajagopal, A., Dembia, C.L., DeMers, M.S., Delp, D.D., Hicks, J.L., Delp, S.L. (2016) Full-Body Musculoskeletal Model for Muscle-Driven Simulation of Human Gait. IEEE Trans Biomed Eng. 2016 Oct;63(10):2068-79. doi: 10.1109/TBME.2016.2586891.

Rezgui, T., Megrot, F., Fradet, L., & Marin, F. (2013). On the imitation of CP gait patterns by healthy subjects. *Gait and Posture*, *38*(4), 576–581. https://doi.org/10.1016/j.gaitpost.2013.01.022

Ries, A.J., Schwartz, M.H. (2018). Ground reaction and solid ankle-foot orthoses are equivalent for the correction of crouch gait in children with cerebral palsy. Dev Med Child Neurol. 2019 Feb; 61(2):219-225. doi: 10.1111/dmcn.13999.

Rodda, J., & Graham, H.K. (2001). Classification of gait patterns in spastic hemiplegia and spastic diplegia: a basis for a management algorithm. Eur J Neurol , pp. 98-108.

Rose, J., Gamble, J.G., Burgos, A., Medeiros, J., & Haskell, W.L. (1990). Energy expenditure index of walking for normal children and for children with cerebral palsy. Developmental Medicine and Child Neurology 32, 333–340.

Rosenbaum, P. (2007). A report: the definition and classification of cerebral palsy April 2006. Dev Med Child Neurol Suppl; 109:8–14.

Saw, A., Smith, P.A., Sirirungruangsarn, Y., Chen, S., Hassani, S., Harris, G., & Kuo, K.N. (2003). Rectus femoris transfer for children with cerebral palsy: long-term outcome. J. Pediatr. Orthop. 23; 672–678.

Scianni, A., Butler, J.M., Ada, L., & Teixeira-Salmela, L.F. (2009). Muscle strengthening is not effective in children and adolescents with cerebral palsy: a systematic review. Aust J Physiother; 55:81–87.

SimTK Confluence. Musculoskeletal Models. OpenSim Documentation – Models, Data, & Utilities. https://simtk-confluence.stanford.edu/display/OpenSim/ [Accessed October 2020].

SimTK Opensim (2012). User's Guide. Release 2.4. 2016 Oct. Available at: https://opensim.stanford [Accessed October 2020].

Stavsky, M., Mor, O., Mastrolia, S.A., Greenbaum, S., Than, N.G., & Erez, O. (2017). Cerebral Palsy-Trends in Epidemiology and Recent Development in Prenatal Mechanisms of Disease, Treatment, and Prevention. Frontiers in Pediatrics; 5:21 Epub 2017/03/01. 10.3389/fped.2017.00021.

Steele, K. M., DeMers, M. S., Schwartz, M. H., & Delp, S. L. (2012). Compressive tibiofemoral force during crouch gait. Gait and Posture, 35(4), 556–560. https://doi.org/10.1016/j.gaitpost.2011.11.023.

Steele, K. M., Damiano, D.L., Eek, M.N., et al. (2012). Characteristics associated with improved knee extension after strength training for individuals with cerebral palsy and crouch gait. Pediatr Rehabil Med; 5:99–106.

Steele, K. M., Seth, A., Hicks, J. L., Schwartz, M. H., & Delp, S. L. (2013). Muscle contributions to vertical and fore-aft accelerations are altered in subjects with crouch gait. *Gait and Posture*, *38*(1), 86–91. https://doi.org/10.1016/j.gaitpost.2012.10.019.

Steele, K. M., Seth, A., Hicks, J. L., Schwartz, M. S., & Delp, S. L. (2010). Muscle contributions to support and progression during single-limb stance in crouch gait. Journal of Biomechanics, 43(11), 2099–2105. https://doi.org/10.1016/j.jbiomech.2010.04.003.

Steele, K. M., van der Krogt, M. M., Schwartz, M. H., & Delp, S. L. (2012). How much muscle strength is required to walk in a crouch gait? Journal of Biomechanics, 45(15), 2564–2569. https://doi.org/10.1016/j.jbiomech.2012.07.028.

Stout, J.L., Gage, J.R., Schwartz M.H., & Novacheck, T.F. (2008). Distal femoral extension osteotomy and patellar tendon advancement to treat persistent crouch gait in cerebral palsy. J. Bone Jt. Surg. 90; 2470–2484, doi:http://dx.doi.org/10.2106/JBJS.G.00327.

Stredney, D. L. (1982). The Representation of Anatomical Structures through Computer Animation for Scientific. Educational and Artistic Applications. The Ohio State University.

Surer E., Kose A. (2011). Methods and Technologies for Gait Analysis. In: Salah A., Gevers T. (eds) Computer Analysis of Human Behavior (pp. 105-123). Springer, London.

Sutherland, D.H., Cooper, L., & Daniel, D. (1980). The role of the ankle plantar flexors in normal walking. J Bone Joint Surg 1980;62-A:354-63.

Tao, W., Liu, T., Zheng, R., & Feng, H. (2012). Gait analysis using wearable sensors. *Sensors*, *12*(2), 2255–2283. https://doi.org/10.3390/s120202255.

Thelen, D. G. (2003). Adjustment of Muscle Mechanics Model Parameters to Simulate Dynamic Contractions in Older Adults, Journal of Biomechanical Engineering, 125(1), p. 70. doi: 10.1115/1.1531112.

Thelen, D. G., & Anderson, F. C. (2006). Using computed muscle control to generate forward dynamic simulations of human walking from experimental data. J Biomech. 2005/07/19, 39(6), pp. 1107–1115. doi: S0021-9290(05)00099-0 [pii] 10.1016/j.jbiomech.2005.02.010.

Trinler, U., Hollands, K., Jones, R., & Baker, R. (2018). A systematic review of approaches to modelling lower limb muscle forces during gait: Applicability to clinical gait analyses. *Gait and Posture*, *61* (November 2017), 353–361. https://doi.org/10.1016/j.gaitpost.2018.02.005.

Trinler, U. K. (2016). Lock Subtalar Mtp Joint Opensim. [Unpublished Ph.D. dissertation]. School of Health Science, University of Salford, UK.

van der Krogt, M.M., Bar-On, L., Kindt, T., Desloovere K., & Harlaar J. (2016). Neuro-musculoskeletal simulation of instrumented contracture and spasticity assessment in children with cerebral palsy. J. Neuroeng. Rehabil. 13 (2016) 64, https://doi.org/10.1186/s12984-016-0170-5.

van Gelder, L., Booth, A. T. C., van de Port, I., Buizer, A. I., Harlaar, J., & van der Krogt, M. M. (2017). Real-time feedback to improve gait in children with cerebral palsy. *Gait and Posture*, *52*, 76–82. https://doi.org/10.1016/j.gaitpost.2016.11.021.

Ward, S. R. et al. (2009). Are current measurements of lower extremity muscle architecture accurate?. Clinical Orthopaedics and Related Research, 467(4), pp. 1074–1082. doi: 10.1007/s11999-008-0594-8.

Waters, R.L., & Mulroy, S. (1999). The energy expenditure of normal and pathologic gait. Gait and Posture 9, 207–231.

Wickiewicz, T. L. et al. (1983). Muscle architecture of the human lower limb. Clinical Orthopaedics and Related Research, pp. 275–83. doi: 009-921X/83/1000/275.

Wilson, A., & Lichtwark, G. (2011). The anatomical arrangement of muscle and tendon enhances limb versatility and locomotor performance. Philosophical Transactions of the Royal Society B: Biological Sciences, 366(1570), 1540–1553. https://doi.org/10.1098/rstb.2010.0361.

Winter, D.A. (1980). Overall principle of lower limb support during stance phase of gait. J Biomech 1980;13:923 /7.

Winters, J. M., & Stark, L. (1987). Muscle models: what is gained and what is lost by varying model complexity, Biol. Cybern., 55, 403–420.

Winters, T.F., Gage, J.R., & Hicks, R. (1987). Gait patterns in spastic hemiplegia in children and young adults. The Journal of Bone and Joint Surgery; 69:437-441.

Winters, J. M. (1995). An improved muscle-reflex actuator for use in large-scale neuromusculoskeletal models. Annals of Biomedical Engineering, 23(4), 359–374. https://doi.org/10.1007/BF02584437.

Yamaguchi, G. T., & Zajac, F. E. (1989). A planar model of the knee joint to characterize the knee extensor mechanism. Journal of Biomechanics, 22(1), pp. 1–10. doi: 10.1016/0021-9290(89)90179-6.

Zajac, F. E. (1989). Muscle and tendon: properties, models, scaling, and application to biomechanics and motor control. In Critical reviews in biomedical engineering (Vol. 17, Issue 4, pp. 359–411).

Zajac, Felix E., Neptune, R. R., & Kautz, S. A. (2003). Biomechanics and muscle coordination of human walking: Part II: Lessons from dynamical simulations and clinical implications. Gait and Posture, 17(1), 1–17. https://doi.org/10.1016/S0966-6362(02)00069-3.

Appendix

Table A. Position errors for the pelvis from RRA, in analysing the CP children with crouch gait. Translational errors (tx, ty, and tz) are given in cm and rotational errors (tilt, list, and rotation) are given in degrees.

		Subjects – crouch gait		
Residuals		CP_Sub1	CP_Sub2	CP_Sub3
Pelvis tx	MAX	1,9305	3,2426	1,9108
	RMS	1,1632	1,5374	1,1840
Pelvis ty	MAX	1,9473	4,8024	2,1369
	RMS	1,1204	3,3880	1,5799
Pelvis tz	MAX	1,6229	3,5857	1,9417
	RMS	1,2488	2,5209	1,4580
Pelvis tilt	MAX	0,0208	0,1239	0,0068
	RMS	0,0120	0,0509	0,0040
Pelvis list	MAX	0,0228	0,1034	0,0152
	RMS	0,0093	0,0436	0,0081
Pelvis rotation	MAX	0,0271	0,1502	0,0307
	RMS	0,0149	0,0585	0,0233

Table B. Position errors for the pelvis from RRA, in analysing the TD children simulating crouch gait. Translational errors (tx, ty, and tz) are given in cm and rotational errors (tilt, list, and rotation) are given in degrees.

		Subjects – crouch gait					
Residuals		TD_Sub1	TD_Sub2	TD_Sub3	TD_Sub4	TD_Sub5	TD_Sub6
Pelvis tx	MAX	2,2596	0,8742	0,6484	1,6559	1,8828	1,9657
	RMS	1,6373	0,5424	0,4457	1,2210	1,3300	1,4072
Pelvis ty	MAX	4,0866	2,5971	3,4976	3,0946	2,3346	3,4030
	RMS	2,8207	1,8162	2,4532	1,9660	1,5887	2,3903
Pelvis tz	MAX	0,2203	0,8507	1,1896	0,7886	1,1186	1,3269
	RMS	0,1600	0,4670	0,5971	0,3507	0,6611	0,6965
Pelvis tilt	MAX	0,0415	0,0301	0,0411	0,0376	0,0398	0,0372
	RMS	0,0260	0,0192	0,0264	0,0231	0,0278	0,0249
Pelvis list	MAX	0,0527	0,0383	0,0128	0,0253	0,0423	0,0216
	RMS	0,0353	0,0242	0,0073	0,0162	0,0299	0,0177
Pelvis rotation	MAX	0,0557	0,0368	0,0175	0,0366	0,0354	0,0666
	RMS	0,0368	0,0311	0,0103	0,0233	0,0242	0,0473

Table C. Position errors for the pelvis from RRA, in analysing the TD children performing their normal gait. Translational errors (tx, ty, and tz) are given in cm and rotational errors (tilt, list and rotation) are given in degrees.

		Subjects – unimpaired gait					
Residuals		TD_Sub1	TD_Sub2	TD_Sub3	TD_Sub4	TD_Sub5	TD_Sub6
Pelvis tx	MAX	2,0535	1,9524	1,3417	0,7455	1,8829	2,1110
	RMS	1,4934	1,4337	0,6835	0,5092	1,2403	1,4760
Pelvis ty	MAX	2,6998	3,0680	2,0502	2,4135	2,8687	2,9283
	RMS	1,7487	1,9365	1,0071	1,5600	1,8351	1,7595
Pelvis tz	MAX	0,4885	1,9342	1,9976	2,1195	1,6664	1,8432
	RMS	0,1868	1,1775	1,0569	1,5457	1,0356	1,0750
Pelvis tilt	MAX	0,0104	0,0455	0,0384	0,0322	0,0359	0,0165
	RMS	0,0062	0,0504	0,0203	0,0195	0,0235	0,0109
Pelvis list	MAX	0,0653	0,0448	0,0581	0,0648	0,0220	0,0107
	RMS	0,0456	0,0506	0,0264	0,0406	0,0140	0,0064
Pelvis rotation	MAX	0,0072	0,0234	0,0457	0,0437	0,0167	0,0204
	RMS	0,0044	0,0213	0,0200	0,0278	0,0059	0,0128

Table D. Position errors in the joint degrees of freedom from RRA, for the CP children with crouch gait. The values are given in degrees.

		Subjects – crouch gait		
Degrees of freedom		CP_Sub1	CP_Sub2	CP_Sub3
Right hip flexion	MAX	0,1059	0,3032	0,0568
	RMS	0,0328	0,1179	0,0407
Right hip adduction	MAX	0,0610	0,1482	0,0293
	RMS	0,0440	0,1074	0,0191
Right hip rotation	MAX	0,0415	0,1121	0,0429
	RMS	0,0146	0,0458	0,0261
Right knee	MAX	0,0895	0,1797	0,0571
	RMS	0,0483	0,0639	0,0338
Right ankle	MAX	1,0832	0,8011	0,7968
	RMS	0,5906	0,3617	0,4413
Left hip flexion	MAX	0,0693	0,3100	0,0439
	RMS	0,0210	0,1197	0,0305
Left hip adduction	MAX	0,0943	0,3101	0,0363
	RMS	0,0424	0,1214	0,0245
Left hip rotation	MAX	0,0458	0,0955	0,0201
	RMS	0,0315	0,0340	0,0121
Left knee	MAX	0,0514	0,0756	0,0101
	RMS	0,0286	0,0430	0,0063
Left ankle	MAX	0,8261	1,7287	0,3523
	RMS	0,4241	0,9424	0,1835
Lumbar extension	MAX	0,1392	0,9908	0,1409
	RMS	0,0984	0,4250	0,0859
Lumbar bending	MAX	0,3482	0,2598	0,3490
	RMS	0,2738	0,1335	0,2606
Lumbar rotation	MAX	0,2284	0,4708	0,1025
	RMS	0,1010	0,1804	0,0487

Table E. Position errors in the joint degrees of freedom from RRA, for the TD children simulating crouch gait. The values are given in degrees.

		Subjects – crouch gait					
Degrees of freedom		TD_Sub1	TD_Sub2	TD_Sub3	TD_Sub4	TD_Sub5	TD_Sub6
Right hip flexion	MAX	0,0357	0,1262	0,0297	0,1437	0,1783	0,0589
	RMS	0,0221	0,0791	0,0097	0,0878	0,1224	0,0402
Right hip adduction	MAX	0,0182	0,0265	0,0285	0,0733	0,0340	0,0575
	RMS	0,0092	0,0194	0,0190	0,0565	0,0277	0,0291
Right hip rotation	MAX	0,0493	0,0122	0,0255	0,0109	0,0228	0,0551
	RMS	0,0319	0,0075	0,0146	0,0064	0,0179	0,0392
Right knee	MAX	0,0240	0,1280	0,0304	0,1396	0,0572	0,0223
	RMS	0,0167	0,0778	0,0160	0,0839	0,0373	0,0148
Right ankle	MAX	0,7909	2,7516	0,7668	3,2938	4,8633	0,6093
	RMS	0,1406	1,6952	0,1453	1,9776	3,3284	0,1027
Left hip flexion	MAX	0,1697	0,0339	0,1039	0,0513	0,0452	0,2051
	RMS	0,1122	0,0115	0,0636	0,0157	0,0304	0,1426
Left hip adduction	MAX	0,0415	0,0406	0,0294	0,0439	0,0551	0,0792
	RMS	0,0222	0,0254	0,0202	0,0337	0,0398	0,0601
Left hip rotation	MAX	0,1257	0,0324	0,0179	0,0477	0,0245	0,0215
	RMS	0,0804	0,0075	0,0102	0,0312	0,0157	0,0142
Left knee	MAX	0,0260	0,0180	0,0136	0,0482	0,0093	0,2431
	RMS	0,0155	0,0137	0,0075	0,0122	0,0036	0,1625
Left ankle	MAX	4,4251	0,8466	2,6333	0,8780	0,2253	3,5650
	RMS	2,8240	0,1485	1,6524	0,1716	0,0333	2,4302
Lumbar extension	MAX	0,1877	0,0221	0,1579	0,2346	0,0969	0,1428
	RMS	0,1208	0,0134	0,1164	0,1696	0,0606	0,0946
Lumbar bending	MAX	0,3240	0,5088	0,2888	0,3159	0,2974	0,5011
	RMS	0,2339	0,3727	0,2135	0,2224	0,2228	0,3616
Lumbar rotation	MAX	0,2026	0,1521	0,0814	0,4106	0,1077	0,3319
	RMS	0,1496	0,1035	0,0591	0,2874	0,0604	0,2438

Table F. Position errors in the joint degrees of freedom from RRA, for the TD children performing their normal gait. The values are given in degrees.

		Subjects – unimpaired gait					
Degrees of freedom		TD_Sub1	TD_Sub2	TD_Sub3	TD_Sub4	TD_Sub5	TD_Sub6
Right hip flexion	MAX	0,0618	0,0396	0,0858	0,2778	0,1255	0,1780
	RMS	0,0364	0,0405	0,0233	0,1904	0,0852	0,1268
Right hip adduction	MAX	0,0580	0,0752	0,0553	0,0579	0,0675	0,1271
	RMS	0,0268	0,0868	0,0284	0,0415	0,0452	0,0985
Right hip rotation	MAX	0,0326	0,0432	0,0467	0,1087	0,1229	0,1487
	RMS	0,0213	0,0436	0,0198	0,0692	0,0941	0,1017
Right knee	MAX	0,0275	0,0365	0,0511	0,0289	0,0310	0,0757
	RMS	0,0072	0,0235	0,0157	0,0131	0,0160	0,0517
Right ankle	MAX	0,5587	0,8967	1,3365	4,1085	3,8813	2,9529
	RMS	0,0942	0,3002	0,1805	2,5220	2,8380	1,9857
Left hip flexion	MAX	0,1009	0,0960	0,1573	0,1172	0,0519	0,1058
	RMS	0,0724	0,1052	0,0822	0,0704	0,0310	0,0641
Left hip adduction	MAX	0,0862	0,0404	0,0251	0,0379	0,0850	0,1325
	RMS	0,0539	0,0484	0,0122	0,0201	0,0594	0,1002
Left hip rotation	MAX	0,1734	0,2775	0,1248	0,0657	0,0376	0,0493
	RMS	0,1260	0,3188	0,0657	0,0404	0,0161	0,0132
Left knee	MAX	0,0716	0,1039	0,0304	0,0263	0,0380	0,0260
	RMS	0,0468	0,1225	0,0100	0,0155	0,0133	0,0113
Left ankle	MAX	3,1376	4,8040	3,9078	0,9124	0,6751	0,6262
	RMS	2,1732	5,5963	2,0114	0,1540	0,1142	0,1093
Lumbar extension	MAX	0,0902	0,0245	0,0306	0,1135	0,1078	0,1533
	RMS	0,0623	0,0220	0,0170	0,0771	0,0521	0,0910
Lumbar bending	MAX	0,0215	0,1248	0,0869	0,0962	0,1908	0,2518
	RMS	0,0121	0,1509	0,0446	0,0568	0,1430	0,1911
Lumbar rotation	MAX	0,1119	0,0994	0,0207	0,0424	0,1760	0,3009
	RMS	0,0856	0,1316	0,0082	0,0255	0,1092	0,2295

Table G. Position errors in the joint degrees of freedom from CMC, for the CP children with crouch gait. The values are given in degrees.

		Subjects – crouch gait		
Degrees of freedom		CP_Sub1	CP_Sub2	CP_Sub3
Right hip flexion	MAX	0,3062	0,0772	0,0595
	RMS	0,1492	0,0421	0,0334
Right hip adduction	MAX	0,1776	0,0488	0,0603
	RMS	0,1100	0,0222	0,0374
Right hip rotation	MAX	0,4674	0,4219	0,3277
	RMS	0,2879	0,2578	0,2603
Right knee	MAX	0,1645	0,1184	0,0819
	RMS	0,0767	0,0746	0,0524
Right ankle	MAX	0,4381	0,6849	0,4107
	RMS	0,2081	0,4643	0,2121
Left hip flexion	MAX	0,5550	0,0672	0,0705
	RMS	0,3643	0,0206	0,0339
Left hip adduction	MAX	0,8192	0,0352	0,1559
	RMS	0,4545	0,0158	0,0598
Left hip rotation	MAX	1,8201	0,6488	0,8520
	RMS	0,9856	0,3337	0,6130
Left knee	MAX	0,1474	0,1204	0,1157
	RMS	0,0838	0,0900	0,0274
Left ankle	MAX	0,4092	0,3987	0,7150
	RMS	0,0992	0,1037	0,3565
Lumbar extension	MAX	0,5347	0,0573	0,0497
	RMS	0,2764	0,0233	0,0225
Lumbar bending	MAX	0,1346	0,0440	0,0501
	RMS	0,0766	0,0168	0,0193
Lumbar rotation	MAX	0,8181	0,2947	0,2382
	RMS	0,5574	0,1584	0,1844

Table H. Position errors in the joint degrees of freedom from CMC, for the TD children simulating crouch gait. The values are given in degrees.

		Subjects – crouch gait					
Degrees of freedom		TD_Sub1	TD_Sub2	TD_Sub3	TD_Sub4	TD_Sub5	TD_Sub6
Right hip flexion	MAX	0,3130	0,3782	0,1651	0,0403	0,4821	0,1553
	RMS	0,1969	0,1855	0,0863	0,0184	0,3837	0,1042
Right hip adduction	MAX	0,2339	0,6782	0,1615	0,0610	0,2035	0,1896
	RMS	0,1537	0,3739	0,0546	0,0307	0,1401	0,1195
Right hip rotation	MAX	1,0132	0,6030	0,5682	0,0975	0,2665	0,5184
	RMS	0,5830	0,5113	0,3783	0,0546	0,1926	0,3440
Right knee	MAX	0,4762	0,2051	0,2723	0,0677	1,7400	0,1137
	RMS	0,3061	0,1719	0,0893	0,0528	1,3825	0,0625
Right ankle	MAX	0,4815	1,3965	0,7848	0,3846	2,5758	0,1952
	RMS	0,1168	1,2205	0,1762	0,3456	2,3922	0,0994
Left hip flexion	MAX	0,0954	0,6938	0,2037	0,1426	0,4255	0,0796
	RMS	0,0380	0,5352	0,1150	0,1028	0,2613	0,0468
Left hip adduction	MAX	0,0978	0,7076	0,1487	0,1364	0,2460	0,2124
	RMS	0,0312	0,3926	0,0687	0,0987	0,1574	0,0823
Left hip rotation	MAX	0,2633	2,0111	0,1786	0,2558	0,8130	0,2516
	RMS	0,0986	1,2862	0,1054	0,1714	0,4875	0,1454
Left knee	MAX	0,1949	0,5805	0,8784	0,3292	0,3406	0,0298
	RMS	0,0838	0,4390	0,6873	0,2120	0,1950	0,0113
Left ankle	MAX	0,4594	0,4612	1,6475	0,3402	0,4595	0,6074
	RMS	0,4096	0,0896	1,5111	0,1102	0,1211	0,4740
Lumbar extension	MAX	0,0300	0,4003	0,1387	0,0329	0,0669	0,0476
	RMS	0,0157	0,1983	0,0639	0,0181	0,0325	0,0285
Lumbar bending	MAX	0,0516	0,3575	0,0548	0,0435	0,0939	0,0973
	RMS	0,0257	0,1793	0,0273	0,0242	0,0558	0,0423
Lumbar rotation	MAX	0,3751	0,6925	0,2591	0,1511	0,2245	0,2677
	RMS	0,2548	0,4715	0,1293	0,1010	0,1290	0,1836

Table I. Position errors in the joint degrees of freedom from CMC, for the TD children performing their normal gait. The values are given in degrees.

		Subjects – unimpaired gait					
Degrees of freedom		TD_Sub1	TD_Sub2	TD_Sub3	TD_Sub4	TD_Sub5	TD_Sub6
Right hip flexion	MAX	0,4025	0,3282	1,2554	0,4924	0,3258	0,1732
	RMS	0,2581	0,2248	0,4684	0,3736	0,1592	0,0807
Right hip adduction	MAX	0,1638	0,3003	0,5173	0,5083	0,5305	0,1892
	RMS	0,1144	0,1747	0,2368	0,1933	0,2304	0,0783
Right hip rotation	MAX	0,9374	0,5603	1,7297	0,2680	0,3138	0,1036
	RMS	0,3802	0,3359	0,7643	0,1912	0,1125	0,0575
Right knee	MAX	0,5648	0,4553	2,0834	0,8594	0,7243	0,3293
	RMS	0,3862	0,2526	0,5746	0,6726	0,3331	0,0982
Right ankle	MAX	0,5217	0,2825	0,3887	1,1908	0,2491	0,1610
	RMS	0,1679	0,0871	0,1469	0,8046	0,1617	0,0978
Left hip flexion	MAX	0,1212	0,2151	0,3893	0,4727	0,2521	0,2898
	RMS	0,0734	0,0590	0,2652	0,2255	0,1865	0,2054
Left hip adduction	MAX	0,1559	0,2880	0,4041	0,1862	0,2909	0,2167
	RMS	0,1014	0,1251	0,2368	0,0907	0,1940	0,1466
Left hip rotation	MAX	0,3332	0,1289	0,2883	1,3430	0,5175	0,9981
	RMS	0,2236	0,0495	0,1713	0,6914	0,2868	0,4905
Left knee	MAX	0,2033	0,5129	0,9784	0,3782	0,5363	0,5115
	RMS	0,0906	0,1204	0,6410	0,1653	0,3432	0,3047
Left ankle	MAX	0,5717	0,1437	0,7217	0,5612	0,1310	0,1850
	RMS	0,2164	0,0428	0,4816	0,1385	0,0675	0,0829
Lumbar extension	MAX	0,1708	0,1189	0,4212	0,3334	0,0741	0,0887
	RMS	0,0991	0,0914	0,2095	0,1657	0,0384	0,0388
Lumbar bending	MAX	0,1198	0,1095	0,2352	0,2983	0,2654	0,1328
	RMS	0,0616	0,0638	0,1001	0,1048	0,1128	0,0519
Lumbar rotation	MAX	0,1591	0,3735	0,4103	0,4385	0,2910	0,2378
	RMS	0,0835	0,2352	0,2842	0,2596	0,1208	0,1288

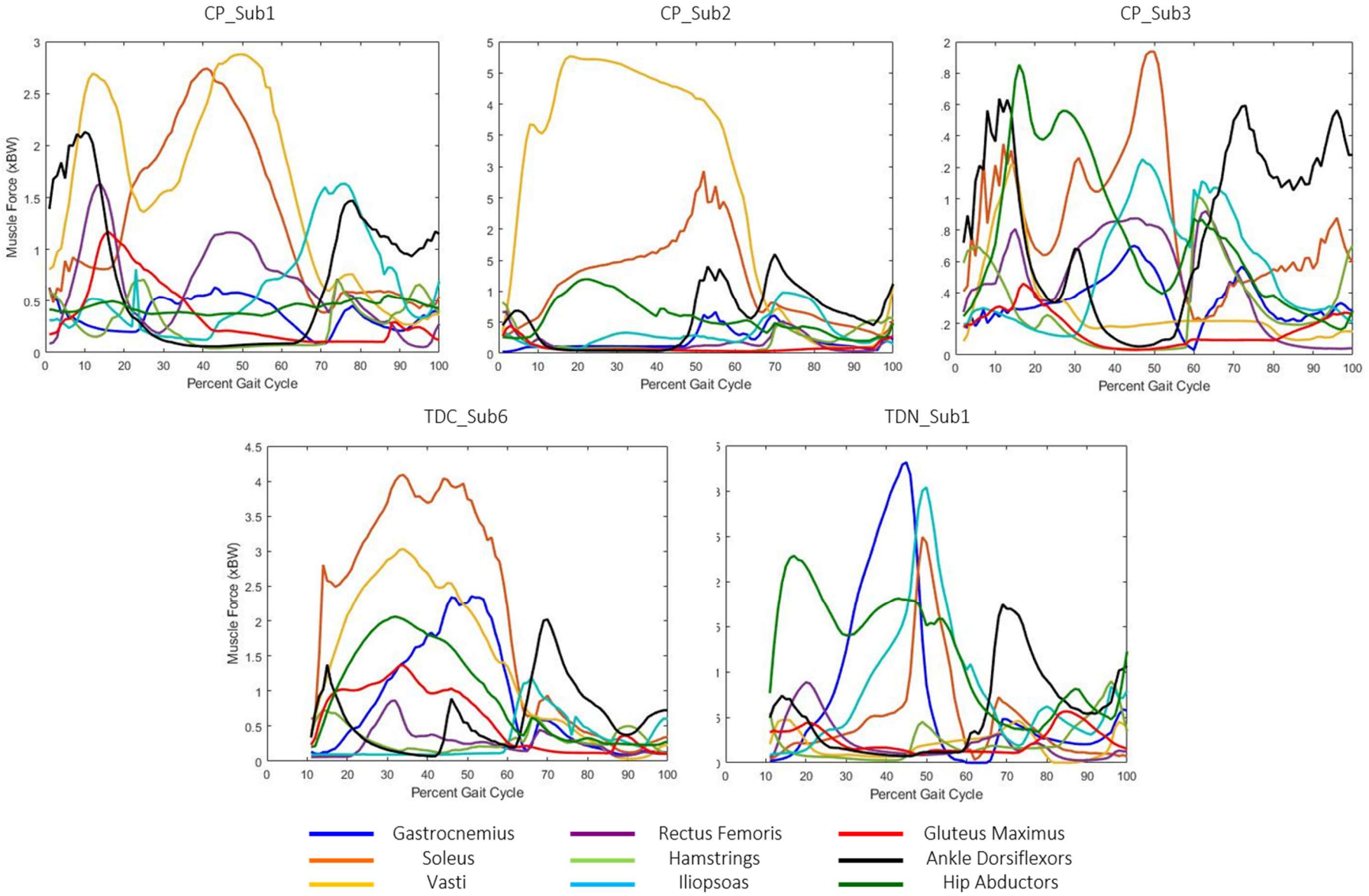

Figure A. Resulting muscle forces normalized by bodyweight (BW) obtained from CMC, for all CP children, subject TD_Sub1 performing normal gait, and subject TD_Sub6 simulating crouch gait.

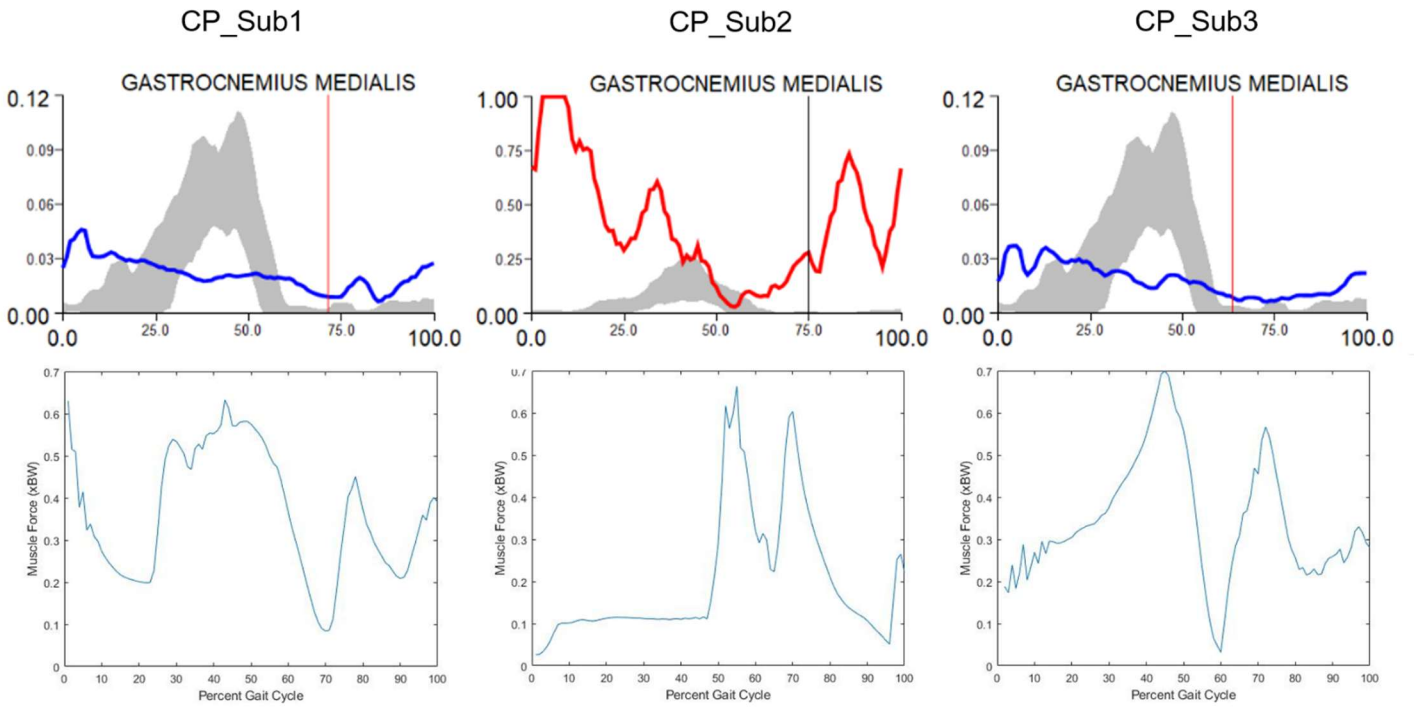

Figure B. Comparison of the experimentally obtained EMG from the gastrocnemius medialis with the force produced by the gastrocnemius throughout the gait cycle, estimated by OpenSim. These results relate to the CP children. The EMG is represented in mV.

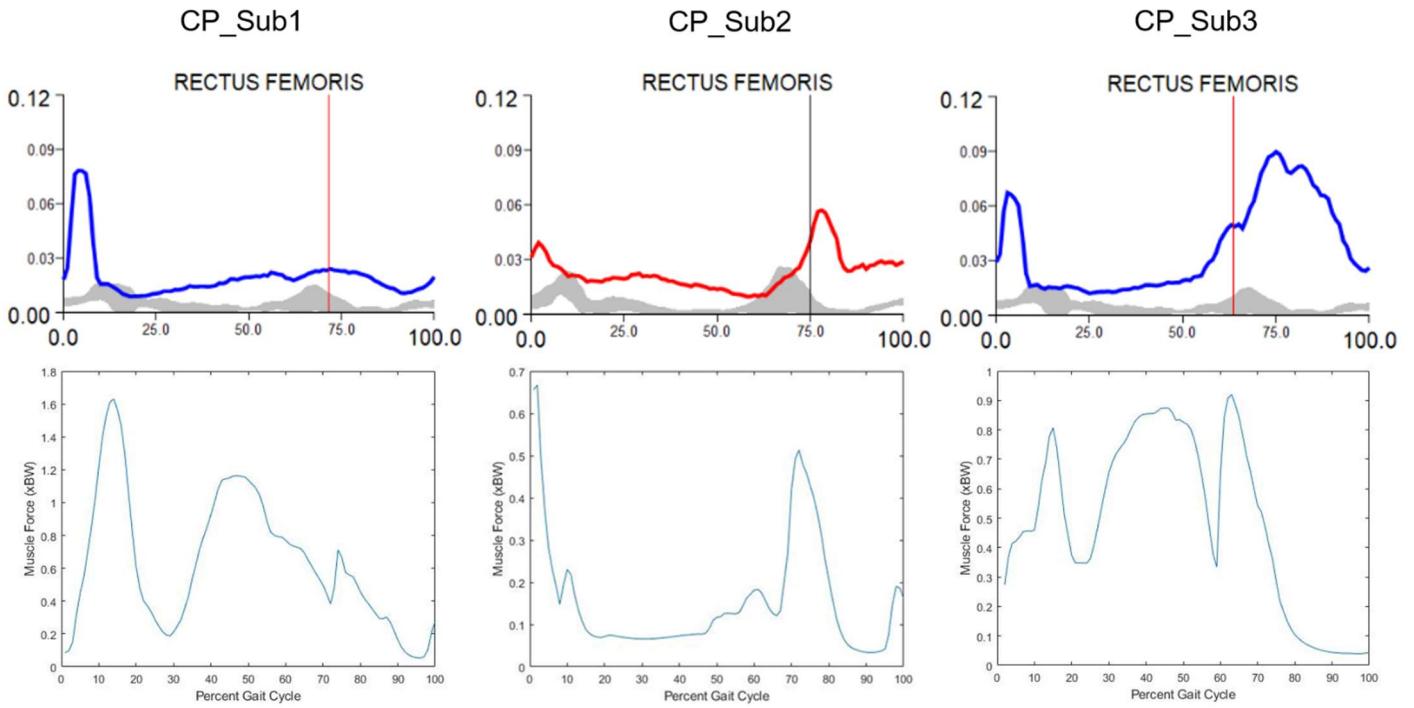

Figure C. Comparison of the experimentally obtained EMG from the rectus femoris with the force produced by this muscle throughout the gait cycle, estimated by OpenSim. The EMG is represented in mV.

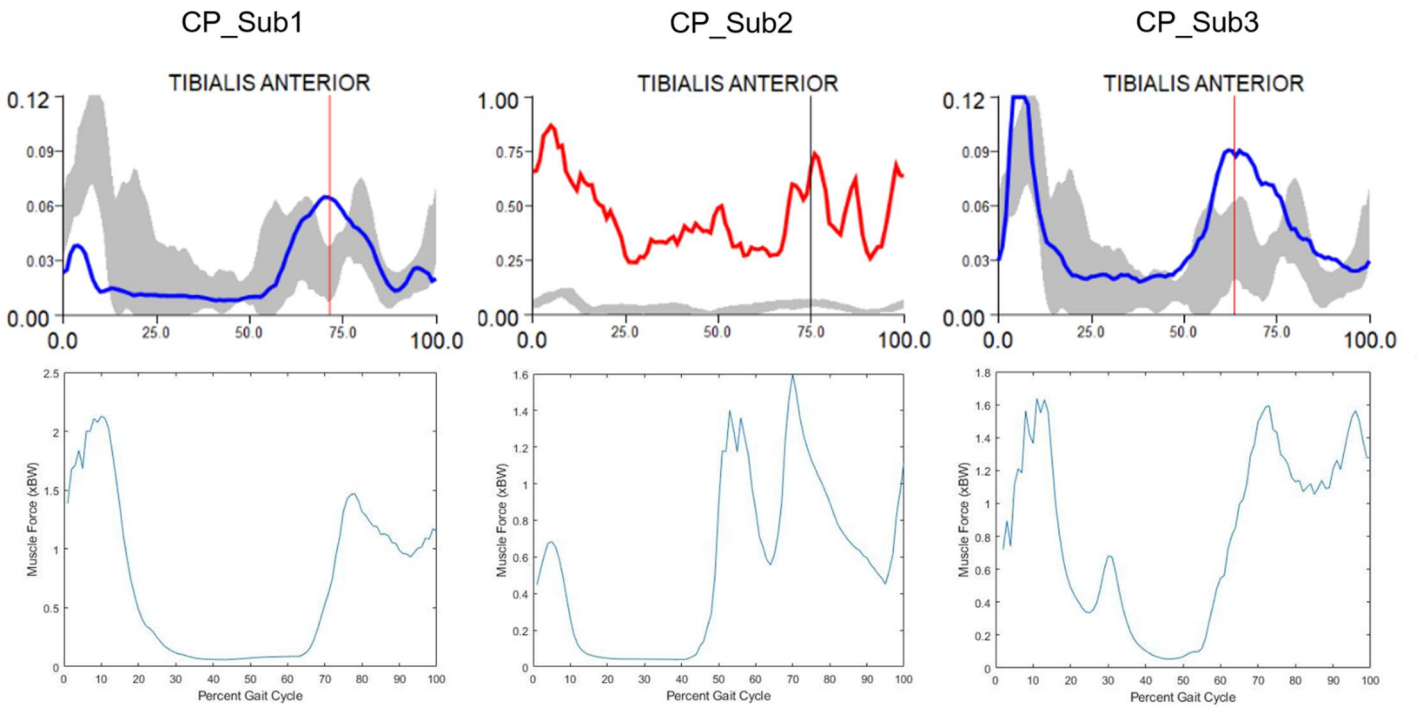

Figure D. Comparison of the experimentally obtained EMG from the tibialis anterior with the force produced by the ankle dorsiflexors throughout the gait cycle, estimated by OpenSim. These results relate to the CP children. The EMG is represented in mV.

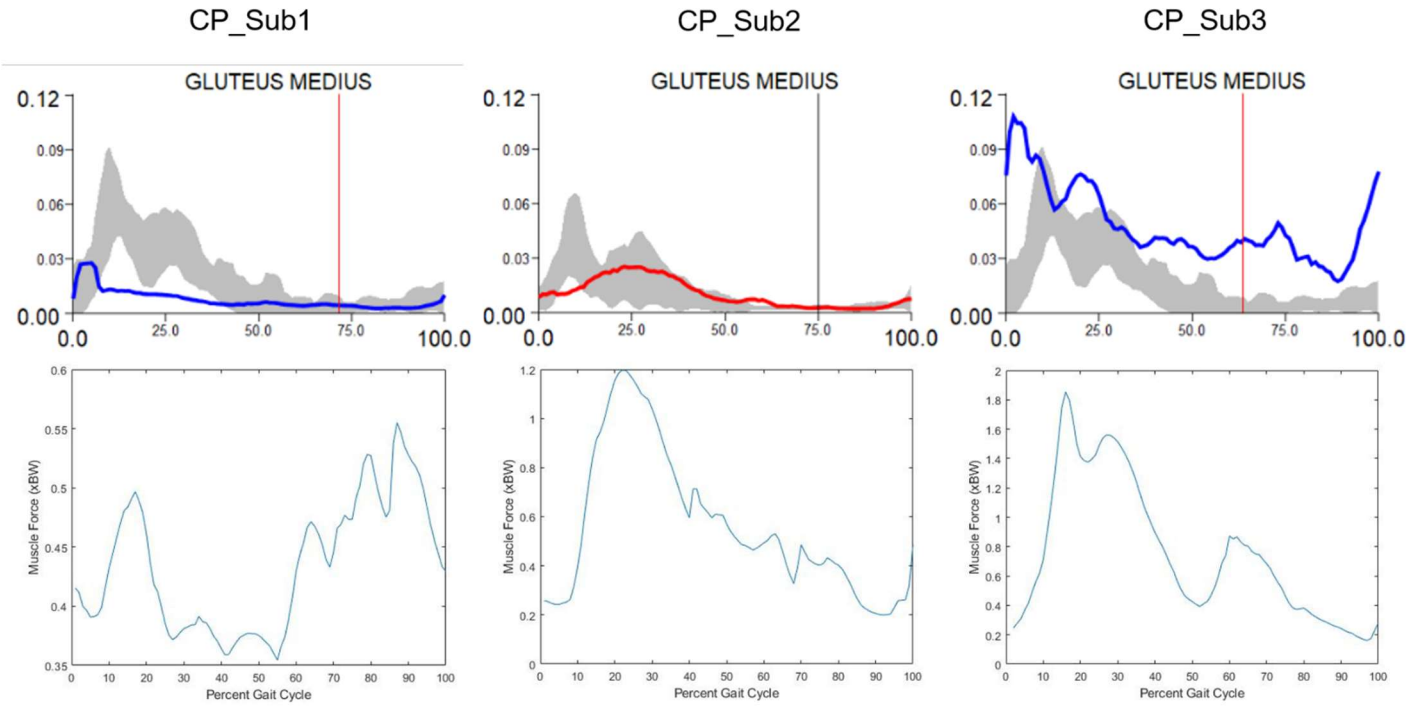

Figure E. Comparison of the experimentally obtained EMG from the gluteus medius with the force produced by the hip abductors throughout the gait cycle, estimated by OpenSim. These results relate to the CP children. The EMG is represented in mV.

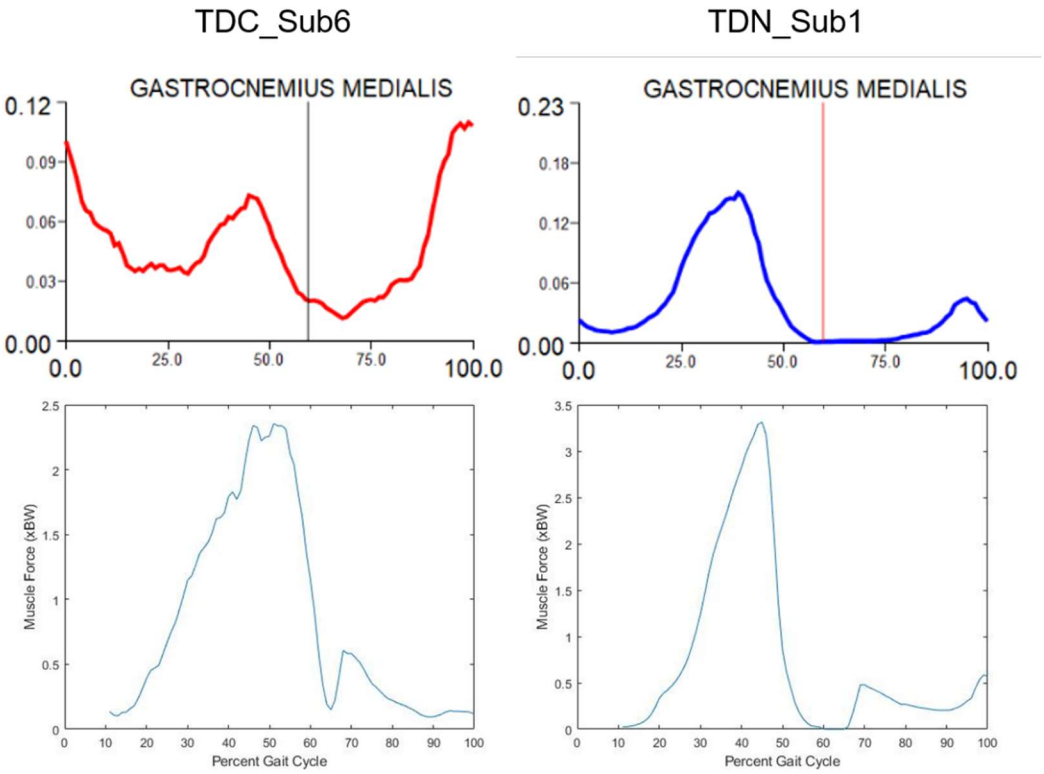

Figure F. Comparison of the experimentally obtained EMG from the gastrocnemius medialis with the force produced by the gastrocnemius throughout the gait cycle, estimated by OpenSim. These results relate to the typically developing children (Sub6 simulating crouch gait and Sub1 performing the unimpaired gait) . The EMG is represented in mV.

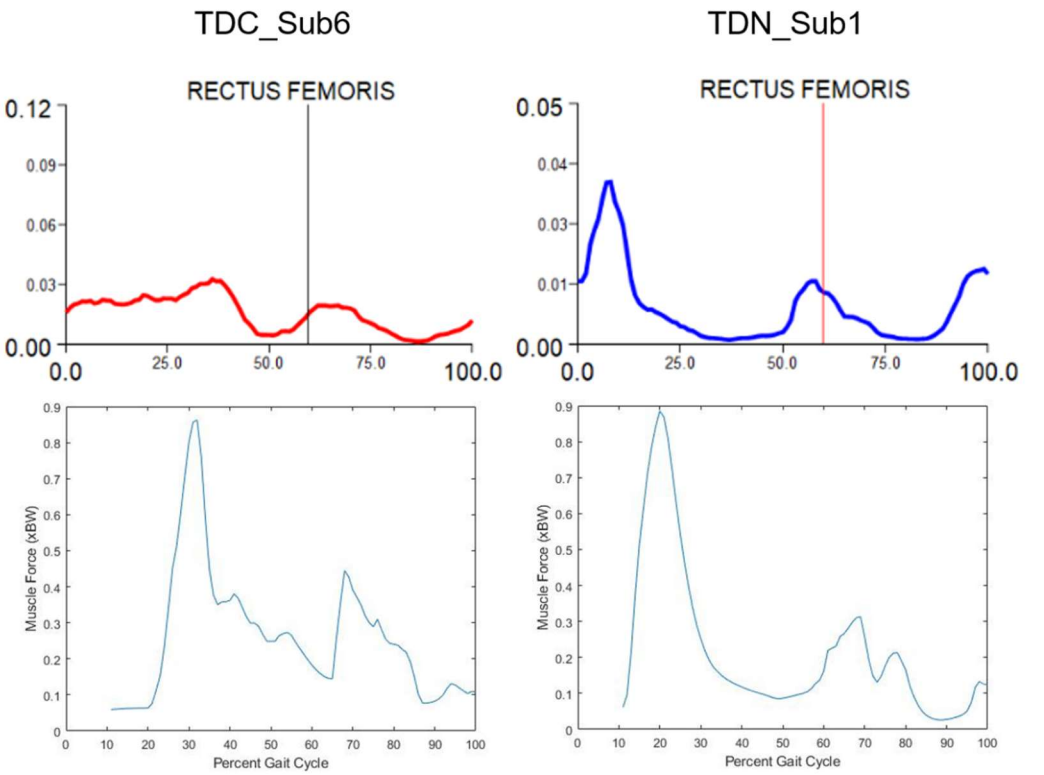

Figure G. Comparison of the experimentally obtained EMG from the rectus femoris with the force produced by this muscle throughout the gait cycle, estimated by OpenSim. These results relate to the typically developing children (Sub6 simulating crouch gait and Sub1 performing the unimpaired gait) . The EMG is represented in mV.

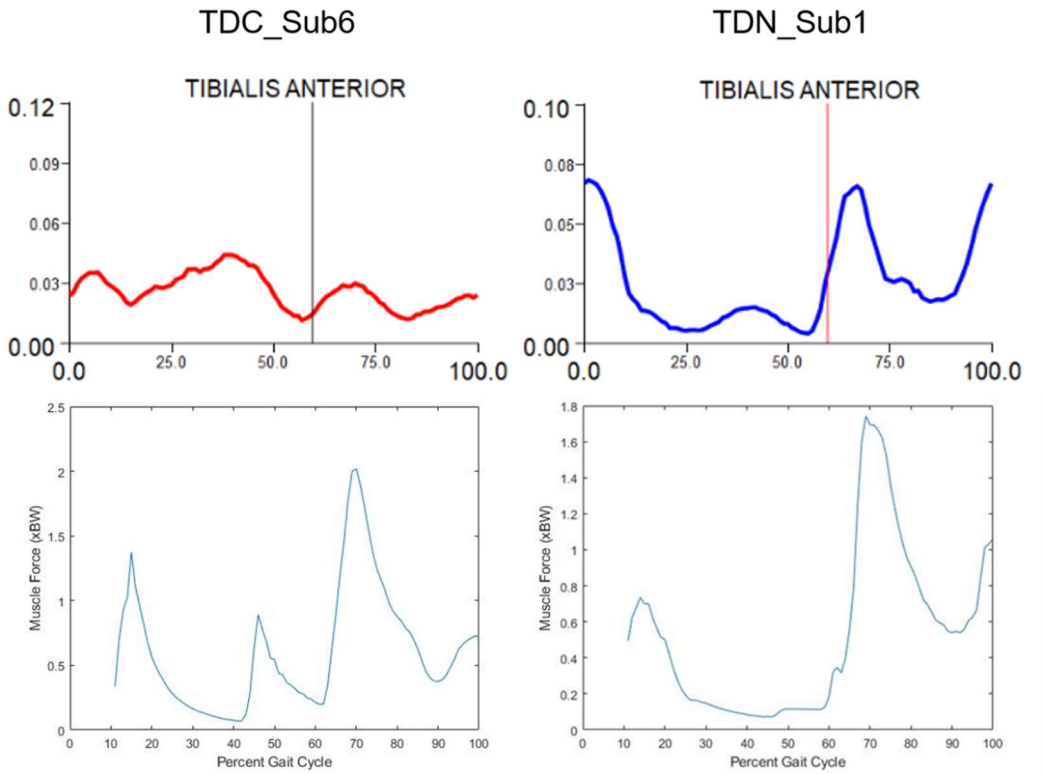

Figure H. Comparison of the experimentally obtained EMG from the tibialis anterior with the force produced by the ankle dorsiflexors throughout the gait cycle, estimated by OpenSim. These results relate to the typically developing children (Sub6 simulating crouch gait and Sub1 performing the unimpaired gait). The EMG is represented in mV.

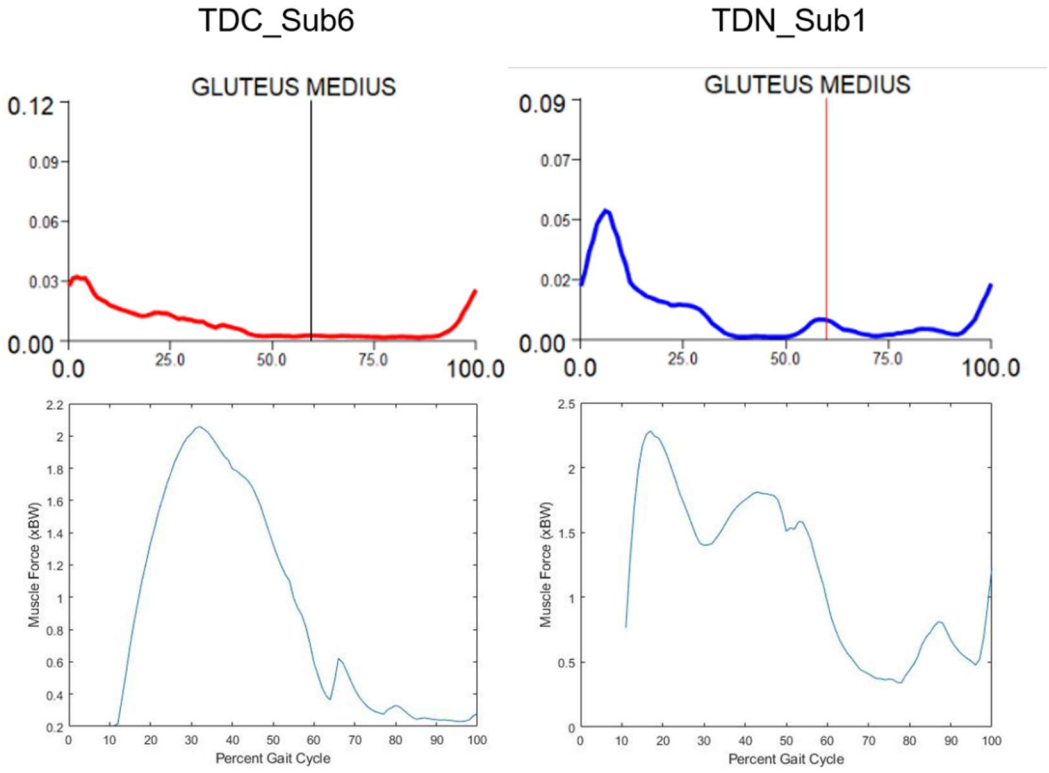

Figure I. Comparison of the experimentally obtained EMG from the gluteus medius with the force produced by the hip abductors throughout the gait cycle, estimated by OpenSim. These results relate to the typically developing children (Sub6 simulating crouch gait and Sub1 performing the unimpaired gait). The EMG is represented in mV.